UNIVERSITÀ DEGLI STUDI DI MESSINA

DIPARTIMENTO DI

SCIENZE CHIMICHE, BIOLOGICHE, FARMACEUTICHE ED AMBIENTALI

DOTTORATO DI RICERCA IN SCIENZE CHIMICHE

XXXVII CICLO 2021-2024

Chemically-tailored nanoplatforms: versatile design strategies for customized antitumoral and antibacterial applications

Roberto Oliva

Supervisor
Prof. Angela Scala

Coordinator
Prof. Concetta De Stefano

Anno Accademico 2023/2024
SSD CHEM-05A

Summary

1. Summary of the Project

The design and development of novel Drug Delivery Systems (DSS) for encapsulation of bioactive compounds has been the main focus of my research during the PhD course. This Thesis describes the design, synthesis, characterization and biological investigation of new engineered biomaterials based on newly-synthetized amphiphilic copolymers, amphiphilic cyclodextrins or commercially available phospholipids. These materials, all sharing the characteristics of biocompatibility and biodegradability, possess the ability to self-assemble into valuable nanostructures and turn out to be able to incorporate antitumoral or antimicrobial drugs, acting as carriers for their payload.

During my PhD research activities, I focused on the development of chemically-tailored nanoplatforms for two common antitumoral drugs, *i.e.* Docetaxel (DTX) and Doxorubicin (DOX), and for two antimicrobial drugs, *i.e.* Linezolid and MEDS433 (***Figure 1***).

DOX and DTX are the two most important chemotherapeutic agents commonly used for the treatment of cancer, both triggering apoptosis. Specifically, DTX is a semi-synthetic analog of Paclitaxel acting as a microtubule-interfering agent able to inhibit microtubule depolymerization with consequent cell cycle arrest at G2/M; DOX is an anthracycline able to interfere with replication and transcription processes via intercalation between DNA bases and binding to the Topoisomerase II enzyme. Moreover, DOX is also able to generate ROS causing oxidative stress. All these mechanisms contribute to the damage of cellular DNA which will ultimately lead to the activation of the apoptotic processes.

While both DTX and DOX are currently used for the treatment of different types of cancer (breast, glioblastoma, osteosarcoma), they possess several drawbacks that limit their therapeutic efficacy, including poor solubility in water, limited lifetime in biological environment and lack of selectivity towards target cells.

Based on these premises, there is an urgent need of suitable delivery nanosystems to improve the biological profile and safety of these antitumoral drugs.

In this framework, my PhD project focused on the synthesis and characterization of novel star-shaped amphiphilic copolymers based on PolyLactic Acid and PolyEthylene Glycol (star PLA-PEG) successfully formulated in nanoparticles (NPs) incorporating DTX and DOX (***Figure 1A***).

Star-shaped polymers have unique properties compared to their linear counterparts, including smaller hydrodynamic radius, lower viscosity, spherical and compact 3D-shape with a high density of functionalizable end-groups and a covalently reinforced core-shell structure similar to that of micelles assuring good drug encapsulation capability.

The novel amphiphilic star PLA-PEG copolymer was synthetized by a proper combination of copper-catalyzed azide-alkyne cycloaddition (CuAAC) and Ring Opening Polymerization (ROP), followed by decoration with the targeting ligand RGD peptide, a well-studied tumor-homing peptide that specifically binds to integrins overexpressed on cancer cells and blood vessels during cancer angiogenesis.

The biological profile of the novel drug-loaded nanosystems was investigated *in vitro* on selected tumoral cells (*i.e.*, U87 Human Glioblastoma and MDA-MB 468 Human Breast Adenocarcinoma for DTX-loaded nanocarriers; MG63, SAOS-2, and U2-OS osteosarcoma cells for DOX-loaded nanocarriers)[1,2].

As a part of my PhD project, I newly synthesized and characterized also a linear amphiphilic PLA-PEG copolymer suitable for nanoformulation and for incorporation of the antimicrobial drug Linezolid (LNZ) (***Figure 1A***).

LNZ is a new-generation oxazolidinone, active and moderately active against Gram-positive and Gram-negative bacteria, respectively. The mechanism of action through which it inhibits bacterial growth differs from all the existing protein synthesis inhibitors since LNZ binds the A-site pocket of the 50S ribosomal subunit with consequent inhibition of the initiation complex and translocation of peptidyl-tRNA from A to P site[3]. This mechanism, occurring at a very early stage of protein synthesis,

confers to LNZ a series of advantages: its action is selective against bacteria without interference with human biosynthetic processes and with low chance to develop drug resistance. This last characteristic makes it particularly efficient in the treatment of infections of bacterial strains resistant to traditional antibiotics, including Methicillin Resistant Staphylococcus Aureus (MRSA) and Multi Drug Resistant-Mycobacterium tuberculosis (Mtb). However, prolonged LNZ administration is often correlated with long-term side effects (*e.g.* myelosuppression and neuropathy).

To overcome these critical drawbacks, there is an urgent need of developing suitable antimicrobial delivery systems to improve the safety profile of LNZ and to reduce the dose, the frequency of dosage and the toxicity related to prolonged administration. In this framework, a novel linear amphiphilic PLA-PEG copolymer was synthetized by a proper combination of carbodiimide-mediated coupling and copper catalyzed azide-alkyne cycloaddition (CuAAC) reactions. The nanoformulation and drug encapsulation was prompted by the self-assembly in water of the amphiphile into NPs consisting of a hydrophobic core incorporating LNZ and a hydrophilic PEGylated shell. The antimicrobial activity of LNZ-loaded NPs was investigated against a panel of Gram-positive bacteria responsible for human infections, such as *Staphylococcus aureus* including MRSA, *Staphylococcus epidermidis*, *Staphylococcus lugdunensis* and *vancomycin-resistant Enterococcus faecium* (VREfm)[4].

During the PhD research, I was involved in the NATO project "VIPER" (*Learning a lesson: fighting SARS-Co**V**-2 **I**nfection and get ready for other future **P**and**E**mic scena**R**ios*) focused on the development of water soluble nanocarriers for MEDS433.

MEDS433 is an *in house* human dihydroorotate dehydrogenase (hDHODH) inhibitor, developed at the University of Turin (Department of Drug Science and Technology) by Marco L. Lolli's group, acting as Broad-Spectrum Antiviral Agent (BSAA) able to reduce the replication of a large virus panel, including SARS-CoV-2. It turned out to be one log unit more potent than the best available and FDA-approved therapy, *i.e.* Remdesivir.

The hDHODH is an enzyme that catalyzes the fourth step in the *de novo* biosynthesis of pyrimidine, active only when a viral infection is ongoing in a cell. Under physiological conditions, the demand of pyrimidines for DNA/RNA is satisfied through the recycling of pre-existing nucleosides; however, during a viral infection, an increment in the need of pyrimidine occurs and the *de novo* biosynthesis of pyrimidines becomes active. Therefore, the use of inhibitor of hDHODH, such as MEDS433, allows to selectively treat infected cells, without effects on healthy cells.

Given the impressive biological performance of MEDS433, the aim of VIPER project was the development of water soluble MEDS433 delivery systems suitable for *in vivo* tests in SARS-CoV-2 infected animal models. Specifically, two different strategies were planned and realized within VIPER project to improve the low water solubility (12 μM) of MEDS433: the first one was based on the use of cyclodextrins and the second one on lipodisks (***Figure 1B and 1C***). I was involved in both the research activities carried out at the University of Messina and at University of Uppsala -Sweden- (during my foreign 6-months abroad), respectively. Both the strategies led to a significant improvement of MEDS433 water solubility which was the main hindrance to its clinical development so far.

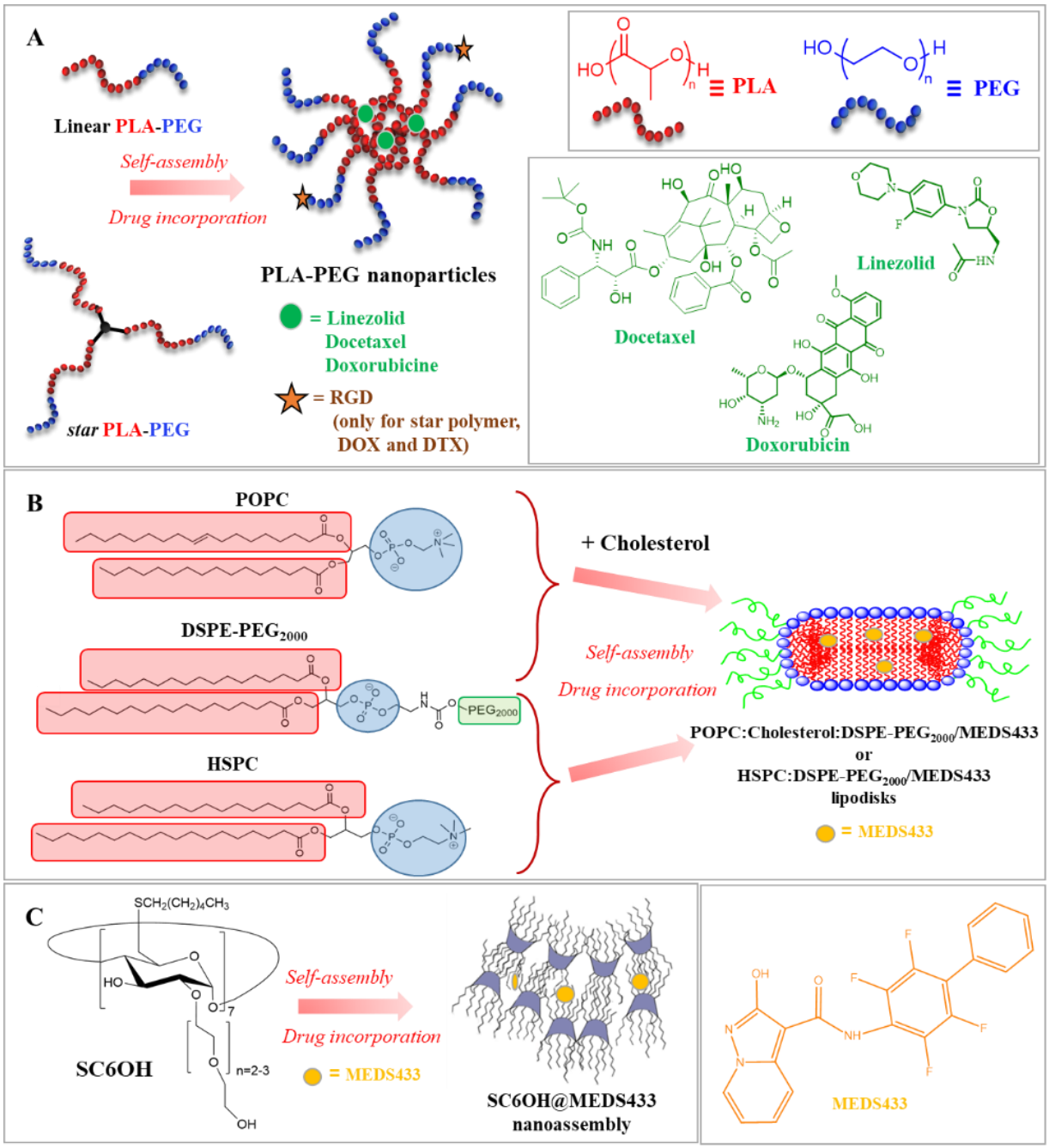

Figure 1 *Overview of nanoplatforms based on amphiphilic polymers (A), phosholipids (B) and amphiphilic cyclodextrins (C) developed within this PhD Thesis for antitumoral and antimicrobial applications*

2. Aim of the work

Over the last decades, in the nanomedical research field, the study of biomaterials has garnered significant attention due to their ability to act as carriers for drug and gene delivery, imaging and theranostics[5]. However, despite the wide range of systems proposed in literature (i.e., polymeric NPs[6,7], inorganic NPs[8,9], liposomes[10,11], nanogels[12,13], dendrimers,[14,15] etc.), only some of them turned out to be effective *in vivo* and therefore were marketed[16].

The design and optimization of a "delivery nanosystem" is crucial to achieve a specific target and application. Specifically, the modulation of size, coating and surface functionalization[17] by proper chemical modification of the starting biomaterial turns out to be essential to get a good colloidal stability, targeting abilities and therapeutic efficacy in the nanomedical field.

For these reasons, over the years, a deepening of the knowledge of the most suitable biomaterials has occurred for specific medical applications and the fine tuning of their chemico-physical and biological properties expanded to best suit their intended purpose.

During my PhD research activity, the design and development of different types of drug-loaded nanocarriers was carried out employing efficient synthetic strategies to properly functionalize the chemical structure of native biomaterials commonly used in nanomedicine (*e.g.*, PLA and PEG, phospholipids, cyclodextrins). Overall, the aim of this work was the development of chemically-tailored nanoplatforms exploiting versatile design strategies for customized antitumoral and antibacterial applications. The results reported in this thesis pointed out that a fine control over the chemical composition, molecular weight, hydrophobic: hydrophilic balance, end-functional groups can be achieved by a proper designing and optimization of all the preparation steps of a multifunctional nanoplatform, having a significant impact on the *self-*

assembly, stability, drug loading, release kinetics, and biological profile, including targeting abilities and therapeutic efficacy.

Physico-chemical characterization of such engineered multifunctional platforms was carried out by complementary techniques including ^{1}H NMR, GPC-SEC, UV/Vis, DLS, zeta potential measurements, Maldi-TOF.

The thesis is structured in four main chapters. Chapter II reports an overview on Nanomedicine and Drug Delivery focusing on biopolymers and polymeric nanoparticles, phospholipids, liposomes and lipodisks, and cyclodextrins. A special focus is devoted to star polymers and copolymers based on Polylactic Acid and Polyethylene glycol.

Chapter III deals with the Results and Discussion concerning the synthesis, physico-chemical characterization and biological investigation of both linear and star-shaped PLA-PEG copolymers; and the formulation of lipodisks and cyclodextrins for MEDS433 incorporation.

Linear and star-shaped PLA-PEG copolymers were newly synthetized by coupling and click chemistry reactions and, after proper nanoformulation, were investigated as antimicrobial and antitumoral nanomedicines, respectively. Chapter III also reports the development of drug-loaded lipodisks and cyclodextrins. Specifically, this section reports the preliminary results of the NATO research project “VIPER” about the development of water soluble MEDS433 delivery systems suitable for *in vivo* tests in SARS-CoV-2 infected animal models. These activities were carried out at the University of Uppsala -Sweden- (during my foreign 6-months abroad) under the supervision of Prof. Katarina Edwards and at the University of Messina, respectively. Specifically, the formulation, physicochemical properties and preliminary biological assays will be discussed.

3. Introduction

3.1. Nanomedicine and Drug Delivery

Nowadays, the clinical treatment of several pathological conditions is encountering more and more challenges. Whether it is to combat the insurgency or diffusion of a tumoral mass or to treat bacterial infections, several complications prevent the simple administration of a drug to constitute an efficient therapy. Although conventional chemotherapy is successful to some extent to destroy cancer cells, many drawbacks and collateral side effects make it uncomfortable or painful for the patient. Specifically, during chemotherapy, the patient is administered one or more cytotoxic compounds which are generally non-selective and therefore distributed all over the body without discriminating healthy from damaged tissues[18].

In other cases, during infectious diseases, a pathogen (*e.g.*, bacteria) may develop resistance mechanisms to the administered therapeutic agent making infection control more complex[19]. Moreover, the drug could be also metabolized, degraded and eliminated too fast, minimizing the effective drug concentration at the target tissues, leading to a reduced therapeutic effect. Therefore, one of the main challenges of modern clinical treatments consists in localizing the pharmaceutical agent in the target tissues.

To overcome all these drawbacks, scientific efforts are currently devoted to harness the power of nanotechnology in diagnosis, treatment, and prevention of contemporary (diabetes, cardiovascular diseases, neurodegenerative disorders, and cancer) and emerging diseases (including coronavirus disease 2019, COVID-19), facilitating the development of personalized medicine[20]. The concept of employing nanotechnology in biomedical and clinical research is best known as *"nanomedicine"*[21] and one of its main fields of research concerns the development of DDS, *i.e.* nanostructures of different chemical nature[18] (polymeric, lipidic, inorganic) that act as

carriers for drugs serving to enhance the selectivity, effectiveness, as well as stability of drug administration (***Figure 2***).

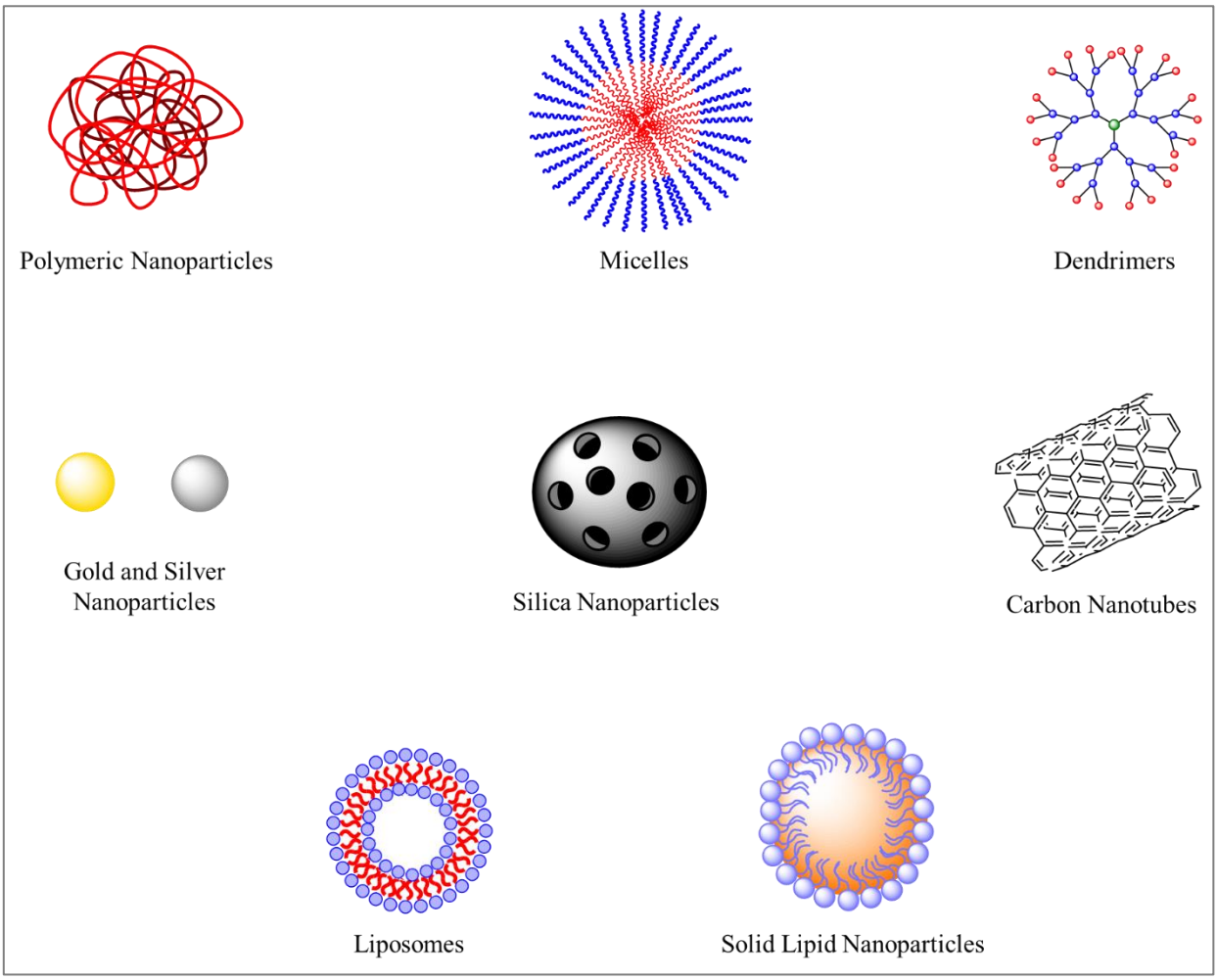

Figure 2 *Different types of Drug Delivery Systems.*

Drug nanocarriers are mainly used to[22]:

-improve solubility and bioavailability of poorly water-soluble drugs;

-improve stability and protection of the drug against degradation: the DDS may be properly functionalized with species providing *stealth* properties (*e.g.* polyethyleneglycol, PEG), making them less recognizable to the macrophages, prolonging the *in vivo* half-life of the drug;

-prevent the rapid development of resistance thanks to the reduced exposition of the drug to the human organism;

-target the damage tissue: nanosized carriers leak preferentially into tumor masses taking advantage of iper-vascularization, enhanced vascular permeability and reduced lymphatic drainage typical of cancer tissues (*"Enhanced Permeability and Retention, EPR"*). This site-specific targeting is called "*passive targeting"*. Moreover, an *active targeting* may be also achieved taking advantage of the chemical functionalization of DDS with specific ligands (folic acid, peptides, aptamers, etc.) recognized by cellular membrane proteins overexpressed on pathological cells, allowing for a selective intracellular uptake and a reduced toxicity;

-control the release: the drug incorporated into a DDS is generally released with a slow, controlled and sustained profile over an extended period of time allowing to reduce the frequency of administration, improving patience compliance and to prolong the therapeutic action.

An ideal DDS must be safe for the human health, therefore the choice of the starting materials for the nanoformulation of the carrier is crucial for the success of a DDS. Ideal building blocks for this purpose own two main features: biocompatibility and biodegradability that are, respectively, the ability of the material to execute its function in a biological host without causing harm and the ability to be degraded without generating any harmful byproduct[23].

3.2. Biopolymers and Polymeric Nanoparticles

Biopolymers are a leading class of functional materials attracting growing interest as an alternative to petroleum-derived plastics due to the more economic production, the lower carbon footprint and renewability. The variety of existing biopolymers with different properties allows to choose the most suitable for a wide array of applications including packaging, paints, films and foams production, biomedical, prosthetics[24].

Naturally derived polymers such as alginate, xanthan gum, chitin and chitosan, gelatin, collagen, hyaluronan, etc. have great potential in the biomedical field.

Alginates and xanthan gum can be extracted from biological sources, *i.e.* respectively from *algae* and *Xanthomonas campestris* bacterial strain[25]. Alginates exist as linear homo or heteropolymeric chains of β-D-mannuronic acid and α-L-guluronic acid linked by (1-4)-glycosidic bonds and their physical characteristics depend on the order in which these units are arranged; xanthan gum is composed of β-D-(1,4)-glucose backbone with a β-D-(1, 4)-glucuronic acid linked to β-D-(1,2)-mannose unit. Both polymers are used in drug delivery thanks to their biocompatibility and versatility: alginates have been formulated in several types of DDS, incorporating bioactive molecules, peptides, proteins and enzymes[26]; xanthan gum undergoes synthetic modification enabling it to form hydrogel for the incorporation of both small bioactive compounds and proteins for oral and parenteral administration[27].

Chitosan is a bio-based polymer composed of N-acetyl-D-glucosamine and β-1-4-D-glucosamine produced by chemical or biological treatment (demineralization, deproteinization and deacetylation) of the chitin extracted from chitinous materials such as crustacean's and insect's shells. Chitosan has been widely used as carrier for the controlled release of bioactive molecules taking advantage of the ability to form a polycationic charged molecule at physiological pH due to the protonation of D-glucosamine. This property bestows to the material targeting ability allowing the selective release of the payload in tissues characterized by low pH values, as in the case of cancerous cells[28].

Collagen is extracted from various animal sources and it's constituted by three, supercoiled polypeptide chains with a glycine unit at every third position oriented towards the axis of the helix, while the remaining peptides are oriented outside and are available for intermolecular and solvent interaction. Collagen is overexpressed in several pathological tissues, including cancer representing a drug targeting site[29]; moreover, its biocompatibility and biodegradability have prompted also the development of collagen-based DDS[30]. For example, a liposomal carrier decorated with a collagen peptide has been loaded with doxorubicin and has been employed in the treatment of a variety of tumor cells overexpressing the CD44 receptor, responsible for the recognition of the collagen moiety and the uptake of the carrier[31]. However, while collagen-based nano-carriers have proven efficient in sustaining drug delivery, they own some drawbacks, since collagen is not readily dispersed in water and may cause antigenicity. By collagen degradation (acid o basic hydrolysis or thermal and enzymatic degradation), gelatin is obtained, a hydrosoluble, biocompatible polymer that can be formulated in porous microspheres using several procedures (emulsion, nanoprecipitation, electrospraying, etc.) and successfully employed as carrier for drugs with different therapeutic actions[32]. Antibacterial vancomycin has been successfully loaded on gelatin microspheres releasing the payload in the target tissues and maintaining good activity[33]; paclitaxel-loaded gelatin carriers have been employed in the treatment of ovarian cancer microscopical carcinomatosis, reducing the mass of tumoral growth and increasing survival time[34].

Hyaluronan is a polymer naturally found in human vitreous humour, joints, connective tissue, umbilical cord, and skin, composed of repeating units of glucuronic acid and N-acetyl-D-glucosamine linked by β-(1-4) glycosidic bonds. It's involved in several biological processes requiring its recognition by different receptors and proteins overexpressed in unhealthy cells; this property and its inherent biocompatibility have made hyaluronan an ideal biomaterial for the formulation of targeted DDS[35].

Furthermore, poly(lactic acid) (PLA), poly(glycolic acid) (PGA), poly(lactic-co-glycolic acid) (PLGA), poly(hydroxy alkanoates) (PHA), poly(ε-caprolactone) (PCL) are synthetic biopolymers widely employed as tunable biomaterials for DDS preparation[36,37,38,39]. They are polyesters that can be naturally degraded by enzymatic or non-enzymatic processes producing biocompatible and not-toxic byproducts, which are eliminated by the normal metabolic pathways. They are easily absorbable, exhibit favorable physico-chemical properties and are approved by both Food and Drug Administration (FDA) and European Medicines Agency (EMA) for application in pharmaceutical and medicinal fields.

3.2.1. Polylactic Acid and Polyethylene glycol

Poly(lactic acid) (PLA) is a polyester obtained by condensation of lactic acid (***Figure 3***).

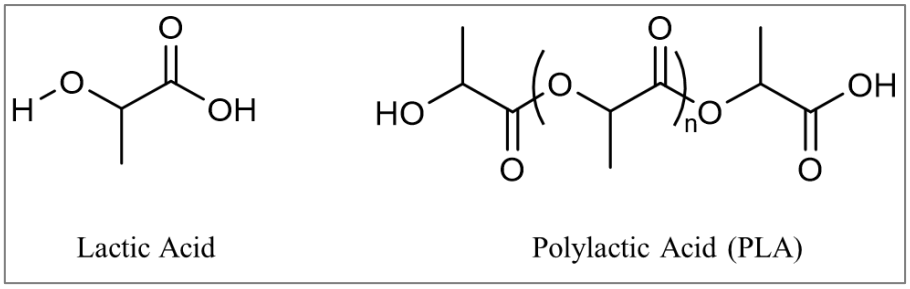

Figure 3 *Lactic acid monomer and PLA polymer structures.*

The lactic acid monomer can be obtained by a synthetic reaction (***Figure 4***) between acetonitrile and hydrogen cyanide, even though fermentation of carbohydrates is the more convenient method allowing to selectively obtain the L- or D- enantiomer by choosing the appropriate bacterial culture.

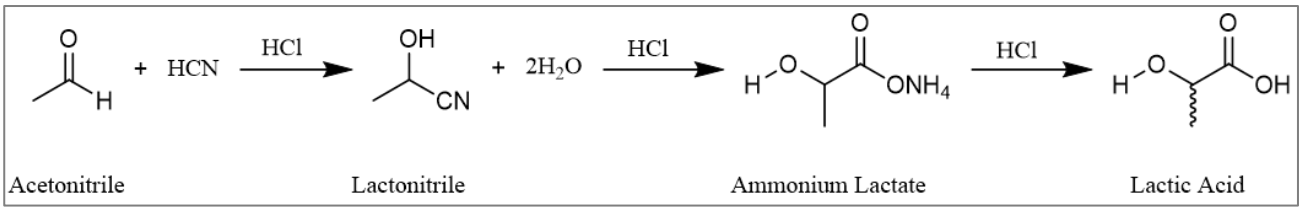

Figure 4 *Synthesis of lactic acid monomer.*

The first synthetic procedure of PLA was the polycondensation of several units of lactic acid, forming ester bonds between the hydroxyl group of one unit and the carboxylic group of a second unit. Over time, however, this procedure has been replaced by other chemical processes due to its inherent disadvantages: the water byproduct must be removed from the reaction mixture operating at high temperatures and low pressure to favor the formation of the polymer. Furthermore, in longer polymeric chains, the *back-biting* phenomenon may occur consisting of the intramolecular reaction of the terminal hydroxyl group with an intra-chain ester bond that reduces the average length of the polymer chain (***Figure 5***).

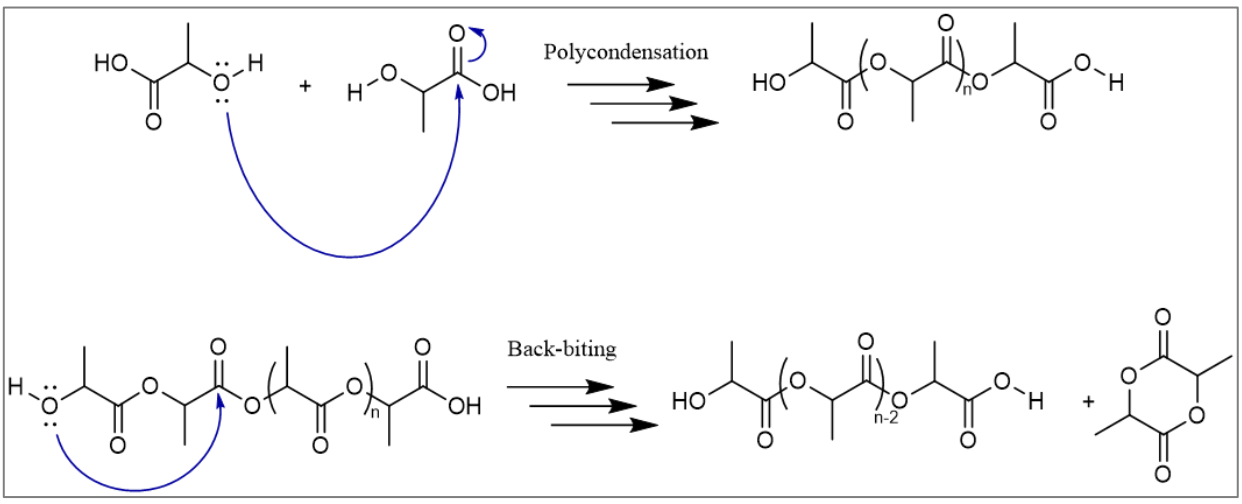

Figure 5 *Polycondensation of monomeric lactic acid and back-biting phenomenon.*

Azeotropic polymerization may be employed to eliminate the water as the polymer is being formed. For this procedure higher temperatures are required together with stabilizers against polymer degradation that need to be separated from the final product. Alternatively, oligomers of lactic acid may be brought up to high temperature

to favor a solvent-free condensation leading to longer polymeric chains. Unfortunately, prolonged reaction times and high energy expenses are needed for these procedures.

The most used and efficient way to produce PLA is the *Ring Opening Polymerization (ROP)* in which the cyclic dimer of the lactic acid, the *lactide*, is opened by an initiator generating an activated linear dimer ready to react with another unit of lactide in a second ROP and the reaction proceeds until a quencher is added. The great advantages of this process are the direct control over the polymerization and the mild reaction conditions not requiring high energy; moreover, the condensation of dimers does not generate water that needs to be removed, the back-biting transesterification is kept low and a low dispersity is achieved.

The ROP procedure can be carried out in different reaction conditions (***Figure 6***): in the cationic ROP, the lactide is protonated by an acid, making it more susceptible to the nucleophilic attack from the initiator. In the anionic ROP, it's the deprotonation of the initiator itself that improves its nucleophilic character, allowing the ring opening of the lactide[40].

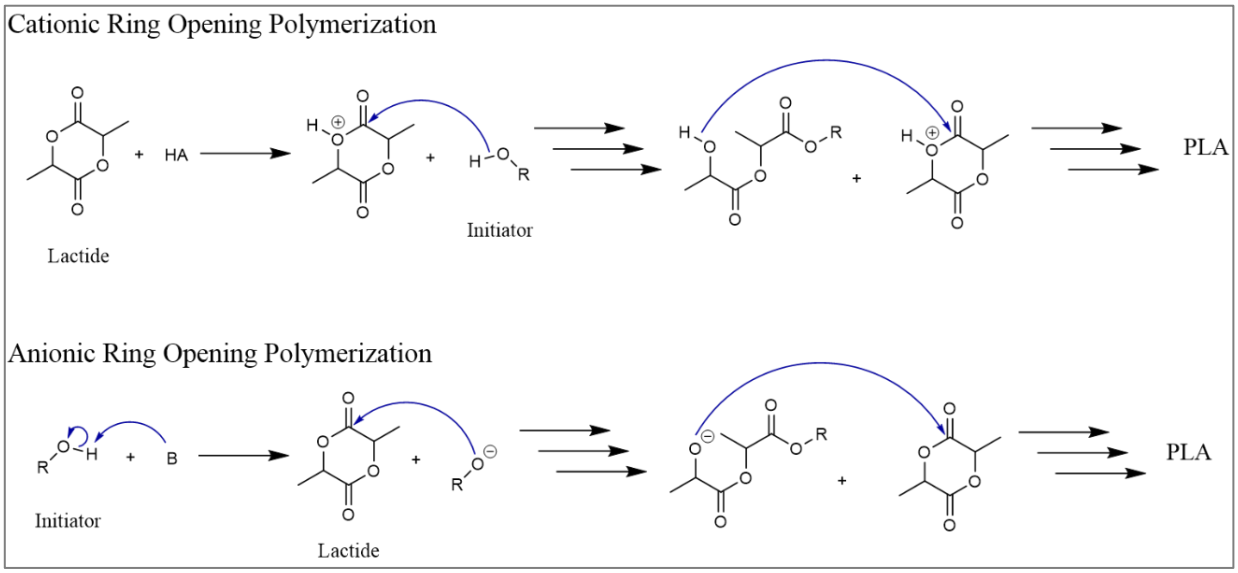

Figure 6 *Cationic and anionic mechanisms of Ring Opening Polymerization for lactide.*

PLA is widely used for several biomedical purposes (*e.g.*, gene and drug delivery, tissue engineering, medical implants and scaffolds) including the formulation of

nanocarriers taking advantage of the ability of polymer chains to *self-assemble* into polymeric nanoparticles (NPs). Moreover, in the presence of a drug to be incorporated, a DDS is generated[41]. While the PLA lipophilicity mainly favors the loading of hydrophobic drugs, its low water-solubility requires the covalent conjugation with hydrophilic species to obtain an amphiphilic copolymer able to self-assemble in water into NPs or micelles with different morphology consisting of a hydrophobic core and a hydrophilic shell. The self-assembly is a self-organizing process driven by non-covalent interactions, including hydrophobic, van der Waals, π–π, electrostatic, hydrogen bonding, etc. (***Figure 7***).

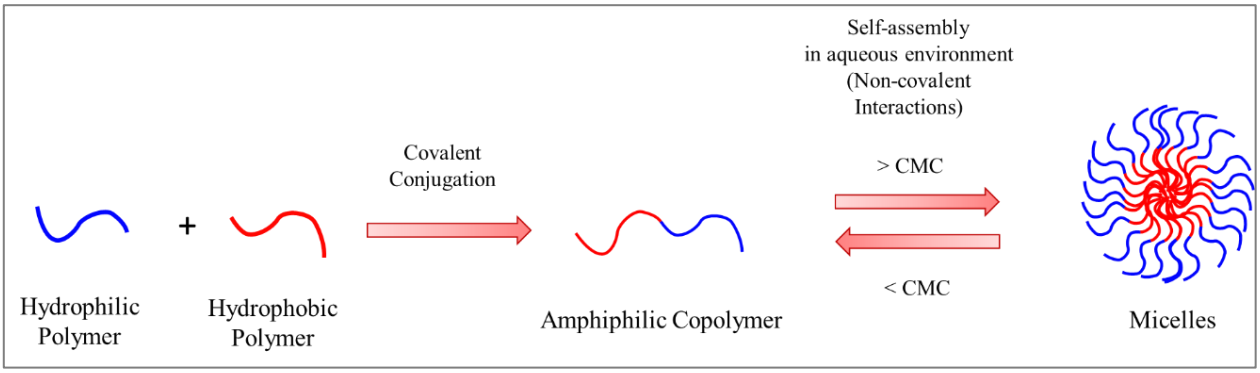

Figure 7 *Self-assembly of amphiphilic copolymers (i.e. PLA-PEG) in aqueous environment.*

One of the most used hydrophilic polymers in nanomedicine is the polyethylene glycol (PEG)[42] obtained by polymerization of ethylene glycol units (***Figure 8***). The conjugation of PEG to another entity (*e.g.*, nanoparticle or hydrophobic polymer) is generally called *PEGylation.* This approach not only impart *"stealth"* properties but also modulates and improves the pharmacokinetic and pharmacodynamic profile of the final species[43]. PEGylation has become a mainstay in DDS formulation since it improves solubility, reduces toxicity and immunogenicity, increases stability and protection against degradation, extends blood circulation time and, consequently, bioavailability and biological activity. Moreover, PEGylation confers *stealth properties*, since the presence of PEG at the NPs surface produces a hydrated cloud that reduces the interaction with blood components and other NPs and the recognition

by the mononuclear phagocytic system, avoiding their capture by macrophages and thereby increasing *in vivo* half-life. Moreover, the hydrated PEG shell on NPs surface prevents aspecific absorption and aggregation of plasma or intracellular fluids proteins on NPs surface leading to the formation of the so-called *protein corona* that can unpredictably modify NPs outcomes including uptake, biodistribution, biological function and toxicity[44].

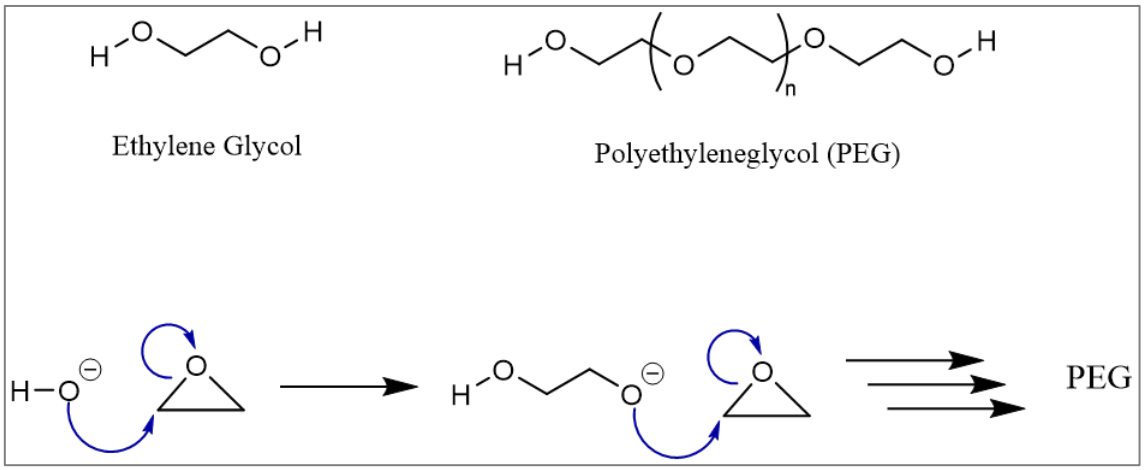

Figure 8 *Ethylene glycol monomer and PEG polymer structures (up). Polyethyleneglycol (PEG) obtained by polymerization of ethylene oxide (down).*

The effect of molecular weight (MW) and coverage density of PEG on NPs surface have been widely studied pointing out that PEG with relatively low MW (2-5 kDa) is preferable for nanomedical purposes. Specifically, oligomers with MW below 400 Da are toxic for humans as result of the oxidation into diacid and hydroxy acid metabolites by aldehyde and alcohol dehydrogenase; this degradation significantly decreases with increasing molar mass. On the other hand, the MW of PEG should not exceed the renal clearance threshold to allow its complete excretion. Specifically, PEG with a MW below 20 kDa is easily secreted in the urine, while the clearance through the liver becomes predominant for PEG with higher molar mass and the renal elimination rather slow. [45]

Another advantage offered by *PEGylation* is represented by the versatility of PEG chemistry since PEG can be functionalized with several types of terminal groups[46]

(***Figure 9***) allowing the covalent grafting of different ligands, including fluorescent probes and/or targeting moieties by classical coupling methods (NHS/amine, maleimide/sulfhydryl, etc.) or click chemistry reactions[47].

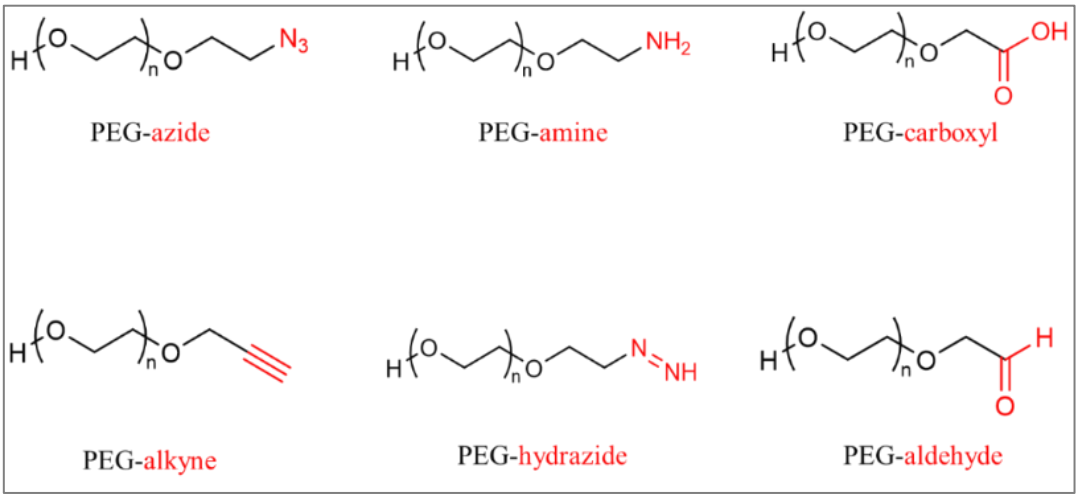

Figure 9 *Some representative terminal functional groups (red) enabling covalent conjugation of PEG with other species.*

Overall, PEG is the most frequently employed hydrophilic component of amphiphilic copolymers; however, hyaluronic acid (HA) and polyethylenimine (PEI) (***Figure 10***) represent valid alternatives for DDS preparation.

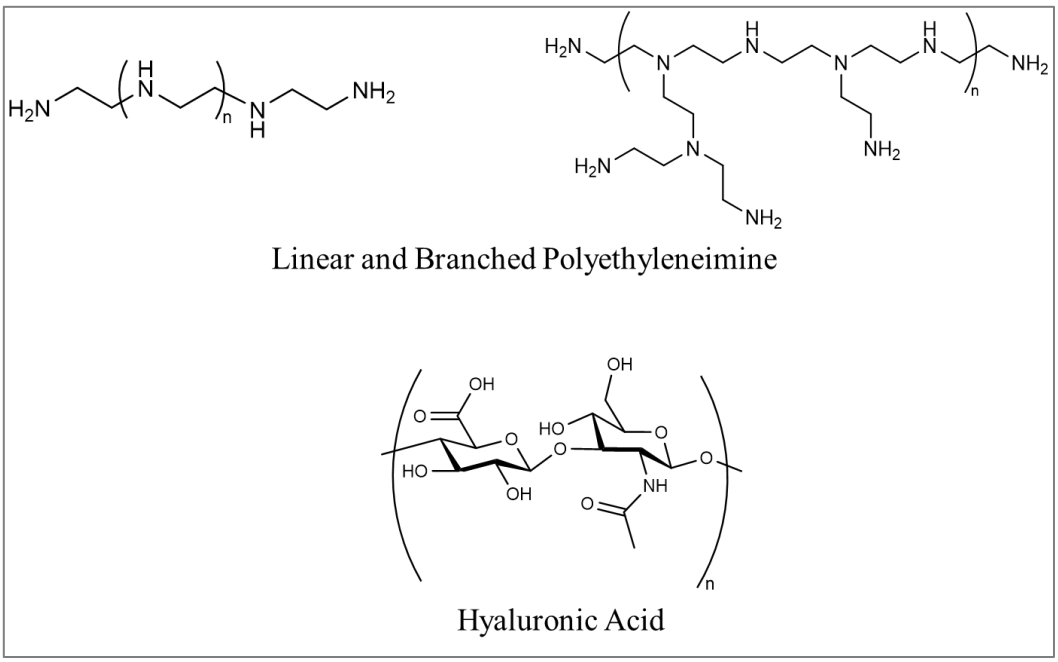

Figure 10 *Chemical structures of hyaluronic acid and polyethyleneimine.*

In the framework of nanomedicine, the advantage of HA compared to PEG consists of its targeting capability given its recognition by CD44 membrane receptors that are overexpressed in cancer cells[48].

PEI is a synthetic polymer, linear or branched, whose structure is characterized by the presence of amine functional groups that turned out to be useful for successful gene delivery involving electrostatic interactions between negatively charged nucleic acid phosphate groups and polycationic PEI[49,50].

Regardless of the composition, amphiphilic polymers can all be formulated into NPs following different methods and, during self-assembly, they can incorporate drugs or other bioactive molecules. Such nanoformulation methods include nanoprecipitation, emulsion-diffusion, emulsion-evaporation, salting out and dialysis and each of them offers its own advantages and disadvantages[51]:

-in the *nanoprecipitation* method, a solution of polymer and drug in a volatile organic solvent is added dropwise to stirring water. As the organic solvent is displaced by the aqueous solvent and evaporates, the *self-assembly* of the polymeric chains is prompted and the NPs incorporate the drug as they form. This procedure is easily carried out without particularly expensive requirements; however, it is not indicated for the incorporation of hydrophilic drugs. Furthermore, the NPs may be obtained with high dispersity of size depending on the intensity of the stirring.

-in the *emulsion* method, an organic solution of polymer and drug is added dropwise to stirring water containing a stabilizing agent that favors the formation of an *o/w* emulsion. As the organic solvent evaporates or diffuses to the volume of water, the NPs are obtained as an aqueous suspension. Emulsion methods can be adapted to incorporate both lipophilic and hydrophilic drugs and, generally, NPs with low size dispersity are obtained.

-in the *salting-out* method, an organic solution of polymer and drug is poured into an aqueous solution containing both stabilizer and a salting-out agent. The solution is gradually diluted with water to favor the diffusion of the organic solvent in the aqueous environment prompting the polymer *self-assembly*. This procedure allows a fine control of the physical features of NPs by choosing the appropriate stabilizers and salting-out agents but requires thorough purification of the NPs suspension to eliminate the presence of salts.

-in the *dialysis* method, a solution of polymer and drug in a non-volatile organic solvent (*i.e.*, DMSO, DMF) is added dropwise to stirring water. The displacement of the organic solvent prompts the *self-assembly* of polymers into NPs incorporating the drug. The solution is transferred into a dialysis bag and put into a high volume of water. The porosity of the bag allows the organic solvent to filter out together with unloaded drug, while retaining the purified suspension of NPs.

The *self-assembly* ability of amphiphilic copolymers is a remarkable property that allows not only their nanoformulation and drug incorporation but also ensure, in principle, stability of the NPs in the biological environment. However, local environment changes including serum absorption, ionic strength variation and high dilution could have a profound impact on NPs since their *core-shell* structure is based on non-covalent interactions. Therefore, polymeric NPs might disaggregate upon dilution in physiological fluids at concentrations below the Critical Micellar Concentration (CMC) causing a burst release of the drug (***Figure 11***).

CMC value represents the concentration of amphiphilic molecules (*i.e.*, PLA-PEG copolymers) at which both the solvent-air interface and the bulk of the solution are saturated and it is defined as the lowest concentration of polymer required to form micelles. Every raise of concentration from this value causes the *self-assembly* into micellar structures, any further dilution causes the micellar disassembly[52], therefore below the CMC all the amphiphilic molecules exist only as monomers.

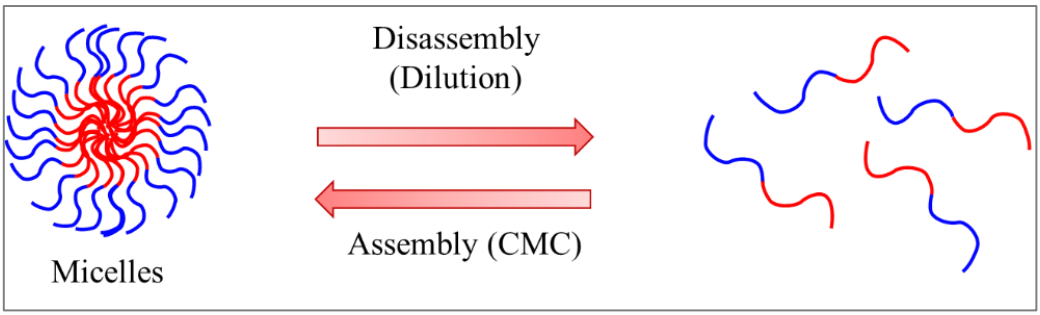

Figure 11 *Conventional polymeric micelles obtained from linear amphiphilic copolymers (i.e. PLA-PEG) disassemble in high dilution conditions.*

Several methodologies can be used for CMC determination and they all rely on the detection of the change of a property of the sample depending on the formation of micelles. For example, the light scattered from amphiphilic polymer solutions at increasing concentration may be detected and its steep increase in intensity identifies the CMC; alternatively, the spectral properties (fluorescence and absorbance) of a lipophilic probe (*i.e.* pyrene) may be used for CMC determination since they are affected by micellization due to variation of the chemical environment[44].

3.2.2. Star polymers

The instability of conventional polymeric micelles formed by linear amphiphiles prompts the development of alternative DDS able to avoid uncontrolled drug release and to ensure a satisfactory thermodynamic as well as kinetic stability. With this purpose, amphiphilic copolymers with a more complex branched structure, called *"star polymers"* consisting of several polymeric linear arms covalently linked to a *core* have been synthetized[53]. Micelles formed by self-assembly of star copolymers exhibit an excellent *in vivo* stability due to their covalently reinforced core-shell globular structure that prevents disassembly upon dilution (***Figure 12***) respect to conventional micelles obtained by their linear counterparts.

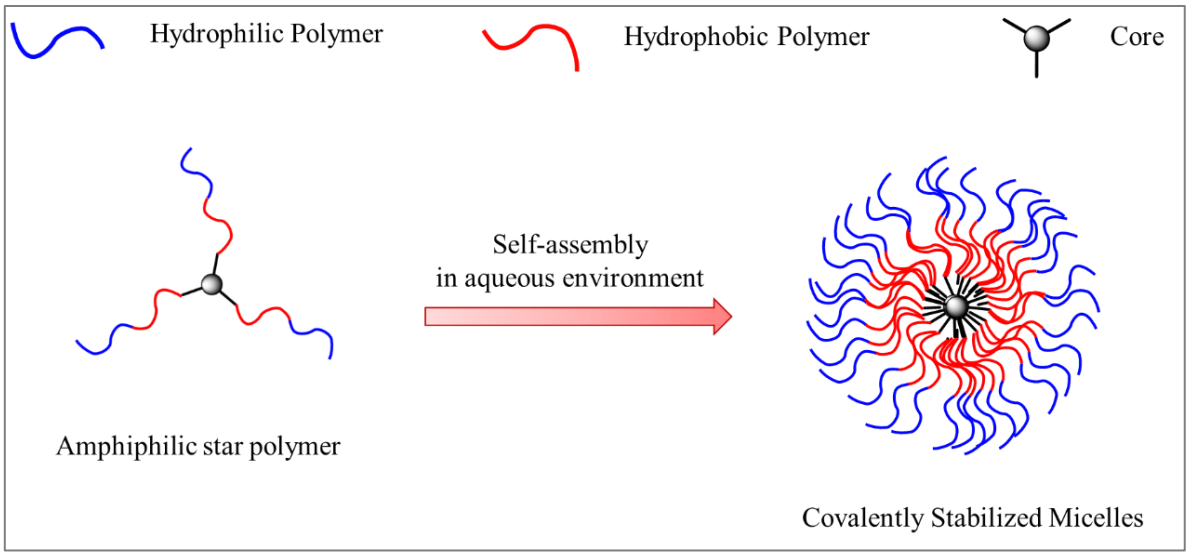

Figure 12 *Covalent bonds between amphiphilic polymers reinforce the micellar aggregate at higher dilutions.*

The synthetic approaches for the preparation of star polymers include the *core-first* and the *arms-first* processes (***Figure 13***). In the core-first approach, a pre-synthesized multifunctional initiator (*i.e.*, the core) is used to produce star polymers by divergently growing linear polymers (*i.e.*, the arms). To obtain star polymers with well-defined structures (*i.e.*, the same arm number and arm length), the initiating sites of the core should have equal reactivity and 100% initiation efficiency. Many polymerization techniques satisfy these requirements allowing to obtain different star polymers with high yields, as the final polymeric product may be easily separated from the small molecule initiators.

The arms-first approach produces star polymers by crosslinking linear polymers via a polymerization or coupling reaction in a convergent way. In this approach, the synthesis of linear polymers is performed in a separate step, ensuring a great control over the length of the arms and the linear polymers may be fully characterized before the coupling to the core.

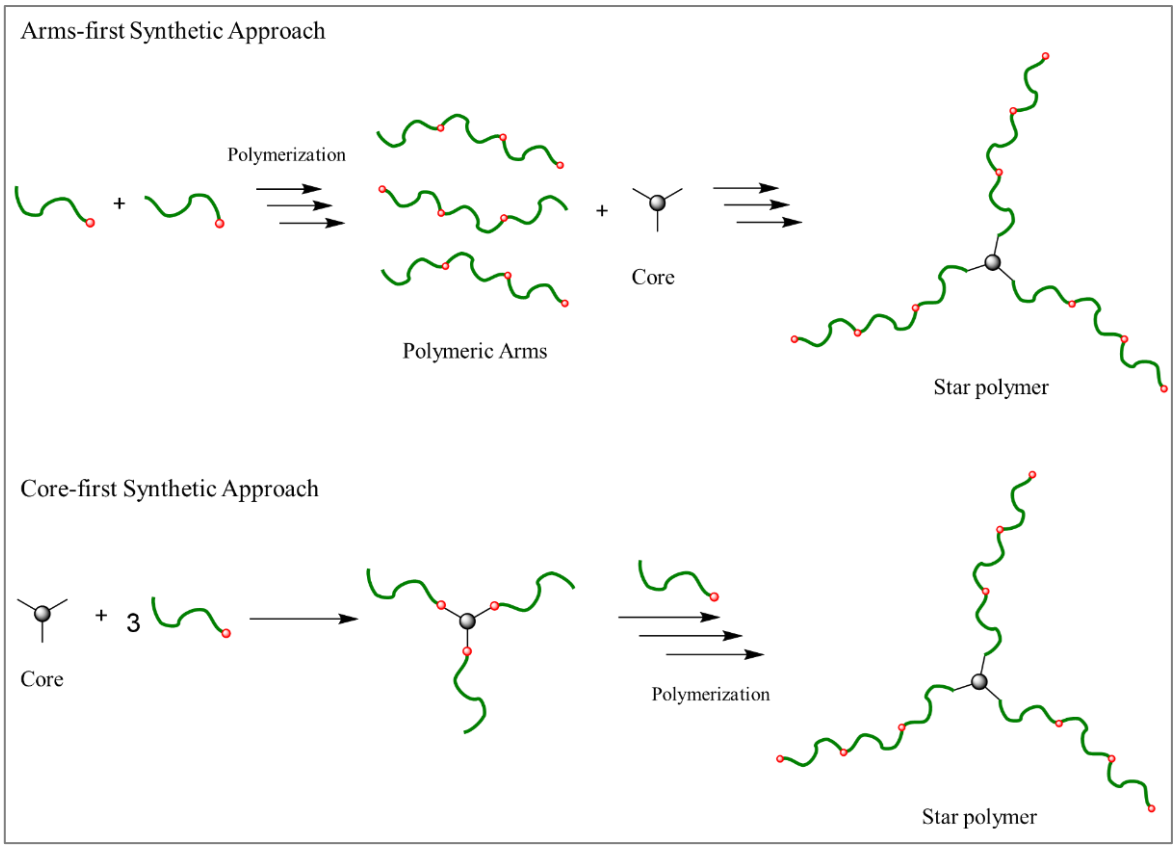

Figure 13 *Different approaches for the synthesis of star polymers.*

The choice of the synthetic route may also depend on the desired star polymer. *Homo-arms* star polymers, possessing arms identical in chemical composition and length, can be obtained by both core-first and arms-first approach. Mikto-arms star polymers, owning arms differing for length, composition or terminal groups, are more easily obtained by arms-first approach (***Figure 14***)[54].

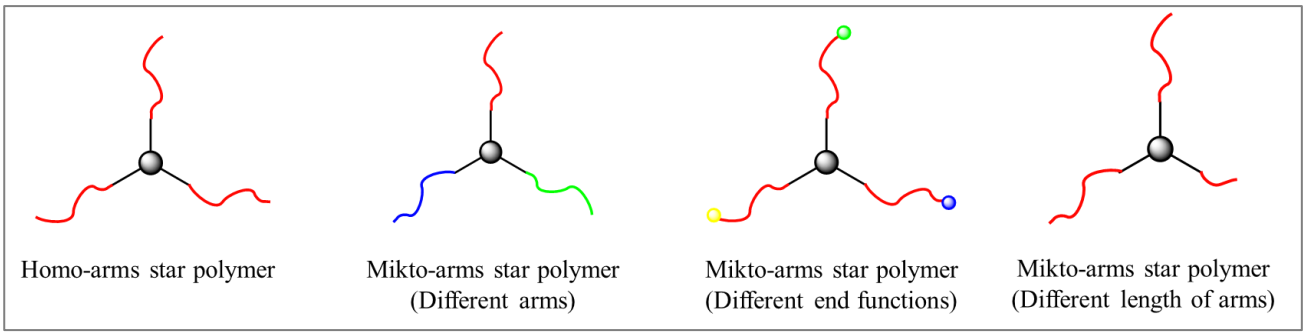

Figure 14 *Homo-arms star polymers have identical branches. Mikto-arms star polymers may have different branches in terms of chemical nature, eng-functionalities or length.*

Alternatively, for the synthesis of mikto-arms star polymers, a combination of the two procedures may be employed, called *in-out* approach (***Figure 15***): in an initial arms-first process, polymers may be directly linked to some functional groups of the core; in the successive step, other core functionalities are involved allowing the grow of other polymer chains[55].

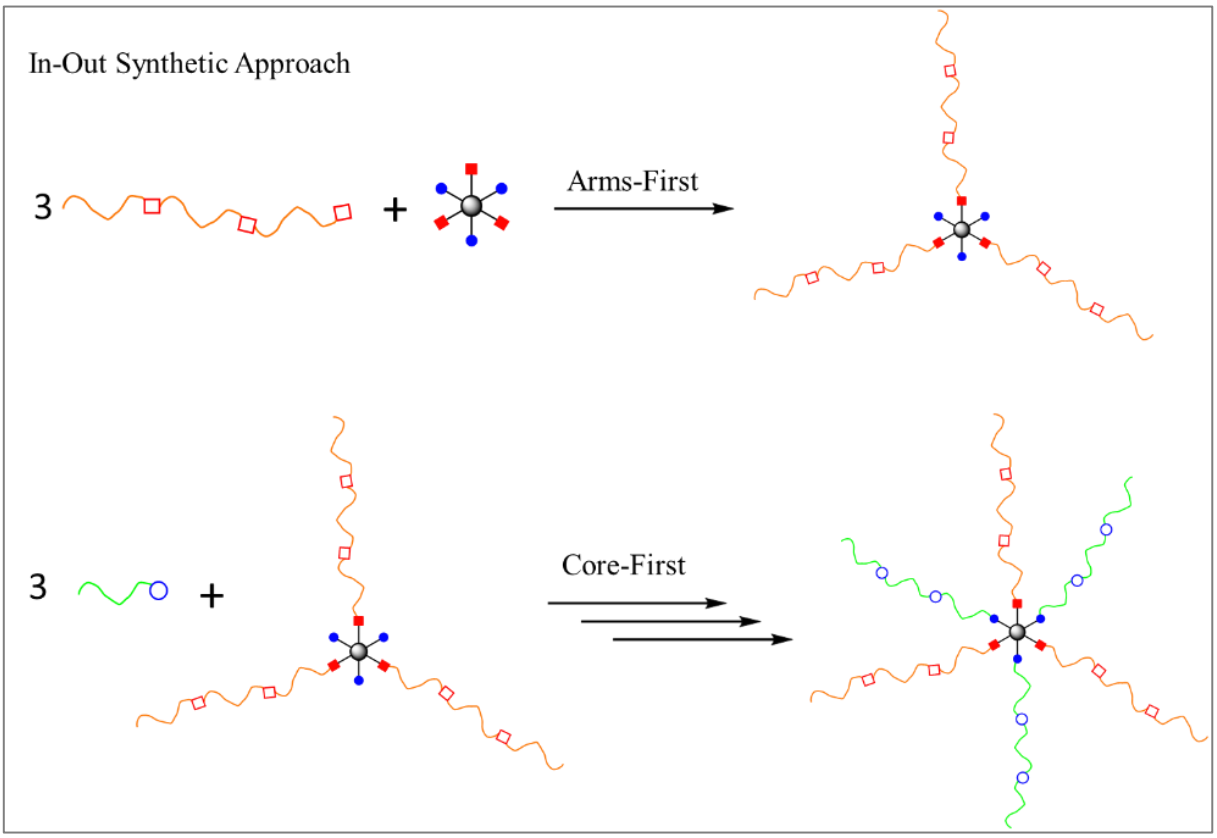

Figure 15 *The "In-Out" synthetic approach consists of an initial arms-first step and a successive core-first procedure.*

The advantages of amphiphilic star polymers respect to their linear counterparts are not limited to the higher stability of the DDS they self-assemble into. Star polymers own a higher number of end-groups and peripheral functionalities suitable for chemical functionalization, including the decoration with targeting ligands or fluorescent probes, allowing a fine tuning of the final properties of the nanocarrier[1].

Various morphologies such as micelles, vesicles, NPs can be obtained as supramolecular nanostructures derived by self-assembly of amphiphiles[56] and, among them, spherical micelles are the most prevalent structure. They can be classified as

“small simple” (< 30 nm) and “large complex” (> 30–50 nm) micelles depending on the arms number, block length and polymeric chain architecture.

The multimicelle aggregate mechanism (MMA) has been proposed to explain the formation of large complex micelles from amphiphilic star copolymers, involving a multi-step aggregation process of small micelles associated by inter-micellar interactions such as hydrogen bonds[57]. Unimolecular micelles (UMs) or multimolecular micellar aggregates (MMAs) may be formed by self-assembly of star polymers. Generally, UMs are observable at low concentration of amphiphilic star polymers in aqueous solution, when no aggregation of the single entities occurs; whereas they form MMAs with unique nanostructure at high concentration. Different MMAs can be formed depending on their mechanism of aggregation (***Figure 16***). In one case, the hydrophilic shells of single UMs are subject to sufficient interactive force to aggregate and form Unimolecular Micelle Aggregates (UMAs) in which the UMs forming the bigger aggregate are still recognizable as distinct micellar structures, each with their respective cores and shells. In the other, the high incompatibility between the lipophilic and hydrophilic component of a single UM induces a phases separation arranging the whole structure in a cone-like shape. Separate cones will aggregate, bringing together the lipophilic domain to form the core of a *microphase-separated small micelle*, while the hydrophilic domains form the shell. Such micelles will be further able to form Small Micelle Aggregates (SMAs) (***Figure 16***).

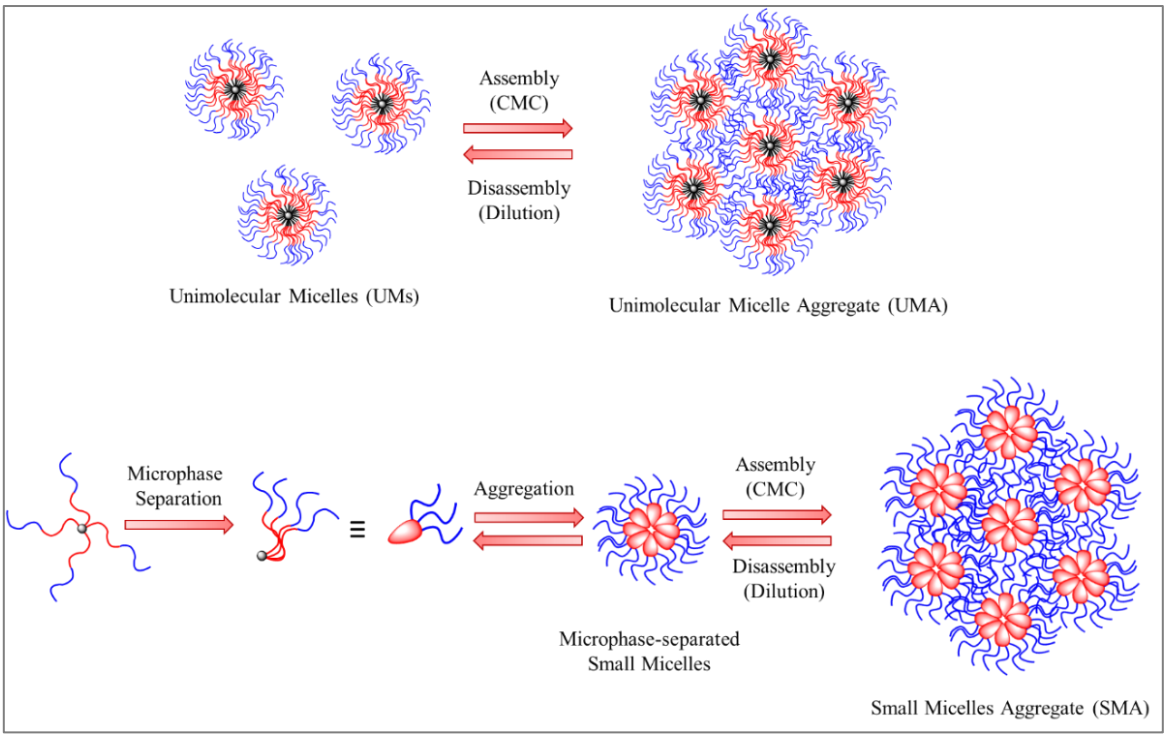

Figure 16 *Mechanism of micellar aggregation.*

3.3. Phospholipids, Liposomes and Lipodisks

Liposomes are the first nanomedicine translated into clinical use. Specifically, the first clinically approved and commercialized nanomedicine was Doxil® (1995), a PEGylated liposomal doxorubicin formulation[58]. Currently, liposomes are widely used in nanomedicine for delivery of drugs, genes and for vaccines[59]. It is noteworthy that the nanotechnology based on the use of lipid NPs and liposomes has been recently exploited for producing mRNA vaccines *Moderna's Spikevax* (mRNA-1273) and *Pfizer/BioNTech's Comirnaty* (BNT162b2) against Covid-19. Interestingly, AFM, DLS and TEM characterizations of *Comirnaty* vaccine has revealed close morphological similarity (similar size and envelope lipid composition) with Doxil®[60].

Overall, liposomes are the most successful nanomedicines accounting for over 60% of the marketed nanoproducts due to the high drug-loading capacity compared to

other nanocarriers, safety and ability to protect the drug from degradation. These are three essential requirements for clinical translation of nanomedicines[16].

Liposomes are spherical vesicles characterized by a bilayer of lipids enclosing an internal aqueous cavity. They are mainly composed by synthetic and/or natural phospholipids, therefore inherently holding the essential requirements of biocompatibility and biodegradability. Phospholipids are constituted by two fatty acids and a phosphate group esterified to the three hydroxyl groups of glycerol. The fatty acids are the hydrophobic tails and the phosphate group represents the hydrophilic head; this amphiphilic nature bestows to phospholipids *self-assembly* properties enabling them to form the typical spherical bilayer of the liposomes[61] (***Figure 17***). Structurally, they resemble the lipid membrane of living cells, but liposomes have a spherical structure formed when phospholipids in aqueous environment orient the lipophilic tails towards the inside of a bilayer and the polar heads towards the outside and the core of the structure.

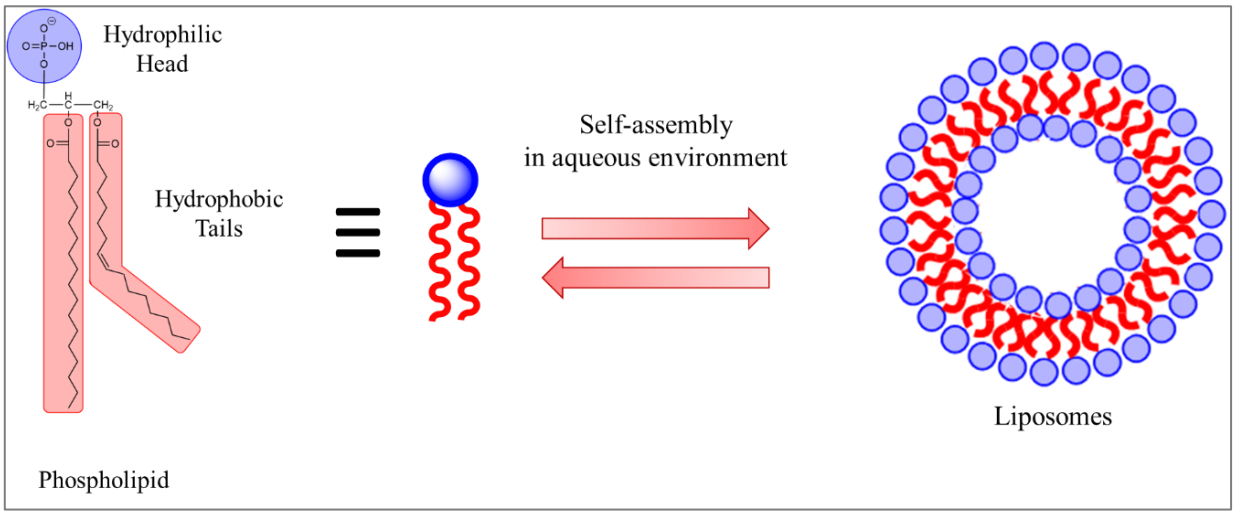

Figure 17 *Phospholipids self-assemble into liposomes in aqueous environment.*

This architecture turns out to be ideal for incorporating both hydrophobic and hydrophilic bioactive compounds as the former can be incorporated in the lipophilic bilayer and the latter in the hydrophilic core. Thus, liposomes are powerful DDS able

to improve drug solubility and stability in biological environment, reduce toxicity, and extend the blood circulation time improving drug bioavailability.

Different phospholipids – natural or synthetic – can be formulated into liposomes with different properties and applications, based on their composition (***Figure 18***). Conventional liposomes, typically formed by natural phospholipids, were the first investigated nanocarriers including cholesterol in the formulation as it was demonstrated to improve integrity of the bilayer, at the same time reducing leakage of loaded drug and increasing *in vivo* stability[62]. However, fast clearance, tissue adhesion or aggregation of liposomes still drastically reduced their permanence in biological environment, therefore the association of hydrophilic species to the liposomes has been established as a mean to further enhance steric stability[63]. *PEGylatio*n is reported to provide phospholipids with a hydrosoluble shell preventing aggregation and bestowing *stealth* properties[64]; however also glycoproteins[65], polysaccharides[66] or other synthetic hydrophilic polymers[67] have been conjugated to liposomal structures to grant enhanced steric protection.

Furthermore, targeted liposomes can be produced with the inclusion of specific moieties in the structure allowing broad spectrum of activity against several pathologies. Studies performed on liposomes decorated with different fatty acids (oleate, linoleate, linoleate) have confirmed an increased permeability into lipophilic environment such as skin compared to the undecorated carrier, granting at the same time a higher stability and longevity of the whole system[68].

The decoration of liposomes with folic acid granted a heightened uptake of the carriers into macrophages by folate receptor, allowing a selective and prolonged release of the incorporated genistein, an anti-inflammatory agent[69].

Oligopeptides have been also included in liposomes and a systematic study of the effects exerted by increasing amounts of glutamic hexapeptide on the performance against bone tissues diseases was recently reported[70]. Specifically, it was observed *in vitro* that the highest quantity of included oligopeptide favored recognition and elimination of liposomes by macrophages, while *in vivo* this effect is counterbalanced

due to the dramatic increase in permeation of bone tissues granted by the high affinity of the oligopeptide to hydroxyapatite, overall improving the performance of the decorated DDS.

Also aptamers have been formulated alongside phospholipids to obtain targeted liposomes for selective cellular uptake, as in the case of liposomal DDS decorated with the aptamer AS1411 which, compared to undecorated liposomes, manifested an improved internalization into breast cancer cells *via* specific membrane receptors[71].

Furthermore, several examples of stimuli-responsive liposomes can be found in literature in which the release of the payload is triggered by changes of physical and/or chemical conditions of pathological tissues, including temperature, light, or pH[72]. More recently, also the interest in enzyme-responsive liposomes has grown[73]. Taking advantage of the highly selective and efficient enzymatic activity, chemical bonds and/or linkers (i.e., enzyme-sensitive groups including esters, phosphate, β-galactose groups) appropriately included in the liposomal structure may be selectively hydrolyzed inside target cells, compromising the structural integrity of the carrier and promoting the payload release[74].

The latest generation of liposomes are ionic, allowing the efficient inclusion of nucleic acids or oligonucleotides *via* electrostatic interactions[75]. They own good stability due to the same-charge repulsion that prevents liposome aggregation. Cationic liposomes are able to cross the blood-brain barrier (BBB) via receptor- or absorptive-mediated transcytosis. *In vivo* delivery of plasmid β-galactosidase has been recently achieved using cationic liposomes composed of phospholipids DOPE, DOTAP and DSPE–PEG_{2000} (1,2-dioleoyl-sn-glycero-3-phosphoethanolamine, 1,2-dioleoyl-3-trimethylammonium propane, 1,2-distearoyl-sn-glycero-3-phosphoethanolamine-Polyethylene glycol) and decorated with ligands (*i.e.*, PEG for stability, transferrin as targeting ligand and Cell-Penetrating Peptides to enhance membrane penetration) to optimize their biological performances[75].

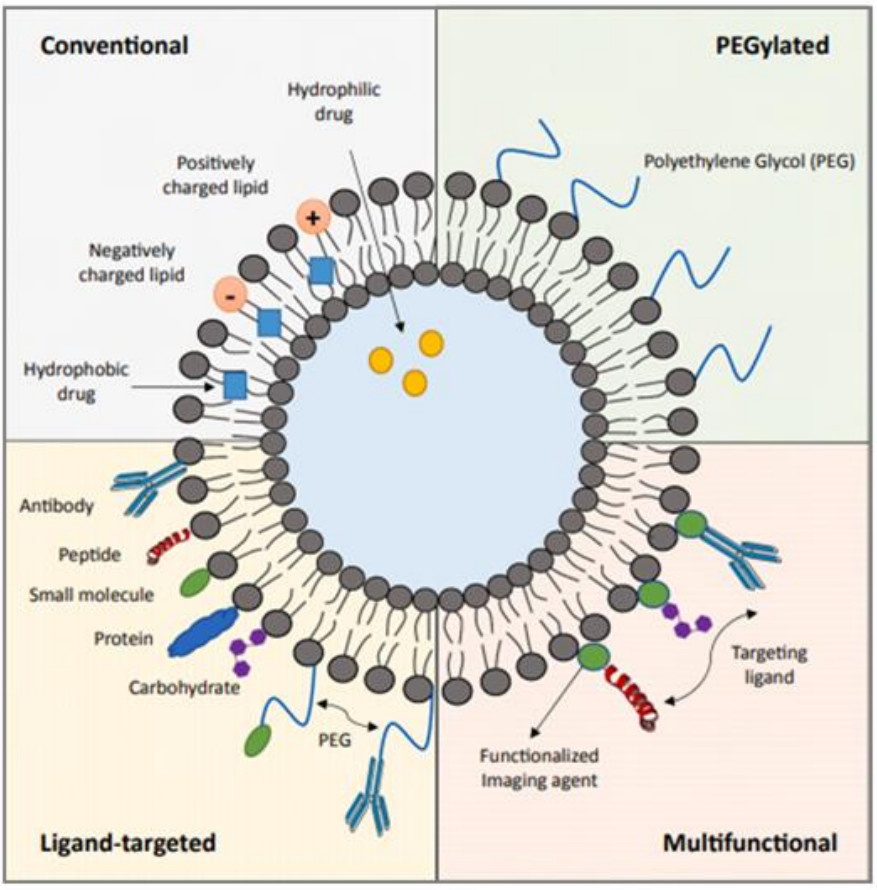

Figure 18 *Different functionalization of liposomal DDS*[76].

Other nanosized lipid bilayer structures that have received significant attention are lipodisks. These nanostructures were first described in 1997[77] and they are composed of a flat phospholipid bilayer assuming a disk-like geometry with PEG chains extending outward from the rim (***Figure 19***). They are typically edge-stabilized by PEG-conjugated lipids.

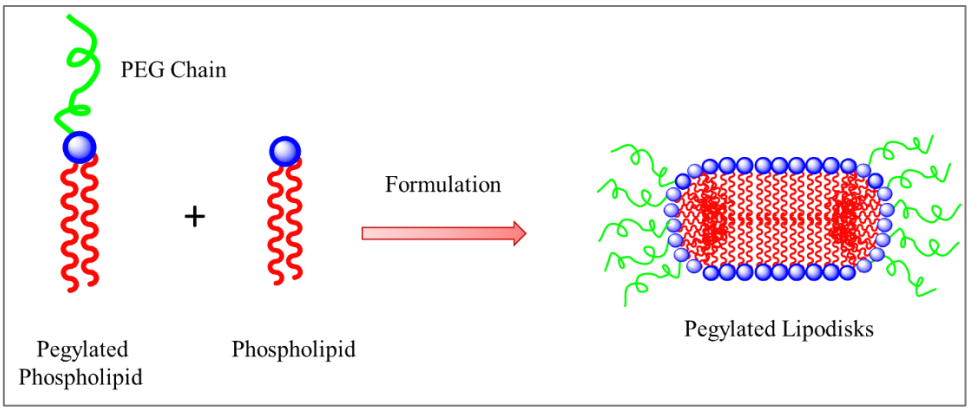

Figure 19 *Phospholipids can self-assemble into lipodisks by varying the lipid constituents and formulation method.*

While initial research on lipodisks focused on their application as biomimetic membranes, overtime the interest in their employment as carriers for bioactive compounds has grown. The main advantage offered by lipodisks in drug delivery applications compared to liposomes is the smaller dimensions, generally around 50-70 nm, that entails different pharmacokinetic properties and favorable tissue localization respect to the bigger liposomes[78]. Moreover, lipodisks are very stable at dilution with the PEG coating offering efficient and long-term steric stabilization.

Lipodisks composition can be modulated to optimize nanoformulation and, more specifically, effects of PEGylated phospholipid length, proportion and density has been studied, highlighting their importance in the formulation of lipodisks. By including PEG-lipids with different length (DSPE-PEG_{750}, DSPE-PEG_{1000}, DSPE-PEG_{2000}), it has been observed that PEG with mass below 1000 Da induces the formation of highly heterogeneous liposomes population and elongated band-shaped structures. On the contrary, the use of PEG chains of 1000 and 2000 Da afforded with equal efficiency lipodisks, without liposomes formation only when 20% molar mass of DSPE-PEG was used, confirming the necessity of the PEG with specific length and proportion to obtain a low-dispersion and homogeneous formulation exclusively populated by lipodisks. Furthermore, the same study reported that lipodisks including PEG percentages below 20% had tendency to aggregate, also pointing out the importance of PEG density around the rim as stabilizing agent[79].

Interestingly, targeting ligands can be also integrated in lipodisks structure with the purpose of refining the performances of the nanocarriers and improving the therapeutic action. Two recent studies discussed the efficacy of Epitelial Growth Factor (EGF)-targeted lipodisks to deliver their respective payloads (p53-activating peptide VIP116 or the membranolitic protein mellitin extracted from bee venom) in target tumoral cells[80,81]. In both studies, the presence of EGF as targeting ligand dramatically enhanced the cellular uptake by target cells overexpressing EGF receptors and, as a consequence, an heightened accumulation of therapeutic peptide was achieved in tumoral cells respect to non-targeted lipodisks with a significantly improved cell-killing effect.

3.4 Cyclodextrins

Cyclodextrins (CD) are natural cyclic oligosaccharides with a truncated cone shape formed by units of D-(+)-glucopyranose linked together by α-1,4-glicosidic bonds. Depending on the number of sugar units, three different families of CD are formed, such as α-, β- and γ-CD (***Figure 20***)[82].

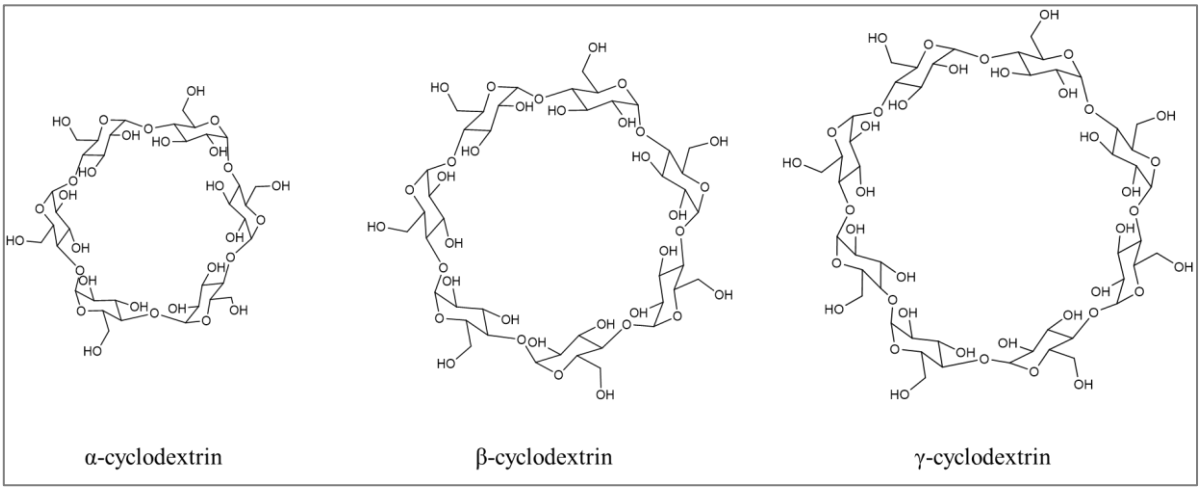

Figure 20 *Top view of α-, β- and γ-CD*

CDs are characterized by a hydrophilic surface due to the presence of primary OH groups located on the wide rim and secondary OH groups on the other rim and an apolar cavity. The abundant hydroxyl groups of CDs enable their chemical modification. Moreover the rigid ring structure, with a hydrophilic outer surface and a hydrophobic cavity, allows the formation of inclusion complexes with hydrophobic compounds with matched sizes and shapes by host-guest non-covalent interactions (van der Waals and hydrophobic interaction, electrostatic and hydrogen bonding) with several applications in food-industry[83], cosmetic[84], environmental[85], agriculture[86] and biomedical fields[87].

The host-guest interactions typical of CDs are widely exploited in nanomedicine for the delivery of bioactive compounds that are typically included inside the CDs cavity.

The main advantages of the use of CDs as drug carriers are the increase in aqueous solubility and stability in biological environment, the improvement of transport across the biological barriers, the increase of bioavailability, a more controlled release[82] as well as an unpleasant taste and smell can be masked, ensuring higher patience compliance[87].

Literature data report the successful application of CDs for the delivery of a wide array of drugs[88] exploiting different administration routes [89] (oral, nasal, sub-cutaneous delivery), attesting for high flexibility offered by these biomaterials.

Over the time, the optimization of CDs performance through suitable chemical modification of their native structure has become a common practice. As an example, the CD thiolation lead to an increased permeation of biological mucus barriers and offered the possibility of crosslinking by formation of disulfide bonds to form a latticed structure, able to gelify in solution affording a delivery system whose characteristics are totally different from the native components[90].

The hydroxyl group in the C-6 position is the most reactive; the hydroxyl in the C-2 position is the most acidic, due to both the presence of hydrogen bonds and the electron-withdrawing effect exerted by the anomeric acetal function; the C-3 position

is the most sterically hindered. Thanks to these differences in the reactivity, the chemical modification of the three hydroxyl groups can be selective allowing the synthesis of amphiphilic macrocycles that self-assemble in water in micelles or vesicles, resulting more versatile than native cyclodextrins, as powerful drug nanocarriers[91,92,93,94,95].

CDs may also be associated, as stabilizing agents, to other DDSs[96]. Solid-lipid NPs[97] and metal NPs[98] have been formulated with CDs as stabilizing agents avoiding phase separation or aggregation of the nanocarriers leading to an increase of their permanence time in biological medium. Moreover, the formulation of mesoporous silica NPs[99] in the presence of different concentrations of CDs enables to finely tune the shape and size of the final DDS, enabling its functionalization with specific targeting and stimuli-responsive group.

4. Results and Discussion

4.1. Linear PLA-PEG copolymers

4.1.1. Synthesis and nanoformulation of amphiphilic PLA-PEG linear copolymer

A linear amphiphilic PLA-PEG was synthetized with a proper combination of carbodiimide-mediated coupling reaction and copper-catalyzed azide-alkyne cycloaddition (CuAAC) (***Figure 21***). Both the reactions offer great advantages in polymer organic chemistry due to the high conversion efficiency and mild reaction conditions. Furthermore, their versatility has been proven in the synthesis of several polymeric architectures, including linear and cyclic structures[100,101].

Specifically, the terminal carboxylic group of PLA was activated by EDCI/HOBt in DCM at room temperature for the subsequent coupling reaction with propargylamine, affording PLA-alkyne. Then, the alkyne terminal moiety introduced on PLA was coupled by CuAAC with the mono-azide methoxy-PEG forming a linear amphiphilic PLA-PEG copolymer bearing a typical triazole ring, without by-products (***Figure 21***)[4].

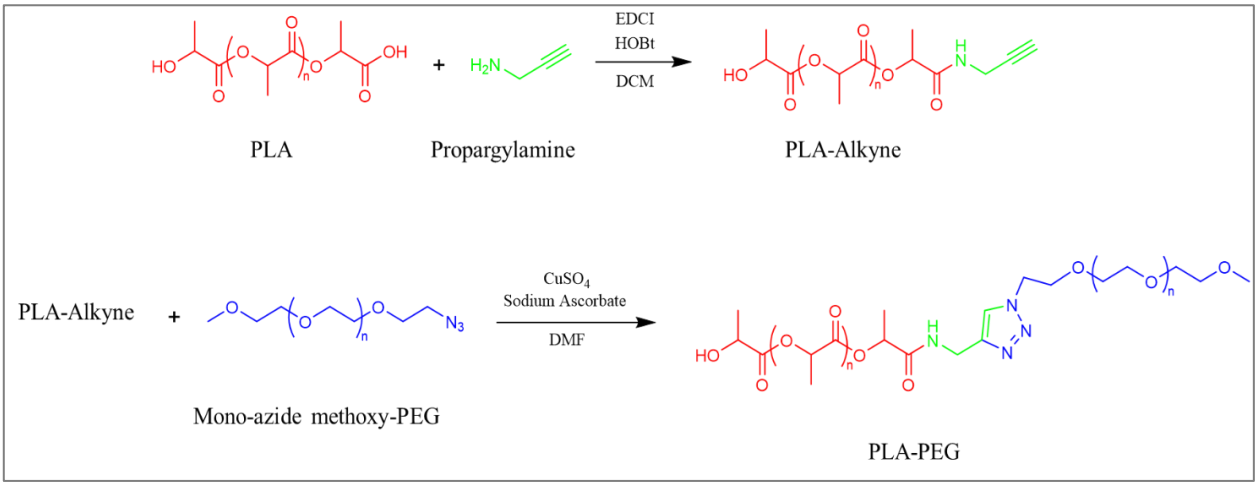

Figure 21 *Two-steps synthesis of linear PLA-PEG amphiphilic copolymer.*

The structure of both the intermediate and the final product was confirmed by ^{1}H NMR characterization (***Figure 22***). In the intermediate PLA-alkyne spectrum (***Figure 22, red line***), characteristic signals of polymeric protons are immediately recognizable at 1.5 ppm $(CH_3)_n$ and 5.2 ppm $(CH)_n$. The presence of resonance at 4.1 ppm (CH_2 protons of propargylamide moiety, shifted from 3.5 ppm of starting propargylamine) and at 6.6-6.4 ppm (amidic NH signals) confirmed the successful coupling of the two reagents.

In the final PLA-PEG spectrum (***Figure 22, blue line***), beside the polymeric protons related to the lactoyl repeating moiety of PLA (unshifted from the previous spectrum) and to the ethylene oxide units of PEG $(CH_2\ CH_2O)_n$ at 3.7 ppm, the presence of the typical H-5 proton signal of the triazolic ring at 7.3 ppm confirmed that the *click* coupling between azide and alkyne has been successfully performed.

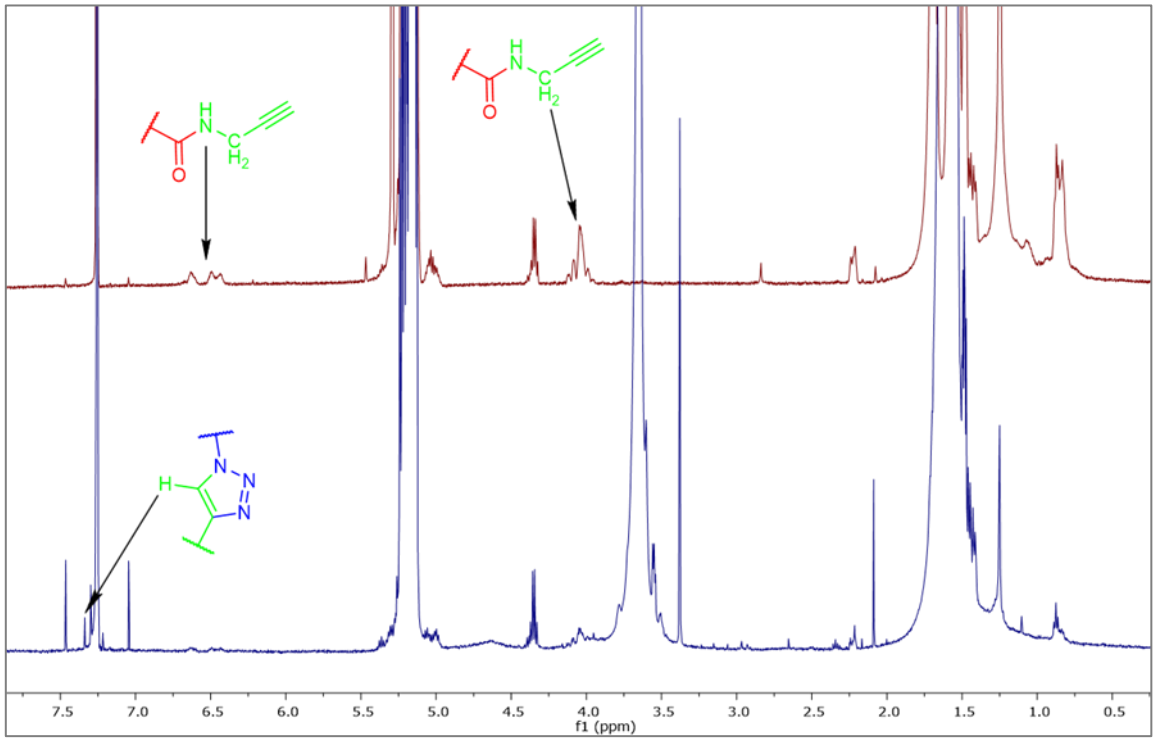

Figure 22 *Stacked NMR spectra of PLA-alkyne precursor (red trace) and PLA-PEG final product (blue trace)*

The newly synthesized PLA-PEG amphiphilic copolymer was nanoformulated to obtain PLA-PEG nanoparticles (NPs) incorporating the antimicrobial drug Linezoliz

(LNZ) exploiting two different methods, *i.e.* nanoprecipitation (in both tetrahydrofuran and acetone) and dialysis.

For nanoprecipitation (***Figure 23***), a solution of PLA-PEG and LNZ (10:3 mass ratio) in organic solvent was added dropwise to a large volume of water. The aqueous medium displacing the organic solvent favored the aggregation of the polymer chains into NPs incorporating the antimicrobial drug. After evaporation of the organic solvent, the centrifugation of NPs suspension allowed to recover PLA-PEG/LNZ NPs as a white powder separated from the unloaded LNZ in the supernatant.

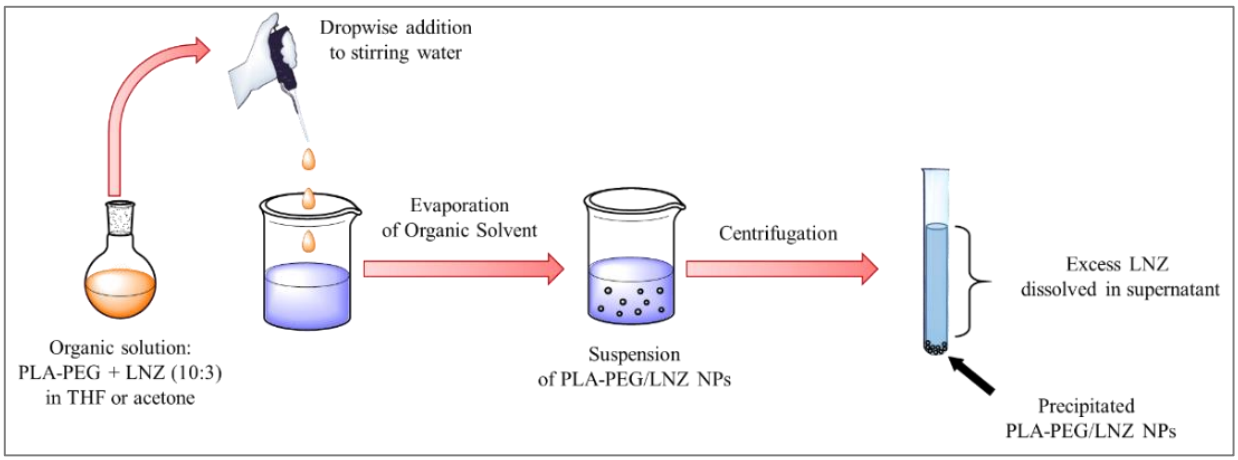

Figure 23 *Formulation of LNZ-loaded PLA-PEG NPs by nanoprecipitation.*

For dialysis (***Figure 24***), a solution of PLA-PEG copolymer and LNZ (10:3 mass ratio) in DMSO was added dropwise to a high volume of water. After stirring, the suspension was transferred into a dialysis membrane of proper cut-off, immersed in water, to remove both the free LNZ and the organic solvent. PLA-PEG/LNZ NPs suspension recovered from the bag was freeze-dried and stored as a white powder. "Empty" (unloaded) NPs were produced following the same procedure, omitting the drug.

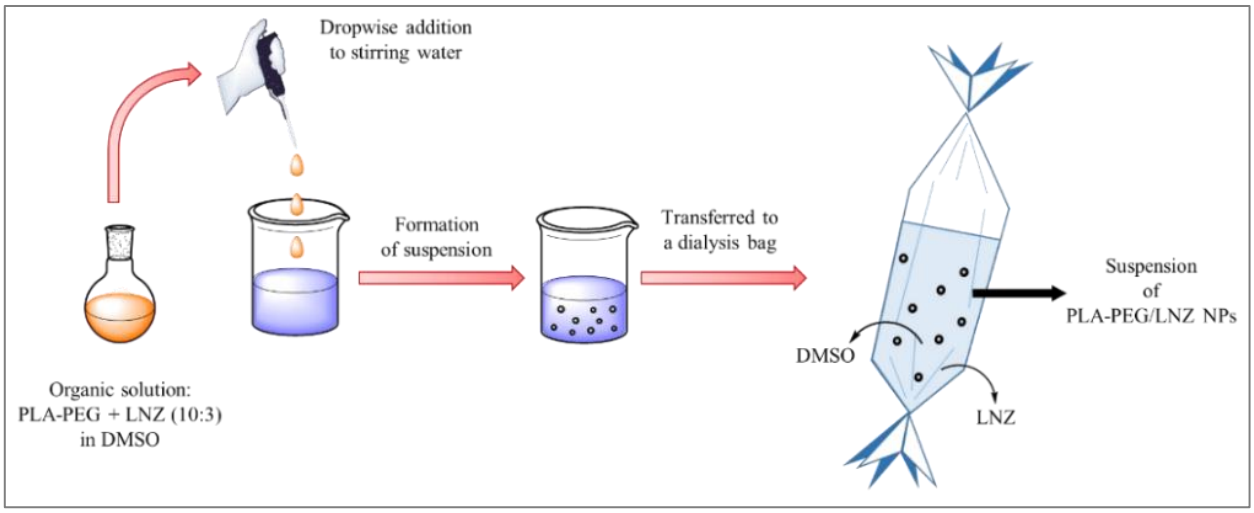

Figure 24 *Formulation of LNZ-loaded PLA-PEG NPs by dialysis.*

The physico-chemical characterization of PLA-PEG/LNZ NPs was carried out with the aim to compare the outcomes of both the nanoformulation methods and to select the best sample for biological investigation.

Empty and drug-loaded NPs were analyzed in terms of size (hydrodynamic diameter) and zeta potential (***Table 1***); specifically, freshly prepared NPs suspension as well as lyophilized and reconstituted NPs were evaluated. A monomodal particle size distribution was observed for all the investigated samples, either as freshly prepared or reconstituted ones, except for PLA-PEG/LNZ NPs prepared by nanoprecipitation in acetone whose hydrodynamic diameter was negatively affected by lyophilization and reconstitution (***Table 1***).

The ζ-potential values of all the investigated samples were negative (ranging from about -31 to -39 mV) (***Table 1***), indicating a good colloidal stability[102].

Table 1 *Physico-chemical charaterization (size, PDI and ζ-potential) of fresh and resuspended NPs.*

		Hydrodynamic diameter (nm ± SD)	**PDI**	**ζ-Potential (mV ± SD)**
Fresh NPs suspension	*PLA-PEG/LNZ Nanoprecipitation (Acetone)*	263 ± 98	0.15	-31 ± 4
	PLA-PEG/LNZ Nanoprecipitation (THF)	206 ± 72	0.10	-34 ± 6
	PLA-PEG/LNZ Dialysis	332 ± 132	0.20	-35 ± 6
	Empty PLA-PEG	180 ± 53	0.1	-38 ± 9
Lyophilized and resuspended NPs	*PLA-PEG/LNZ Nanoprecipitation (Acetone)*	489 ± 86 (92%) 131 ± 16 (8%)	0.05 0.05	-40 ± 5
	PLA-PEG/LNZ Nanoprecipitation (THF)	264 ± 96	0.15	-38 ± 6
	PLA-PEG/LNZ Dialysis	295 ± 48	-	-37 ± 7

^{1}H NMR studies in different solvents were employed to investigate the structure of PLA-PEG/LNZ NPs and to confirm the drug incorporation (***Figure 25***).

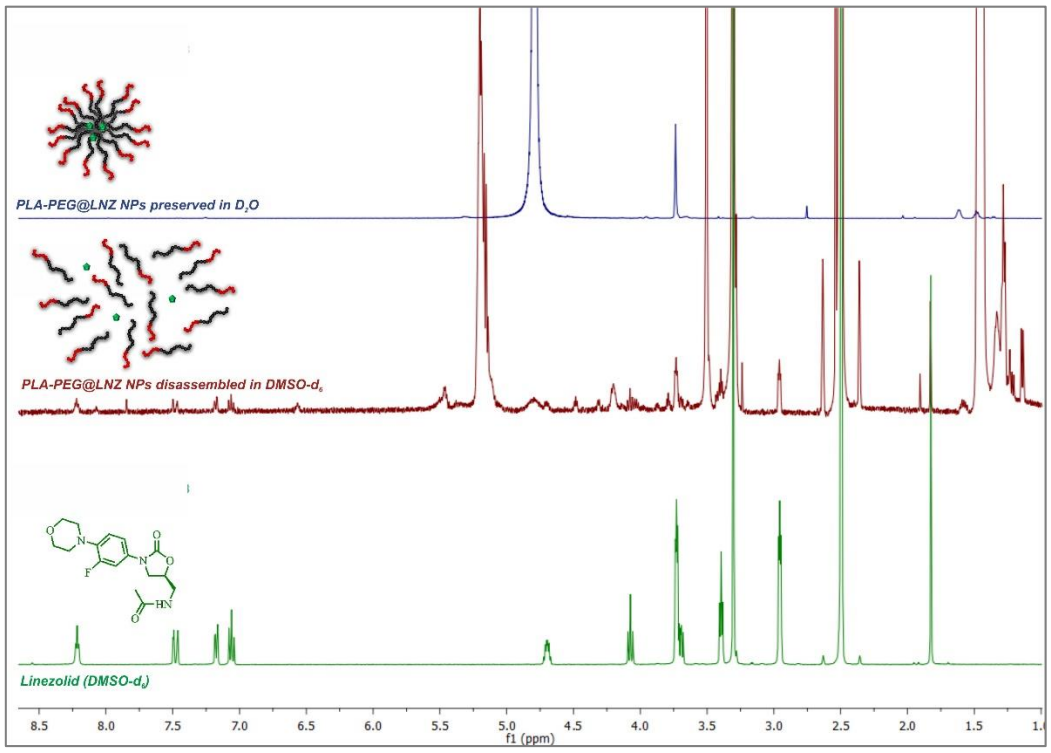

Figure 25 *Stacked spectra of PLA-PEG/LNZ NPs in D_2O (blue trace), disassembled PLA-PEG/LNZ NPs in DMSO (red trace) and free LNZ in DMSO (green trace)*

^{1}H NMR spectrum of the nanoformulated system in D_2O showed exclusively the typical PEG signals at 3.7 ppm, as previously reported for similar systems in aqueous solvents[103], confirming the assembly of the polymer into aggregates with PEG as the outer hydrophilic shell. The spectra of the system performed in DMSO-d_6 shows the signal of both hydrophilic PEG and hydrophobic PLA, attesting for the complete disaggregation of the system in this solvent. More importantly, the resonances of LNZ are visible after disassembly of NPs into DMSO, proving the successful incorporation of the drug into the nanosystem.

Drug Loading (DL) and Encapsulation Efficiency (EE) of PLA-PEG/LNZ NPs were determined by UV-Vis analysis in DMSO, a solvent that typically disassembled nanosystems[103], pointing out that the best "nanoantibiotic" was prepared by dialysis and it was selected for biological investigation (***Table 2***).

Table 2 *Drug Loading and Encapsulation Efficiency achieved with different formulation methods.*

	Drug Loading (%)	**Encapsulation Efficiency (%)**
PLA-PEG/LNZ Nanoprecipitation (Acetone)	0.6	2.6
PLA-PEG/LNZ Nanoprecipitation (THF)	0.9	4.1
PLA-PEG/LNZ Dialysis	3.5	15

4.1.2. Release studies and biological assays

Drug release studies were performed on both PLA-PEG/LNZ NPs and free LNZ in PBS at pH 7.4 using the dialysis bag method and the results were reported as cumulative percentage release (***Figure 26***). The same concentration of LNZ and the same experimental conditions were used to compare the release rate of the two samples. The amount of LNZ released and transferred from the internal to the external jacket of the dialysis membrane was quantified by UV-Vis absorption at predetermined times.

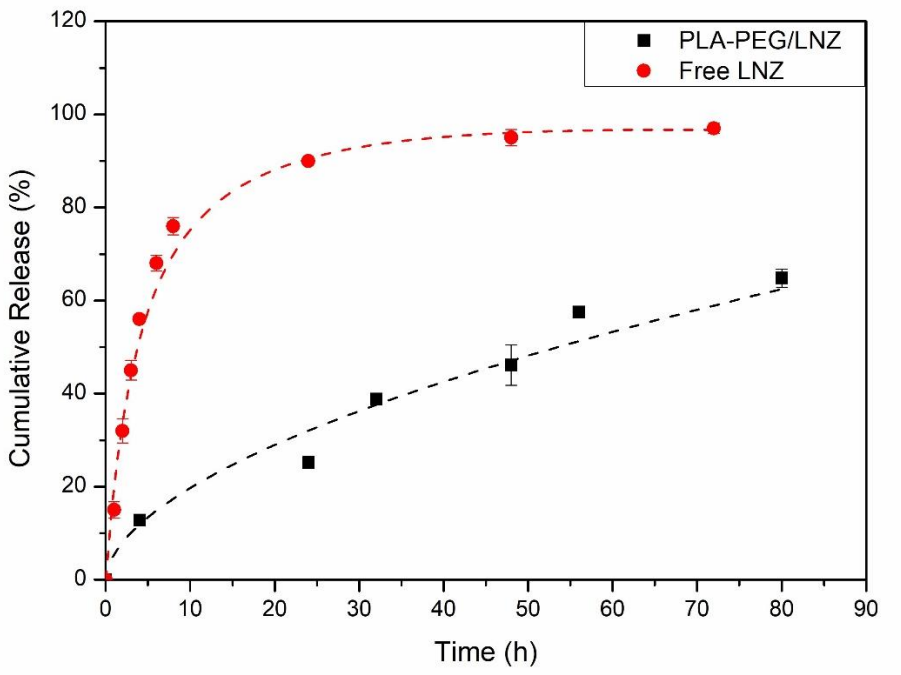

Figure 26 *Cumulative percentage release of LNZ as free drug (●) and from PLA-PEG/LNZ NPs (■) as a function of time, assessed by dialysis in PBS (pH 7.4) at 37 °C. Data are reported as the mean ± SD (n = 3).*

The fast diffusion of free drug across the dialysis membrane led to a very quick release, as expected, reaching 97% within 72 hours, with a *burst* effect consisting of 56% of released LNZ within the initial 4 hours. Conversely, a sustained and controlled drug release was observed for PLA-PEG/LNZ NPs with about 65% of released drug within 80 hours. Specifically, 25% of drug was released in 24 hours and about 50% within 48-56 hours. During the first 4 hours (*burst release* phase), only about 13% of LNZ was released likely due to the diffusion of LNZ from the NPs surface, prior to the onset of the typical polymer erosion, hydrolytic degradation and swelling. In fact, the slight water-solubility of LNZ favored, during NPs preparation, its partial diffusion into the outer aqueous phase with consequent encapsulation of the drug also in the outer layer of NPs[104], according to other antibiotic-loaded NPs (*i.e.*, Amikacin) reported in literature[105].

Overall, the observed release profile of PLA-PEG/LNZ NPs consisting of a rapid drug diffusion in the first hours associated with the presence of LNZ on NPs surface followed by a sustained release might be highly desiderable for treating bacterial

infections since the effectiveness of an antimicrobial delivery nanosystem is highly dependent on the control of the drug release profile.

The biological performance of the nanoformulation was investigated comparing the antibacterial effects of the incorporated LNZ and of the free drug at the same concentration against strains of *Staphylococcus epidermidis*, *Staphylococcus lugdunensis* toward which free LNZ has Minimal Inhibitory Concentration (MIC) of 1 μg/mL, and *Staphylococcus aureus*, *Methicillin Resistant Staphilococcus Aureus* (MRSA), and *vancomycin-resistant Enterococcus faecium* (*VREfm)*, toward which MIC is 2 μg/mL.

The MIC and Minimal Bactericidal Concentration (MBC) data determined by our biological assays confirmed that the native antimicrobial effect of the drug was preserved even after incorporation in polymeric NPs. Moreover, they apparently revealed a reduced effect of the nanoformulation against bacterial cultures compared to free LNZ (4-8 μg/ mL *vs* 1-2 μg/mL) (***Table 3***). However, considering our release study, only about 25% of the encapsulated LNZ was released from PLA-PEG/LNZ NPs within the first 24 hours (the time of the biological evaluation) pointing out that the drug has retained its MIC value and the gradual release of LNZ from NPs provided a long-lasting supplier of drug able to keep concentrations above MIC, thus allowing the maximal effect of the time-dependent antibiotic.

Empty NPs didn't have any effect on the bacterial growth, as expected (***Table 3***).

Table 3 *MIC and MBC values determined by biological assays. Results expressed as μg/mL.*

	***S. Aureus* ATCC 6538**		**MRSA ATCC 43300**		***S. Epidermidis* ATCC 35984**		***S. Lugdunensis* DSM 4804**		**VREfm DSM 17050**	
	MIC	MBC	MIC	MBC	MIC	MBC	MIC	MBC	MIC	MBC
Free LNZ	2	16	2	16	1	16	1	16	2	16
PLA-PEG/LNZ NPs	8	>16	8	>16	4	>16	4	>16	>16	>16
Empty PLA-PEG NPs	-	-	-	-	-	-	-	-	-	-

The effect of PLA-PEG/LNZ NPs, free LNZ and empty PLA-PEG NPs on planktonic growth of MRSA was monitored over 72 hours. Specifically, concentrations of samples equal to MIC, 2 x MIC and 4 x MIC were evaluated (***Figure 27***).

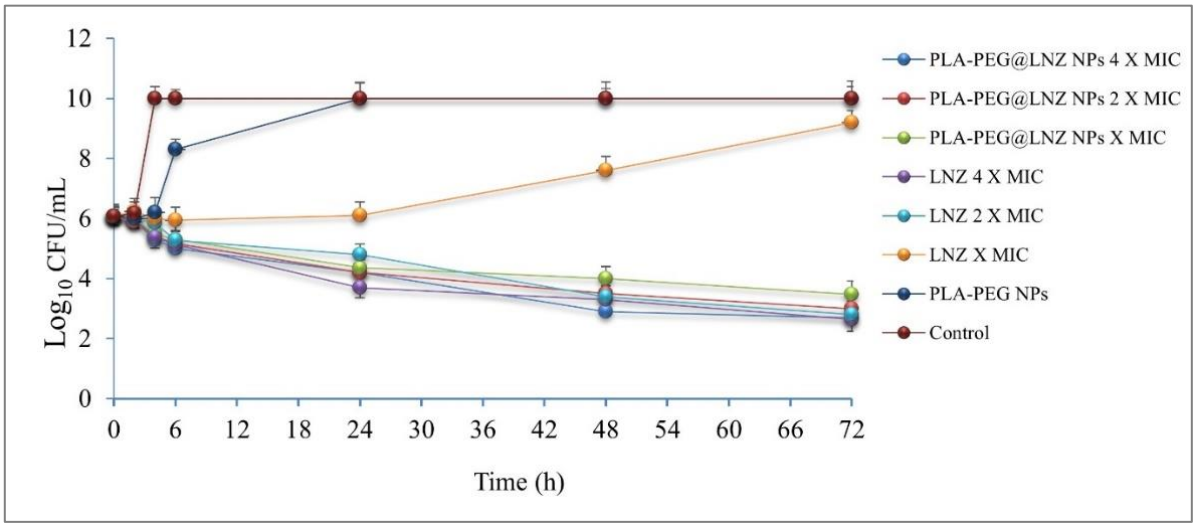

Figure 27 *Effects of PLA-PEG/LNZ, free LNZ and empty PLA-PEG NPs at concentrations of MIC, 2 x MIX and 4 x MIC on planktonic growth of MRSA. Free LNZ at MIC, 2 × MIC, and 4 × MIC correspond to 2, 4, 8 μg/mL, respectively. PLA-PEG/LNZ NPs at MIC, 2 × MIC, 4 × MIC correspond to a LNZ content of 8, 16, 32 μg/mL. According to release data, about 25% of drug was released in 24 h, 46% in 48 h and 60 % in 72 h.*

Free LNZ showed a bacteriostatic effect at 2 μg/mL (MIC value) only up to 24 hours after which the bacterial regrowth was noticed (orange line) likely due to the rapid clearance of free drug at 24 hours. At higher concentrations of free LNZ (4 and 8 μg/mL; LNZ 2 × MIC and LNZ 4 × MIC, respectively), an evident reduction of bacterial load was detected. Specifically, at concentration of LNZ 4 × MIC (violet line), bacterial count declined up to 24 hours from baseline 1.2 $\times 10^6$ CFU/mL to 4.8 $\times 10^3$ CFU/mL (2.4 Log decrease). Then, bacterial cells entered in a persisting phase with a small proportion of viable bacteria survived beyond 48 hours (2 $\times 10^3$ CFU/mL; 2.78 Log decrease) that further reduced to 4.5 $\times 10^2$ CFU/mL (3.43 Log decrease) at 72 h. Also for LNZ 2 × MIC (light blue line) a similar trend was observed. The growth control reached a maximum of ~10^{10} CFU/mL.

On the contrary, LNZ incorporated in PLA-PEG NPs managed to reduce bacterial proliferation for the whole duration of the experiment at every concentration, including

at MIC. The prolonged effect of loaded LNZ even at the lowest concentration confirmed that the DDS protected the incorporated payload, releasing it slowly over the time and extending its therapeutic window. Interestingly, significant difference was detected between PLA-PEG/LNZ NPs and free LNZ at the MIC (green and orange lines, respectively). In fact, the drug incorporated into the NPs × MIC (green line) was significantly effective in reducing the bacterial load from 1.2×10^6 to $2.3–1 \times 10^4$ CFU/mL (1.72-2.08 Log decrease) over 24-48 hours followed by a reduction to 3×10^3 CFU/mL (2.61 Log decrease) at 72 hours. Thus, one of the main advantages of PLA-PEG/LNZ NPs consisted of the prolonged activity of LNZ loaded into NPs × MIC until 72 hours, compared to free LNZ × MIC that is active only until 24 hours (orange line).

PLA-PEG/LNZ NPs 4 × MIC (blue line) determined reduction of bacterial cells to 1.6×10^4 CFU/mL (1.88 Log decrease) at 24 hours followed by a decrease to 8×10^2 CFU/mL (3.18 Log decrease) at 48 hours and 4.8×10^2 CFU/mL (3.39 Log decrease) at 72 hours, compared to untreated control. A similar trend was also observed for PLA-PEG/LNZ NPs 2 × MIC (red line). It is noteworthy that, although the activity of free LNZ at 2 × MIC and 4 × MIC and drug-loaded NPs appeared similar in the time kill plots, only PLA-PEG/LNZ NPs 4 × MIC determined a reduction of bacterial load of 3 Log in CFU/mL as early as 48 hours.

Further investigation of PLA-PEG/LNZ NPs were performed against MRSA biofilms that are self-produced biological matrixes difficult to eradicate and poorly susceptible to conventional antimicrobial treatments. Biofilms drastically reduce the effect of antimicrobial agents, including LNZ, by preventing their penetration inside target cells[106]. Since LNZ has a relatively poor efficacy in eradicating established *S. aureus* biofilm[107], we would like to test the anti-biofilm ability of our PLA-PEG/LNZ NPs. A 24 h MRSA biofilm was treated with free LNZ and PLA-PEG/LNZ NPs at concentrations 2 x MIC and 4 x MIC and the biofilm retention was evaluated in terms of biomass (by optical density) and cells viability (CFU/mL) after 24 hours of treatment (***Figure 28***). Neglectable effects (~2% biomass reduction) were exhibited by free drug at both tested concentrations, in accordance with literature[106,108], whereas LNZ

incorporated in NPs achieved a concentration dependent reduction of biomass, corresponding to 38% and 27% at 4 x MIC and 2 x MIC, respectively.

Biofilm viability measurements confirmed these results showing that LNZ-loaded NPs 4 x MIC caused a 64% reduction (from baseline 1.6×10^7 to 5.8×10^6 CFU/mL) after 24 hours treatment, whereas a bacteriostatic effect was achieved with a NPs concentration equal to 2 x MIC. Conversely, no effect was observed with free drug and empty NPs revealing an increase of CFU/mL (***Figure 28***).

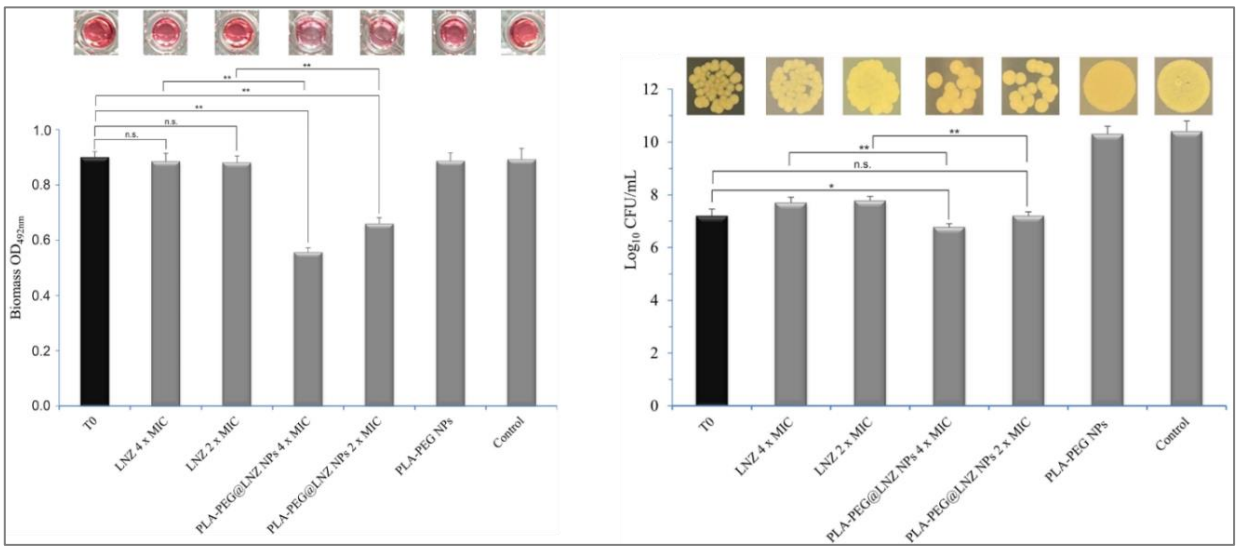

Figure 28 *Efficacy of free LNZ, PLA-PEG/LNZ NPs and empty PLA-PEG NPs at different concentrations on 24 h MRSA biofilm and related photographs. Biofilm retention was expressed in terms of biomass (optical density; left) and cells viability (CFU/mL; right). Black histogram represents the biofilm without treatment at time 0 (T0). Grey histograms represent the biofilm after 24h treatment with free LNZ, PLA-PEG/LNZ NPs, empty PLA-PEG NPs and CAMHB (control).*

Overall, the biological assays demonstrated the inhibitory activity of PLA-PEG/LNZ NPs on MRSA biofilm in terms of biomass and cell viability, while free LNZ exerted a negligible effect and even a biofilm growth revival. Notably, the observed effect of LNZ-loaded NPs 4 × MIC, the best performing sample, should be considered taking in account the outcomes of our release experiment, *i.e.* NPs released only about 25% of the loaded drug within 24 hours which is the experimental time of biofilm evaluation. Overall, the anti-biofilm efficacy of PLA-PEG/LNZ NPs could be

strictly related to the ability of anionic NPs to diffuse through the water pores of the biofilm[109] improving the contact between deepest bacteria and antibiotic[110].

4.2. Star shaped PLA-PEG copolymers

4.2.1. Synthesis of star PLA-PEG and PLA-PEG-RGD and nanoformulation

The synthesis of the star shaped amphiphilic PLA-PEG copolymer was carried out exploiting a multi-step process combining a ring-opening polymerization (ROP) of L-lactide using glycerol as trifunctional core, affording the three-armed PLA, and a series of esterifications and CuAAC reactions, allowing the conjugation of the hydrophilic PEG to the star PLA and the final decoration of end-groups with RGD peptide.

Designing and optimizing all the synthetic steps for polymer preparation is crucial to achieve a specific target and application. Specifically, the modulation of molecular weight, size, and functionalization by proper chemical modification of starting polymers turns out to be essential to get a nanosystem endowed with *self-assembly* abilities, colloidal stability, targeting properties and therapeutic efficacy in the nanomedical field.

The synthesis of star polymers requires a fine control over the molecular weight, the number of the arms and the chemical composition since these features strongly influence polymer micellization, crystallinity, degradation rate, etc[111,112]. Accordingly, we designed the core-first synthesis of an amphiphilic star PLA-PEG copolymer with a specific hydrophobic to hydrophilic ratio (14.000 : 6.000 g/mol) to ensure proper *self-assembly* and micellization in water.

The three-armed star PLA was obtained by ROP reaction of lactide in the presence of glycerol as core-initiator and DBU as catalyst (***Figure 29***)[1]. The reagents were used in a specific ratio (Lactide : Glycerol : DBU 97:1:2) and the reaction time was

controlled by quenching with benzoic acid after 10 minutes to obtain a star PLA with a final molar mass of 14.000 g/mol. The product was isolated by precipitation in cold methanol. This work-up allowed to eliminate any traces of benzoic acid/DBU salt, avoiding instability over the time.

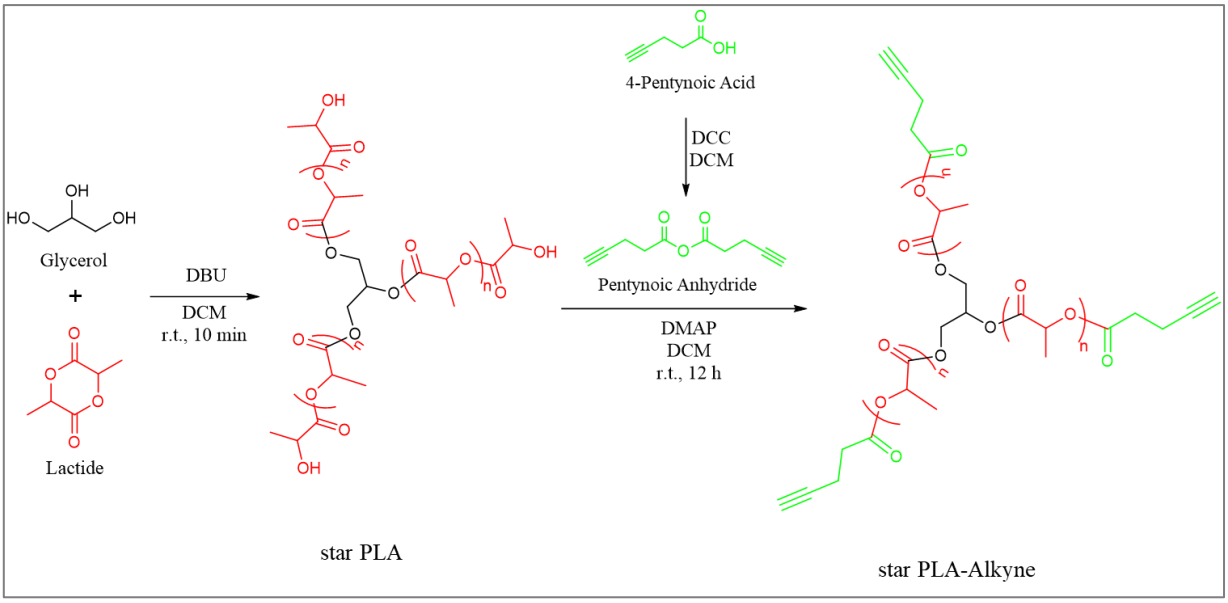

Figure 29 *Core-first synthesis of star PLA-Alkyne*

NMR characterization confirmed the chemical structure and the desired degree of polymerization with a Mn $^{1H\ NMR}$ = 14.000 g/mol. Moreover, kinetic studies determined that the linear polymeric arms grew equally from the three OH-initiating groups of glycerol. Then, the three terminal hydroxyl groups of star PLA were esterified with pentynoic anhydride to insert alkyne functionalities (***Figure 29***).

The comparison of ^{1}H NMR spectra before and after the functionalization confirmed the quantitative esterification (***Figure 30***). Specifically, beside the typical star PLA protons resonances recognizable at 5.15 and 1.57 ppm in both spectra, related to the lactoyl repeating units, the disappearance of the signal at δ 4.36 ppm (CH of the hydroxyl end groups) after reaction with pentynoic anhydride was evident for star PLA-Alkyne, together with the appearance of three signals for the pentynoic moiety (δ 2.65, 2.52, 1.98 ppm) confirming the reaction success.

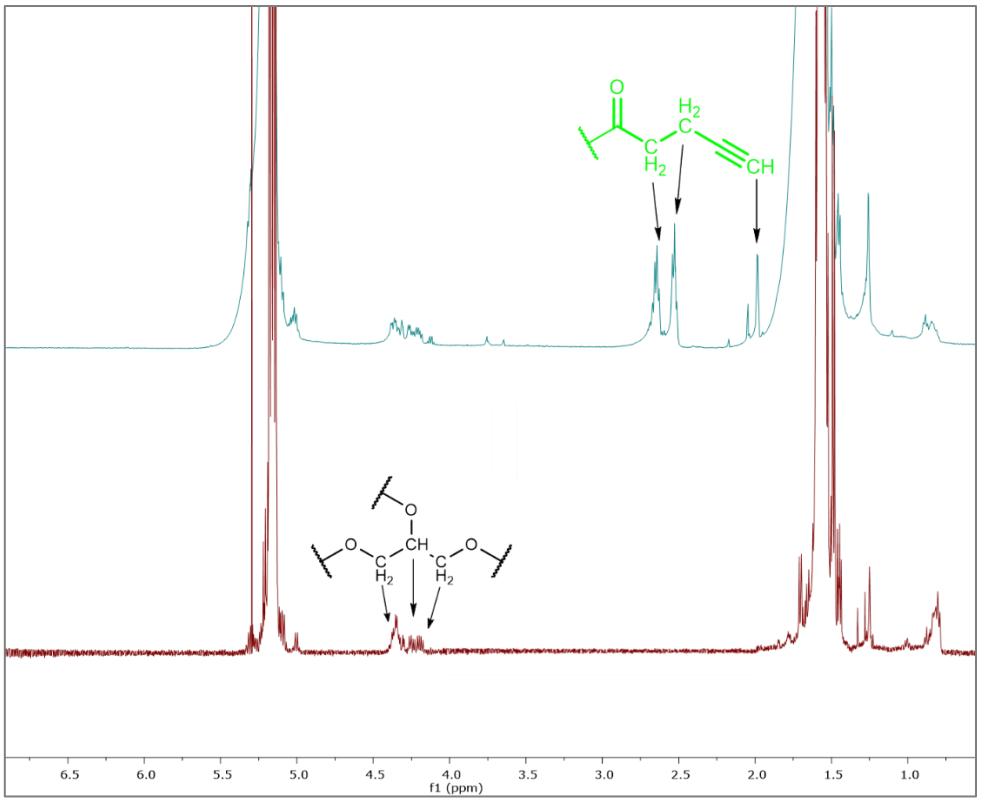

Figure 30 *Stacked NMR spectra of star PLA precursor (red trace) and star PLA-Alkyne (blue trace)*

The hydrophilic portion of the final product consisted of PEG_{2000} that was first mono-functionalized by reaction with tosyl chloride in the presence of TEA and DMAP to get a tosyl leaving group suitable for the reaction with sodium azide, allowing the insertion of one terminal azide group on PEG chain (***Figure 31***). ^{1}H NMR and MALDI-Tof confirmed the structure of monoazide-PEG, according to literature[1,113].

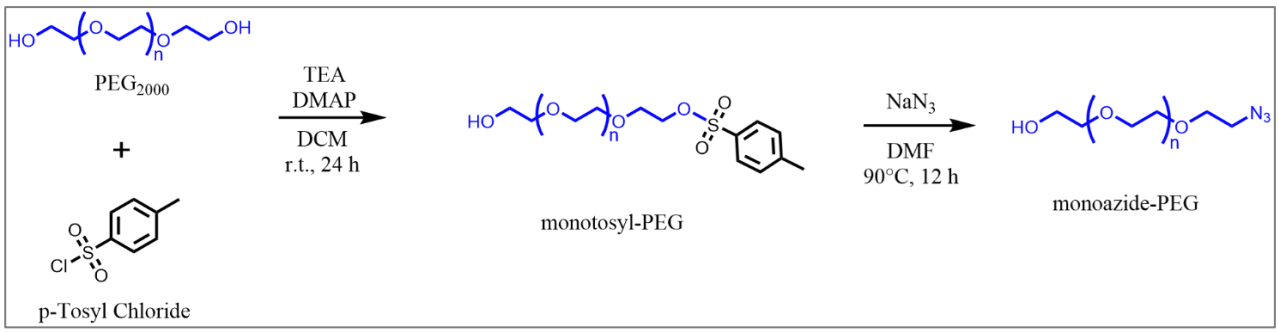

Figure 31 *Two steps synthesis of monoazide-PEG.*

The coupling between monoazide-PEG and star PLA-Alkyne was achieved by CuAAC (***Figure 32***) in THF in the presence of CuBr and PMDETA. To isolate the final product, water was added after organic solvent evaporation and the mixture was centrifuged to obtain the amphiphilic star PLA-PEG as a solid compound in a very good yield (96%).

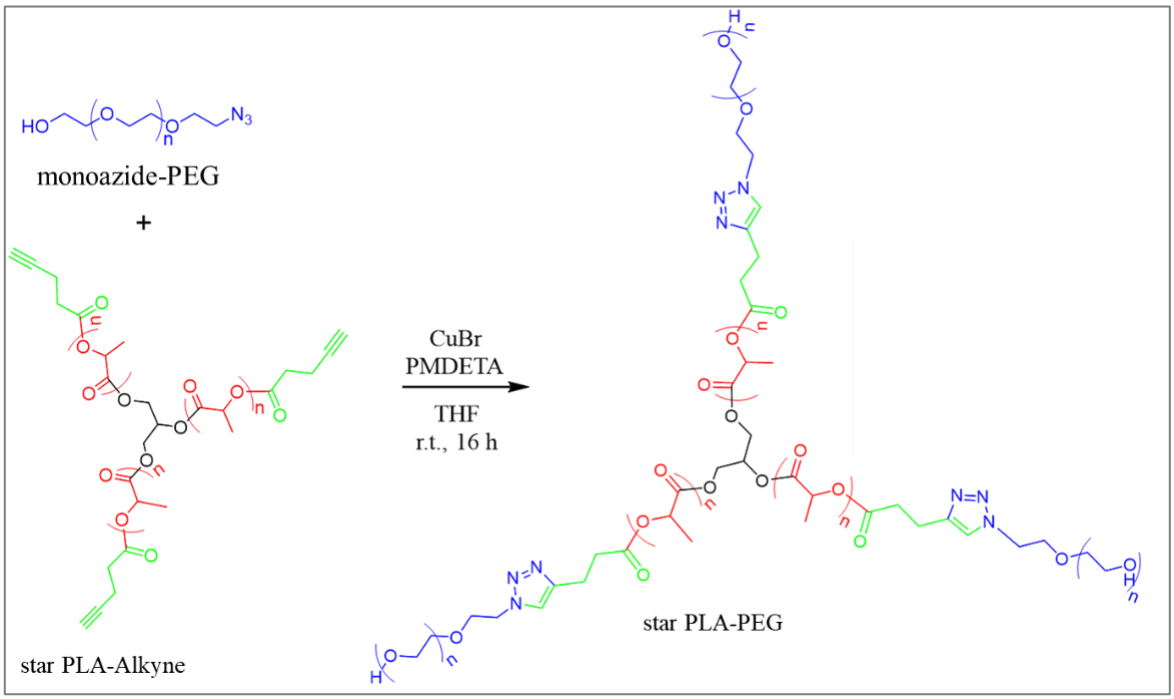

Figure 32 *CuAAC click-chemistry reaction to link hydrophilic and hydrophobic domain leading to star PLA-PEG.*

^{1}H NMR and SEC analysis confirmed the structure of the product (***Figure 33***). Specifically, SEC measurement in THF revealed for the final product an elution volume lower than the precursor, as expected, confirming the success of the *click* coupling (***Figure 33A***). ^{1}H NMR characterization attested for the formation of the triazole ring linking the PLA and PEG moieties as demonstrated by the disappearance of the alkyne proton signal at 1.98 ppm (black dashed circle), converted in the triazole H-5 resonating at 7.58 ppm (black circle), the shift of the azido-methylene protons resonance from 3.39 ppm to 3.06 ppm (blue circles) and the shift of the pentynoic-methylene protons signal (from δ 2.52 to 4.49 ppm, orange circles) (***Figure 33B***).

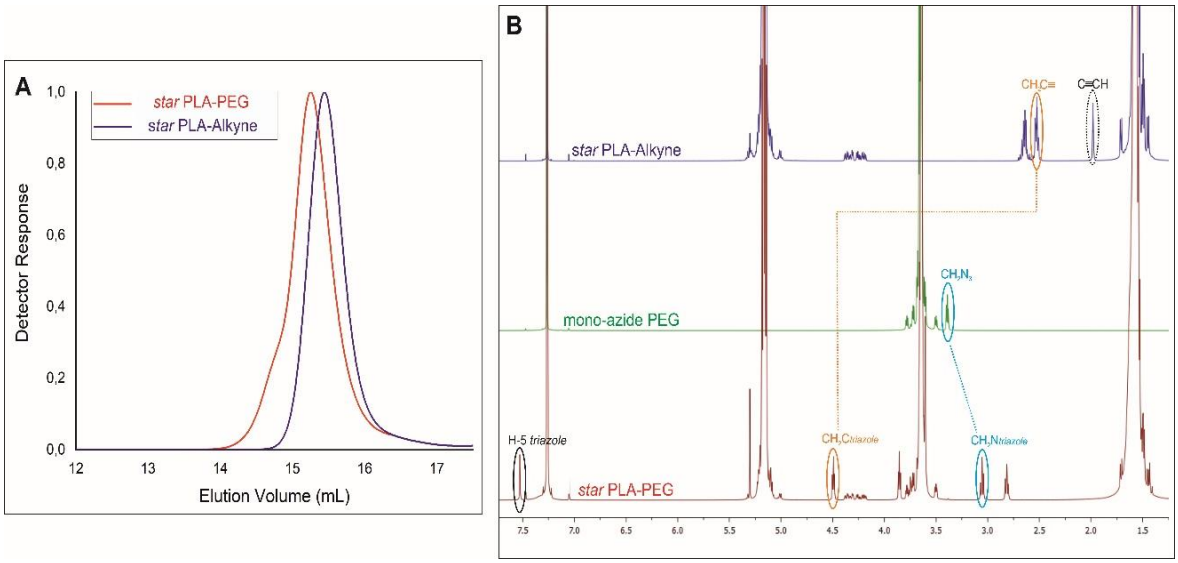

Figure 33 *A) SEC chromatograms of star PLA-PEG (red line) compared to star PLA-Alkyne precursor (blue line). B)* ^{1}*H NMR spectra of star PLA-PEG (red trace), mono-azide PEG (green trace), star PLA-Alkyne (blue trace).*

A terminal alkyne function was then inserted on hydroxyl end-groups of star PLA-PEG to favor the final coupling with azido cyclic-RGDyK peptide (***Figure 34***).

RGD is an oligopeptide known to be recognized and internalized by $\alpha_v\beta_3$ integrin[114], cellular surface receptors overexpressed on cancer cells and blood vessels during cancer angiogenesis. The decoration of polymeric structures with RGD turned out to be an appealing strategy to bestow targeting abilities to the final formulated polymeric DDS. The final CuAAC was carried out in the classical *click chemistry* conditions (*i.e.*, CuBr and PMDETA) in anhydrous DMF with a coupling efficiency of about 50% (~1.5 degree of substitution) (***Figure 34***). The formation of the triazolic linkage between star PLA-PEG and RGD was confirmed by ^{1}H NMR spectroscopy and SEC analysis. The presence of ^{1}H NMR signals resonating at 7.96, 7.43, 7.02 and 6.72 ppm attested for aromatic moieties (tyrosine and benzamide) of the RGD oligopeptide structure. Moreover, SEC analysis carried out with a double detector (differential refractometer and UV–Vis spectrophotometer set at λ_{max} of RGD, 280 nm) also confirmed the successful grafting of RGD peptide on the polymeric architecture.

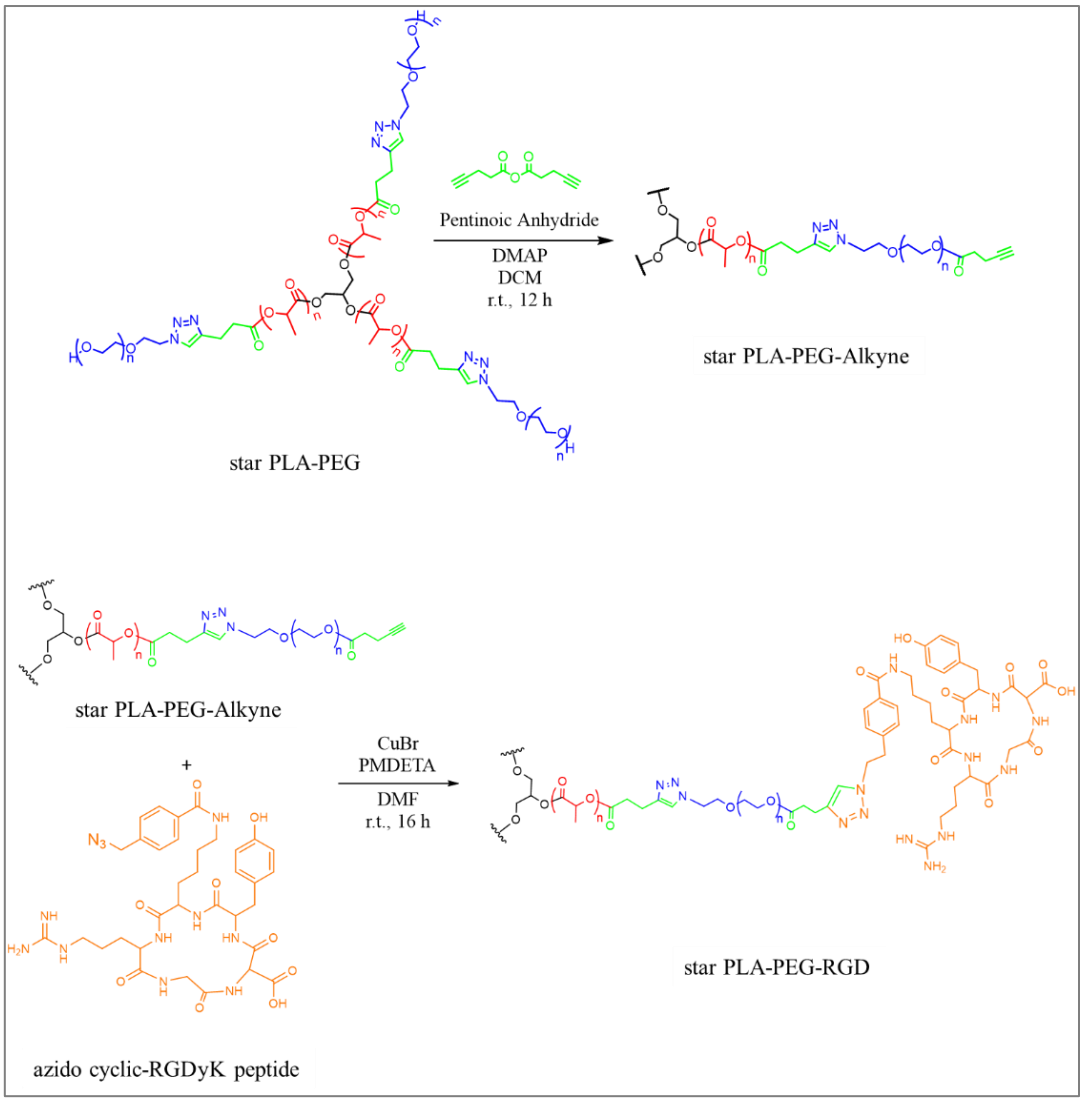

Figure 34 *Final CuAAC click reaction to decorate star PLA-PEG with targeting ligand RGD peptide.*

The newly synthetized star PLA-PEG-RGD was formulated by nanoprecipitation to incorporate Docetaxel (DTX) and Doxorubicin (DOX)[2], using in both cases a blended mixture of star PLA-PEG and star PLA-PEG-RGD in a 9:1 mass ratio. The use of blended polymer mixtures based on RGD-decorated and undecorated polyesters was already reported in literature for NPs formation[115,116] and turned out to be a very good option since even a small quantity of grafted peptide was able to significantly influence the biological outcomes of our system.

The polymer was nanoformulated with DOX using a mass ratio 10:3, while DTX encapsulation was performed using two different polymer: drug mass ratio (10:1 and 10:3). A solution of blended polymers and drug in THF was added dropwise to a high

volume of stirring water. Diffusion of the organic solvent in water causes the aggregation of the polymer chains into NPs incorporating the drug; THF is then evaporated under reduced pressure. DTX formulation was lightly centrifuged (1500 RPM) to separate the insoluble, unloaded drug as a residue obtaining the drug-loaded NPs suspended in the supernatant (***Figure 35***). Conversely, a strong centrifugation (13000 RPM) was carried out for DOX formulation to recover the DOX-loaded NPs as a residue separated from the unloaded DOX dissolved in the supernatant (***Figure 35***).

Similarly, DOX-loaded NPs without RGD were formulated, using only undecorated star PLA-PEG in the formulation and keeping the ratio of polymer to DOX at 10:3. The undecorated NPs have been used to investigate the contribution of the targeting ligand to the performance of our delivery system[2].

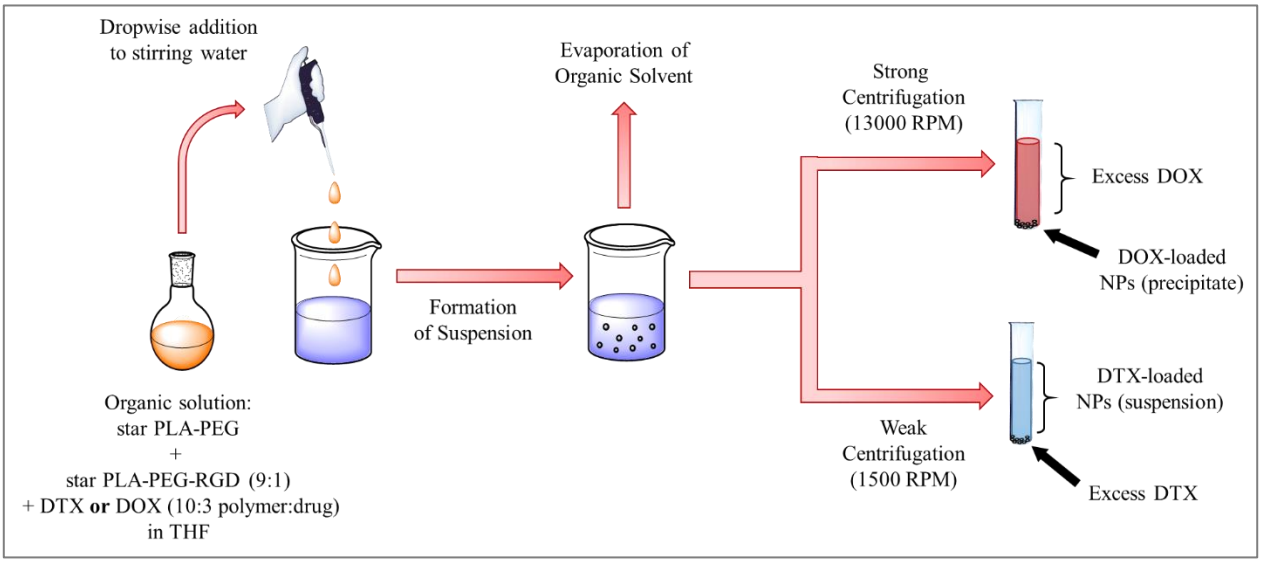

Figure 35 *Nanoprecipitation protocols for DTX- and DOX-loaded NPs formulation.*

Size (hydrodynamic diameter, D_H) and zeta potential (ζ) of the nanoformulations were investigated (***Table 4***). Empty, unloaded NPs, formulated following the same procedure without the drugs, were also analyzed both as a fresh suspension and as a lyophilized and reconstituted sample to investigate the effect of lyophilization on size distribution. Size comparison of empty freshly prepared NPs and re-suspended NPs

after lyophilization demonstrated a slight increase of the mean hydrodynamic diameter (D_H 133 nm *vs* 259 nm).

Mean D_H of DTX-loaded nanoformulation resulted 283 ± 50 nm and 379 ± 138 nm (***Table 4***) for 10:3 and 10:1 nanoformulations, respectively. The second population was negligible (8 %) for the 10:3 formulation (70 ± 9 nm), but more evident (44 %) for the 10:1 (129 ± 29 nm).

DOX-loaded RGD-targeted NPs were characterized by a main population (≅ 90 %) of 349 nm and a second negligible population (≅ 10 %) of about 80 nm, whereas the undecorated DOX-loaded system exhibited a monomodal distribution of 278 nm.

All the nanoformulations were characterized by negative ζ-potential values (ranging from -20 to -29 mV) due to the likely adhesion of hydroxyl groups produced by water dissociation to the PEG hydrophilic shell[117]. The resulting negative surface potential was a desirable property as it entailed good colloidal stability given by same charge repulsion, reduced plasma protein adhesion and reduced aspecific cellular uptake, being an advantage from a biopharmaceutical point of view[118,119].

Table 4 *Physico-chemical characterization (Hydrodynamic Diameter, PDI and ζ-potential) of NPs*

	Hydrodynamic Diameter (nm ± SD)	**PDI**	**ζ-Potential (mV ± SD)**
star PLA-PEG-RGD/DTX (10:3)	283 ± 50 (92%) 70 ± 9 (8%)	0.4 0.4	-25 ± 4
star PLA-PEG-RGD/DTX (10:1)	379 ± 138 (56%) 129 ± 29 (44%)	0.3 0.2	-22 ± 4
star PLA-PEG-RGD/DOX	349 ± 62 (90%) 80 ± 9 (10%)	0.4 0.2	-29 ± 6
star PLA-PEG/DOX	278 ± 52	0.2	-27± 7
Empty star PLA-PEG	251 ± 25	0.1	-27± 4
Fresh empty star PLA-PEG-RGD	133 ± 51	0.4	-22 ± 7
Re-suspended empty star PLA-PEG-RGD	259 ± 76 (93%) 55 ± 6 (7%)	0.4 0.2	-20 ± 4

SEM analysis was performed on star PLA-PEG-RGD and star PLA-PEG-RGD/DOX to investigate morphological characteristics of the NPs (***Figure 36***) and in both cases, smaller average dimensions were detected compared to DLS results, as

expected[120]. In fact, in DLS analysis the aqueous medium which hydrated the dispersed NPs led to the detection of larger particle sizes, influencing their mean hydrodynamic diameter; on the other hand, SEM imaging in dry condition allowed to directly observe the real size of the "dry" NPs since water was removed under vacuum before the measurement.

More specifically, empty NPs exhibited size ranging from about 30 nm to 230 nm (***Figure 36***), the former being individual particle with near-spherical shape and rough surface and the latter being assemblies of the smaller ones. DOX-loaded NPs exhibited rough surface and size from about 50 nm to 220 nm (***Figure 36***). The incorporation of the drug seemed to determine a change in particles' morphology leading to a greater tendency of aggregation into multi-micellar nanoassemblies of higher dimensions whose formation has been already discussed (see Introduction) as a consequence of the covalently reinforced core-shell structure of amphiphilic star polymers[53]. The unimolecular micelles they assemble into below CMC can indeed undergo secondary aggregation into multi-micellar aggregates at higher concentrations due to increasing interactions between their arms (entanglement, overlapping and crumpling)[121]. Generally, as in the case of star PLA-PEG-RGD NPs, the coexistence of the two species, unimolecular and multimolecular aggregates, can be observed since the formation of MMA is a gradual process. However, the direct observation of both the defined core and the isolated arms is difficult for the majority of star polymers, therefore only near-spherical particles are detected without a high definition of the structural details of these complex architectures[54].

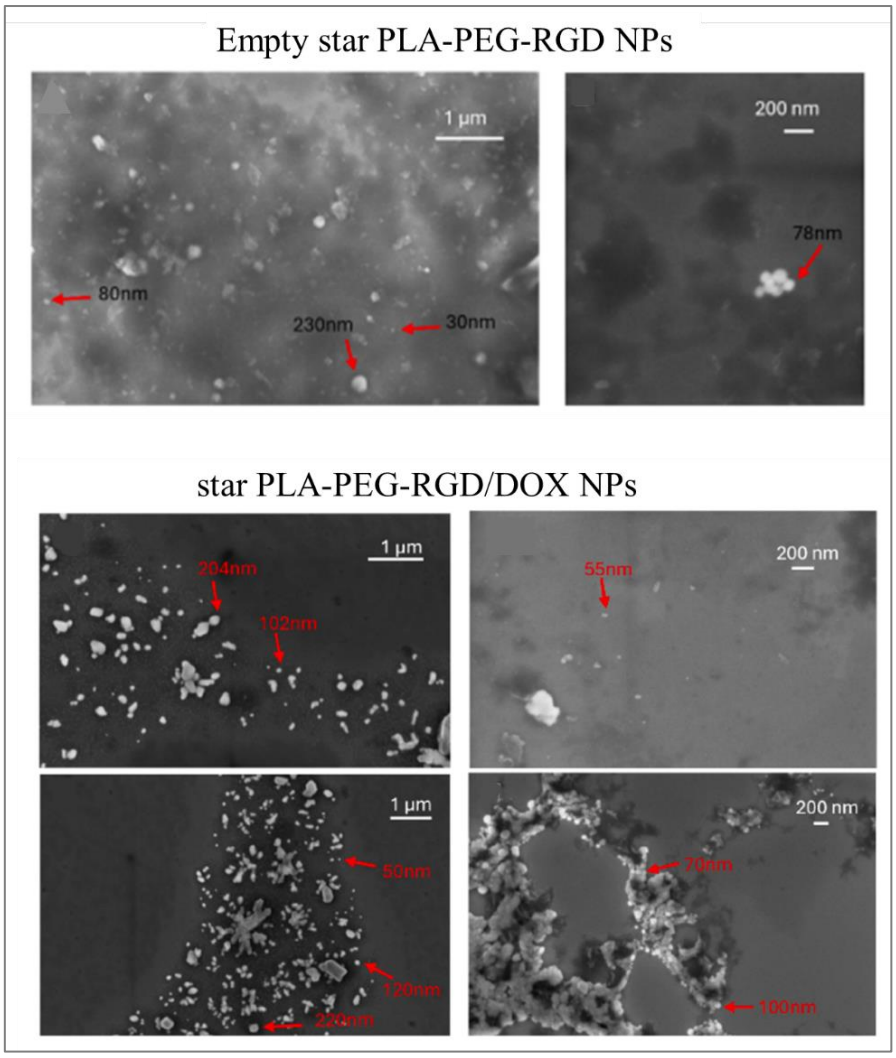

Figure 36 *SEM imaging of empty (up) and DOX-loaded (down) star PLA-PEG-RGD NPs*

Further studies are carried out by ^{1}H-NMR on DOX-loaded star PLA-PEG NPs, in order to achieve structural clarification of the polymeric aggregate and to confirm its ability to incorporate the drug (***Figure 37***).

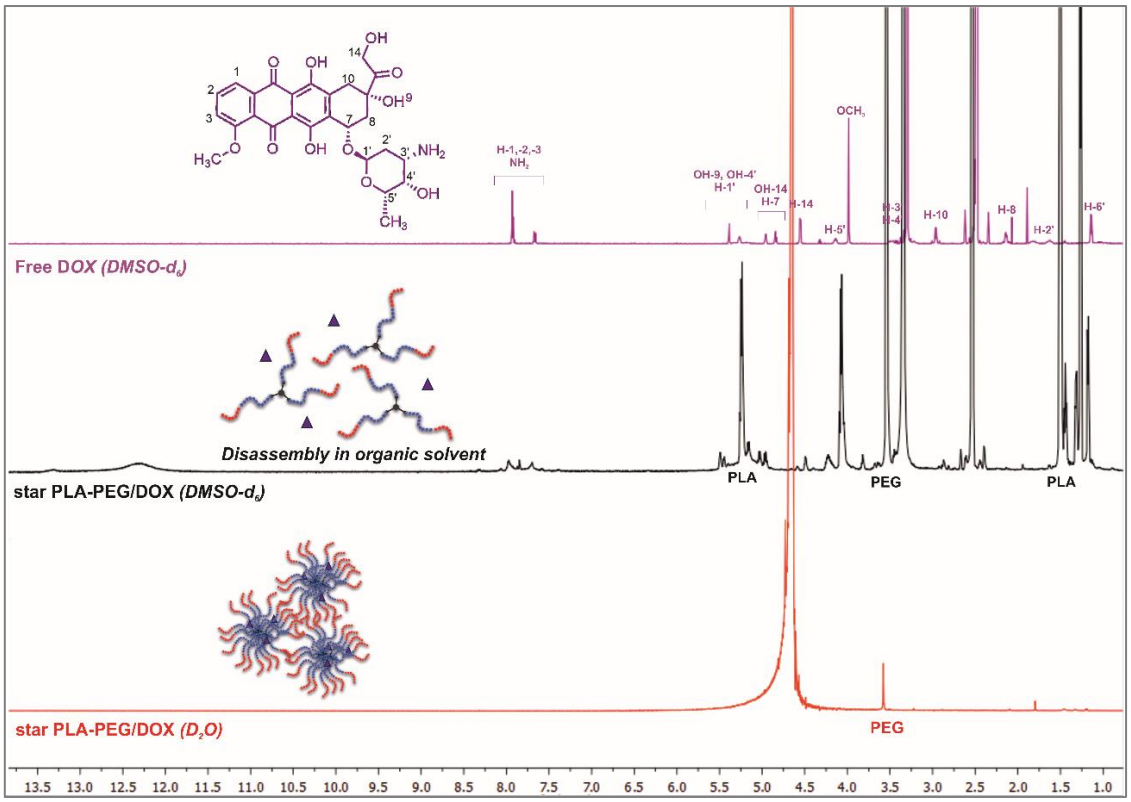

Figure 37 *Stacked NMR spectra of free DOX in DMSO-d_6 (purple trace), disassembled star PLA-PEG NPs in DMSO-d_6 (black trace), star PLA-PEG/DOX NPs in D_2O (red trace)*

In D_2O, the only signal of PEG at 3.7 ppm confirmed the assembly of the polymer into NPs surrounded by a hydrophilic shell. In DMSO-d_6, the typical disassembly of DOX-loaded NPs was highlighted by the presence of all the resonances of PEG, PLA and DOX (***Figure 37)***.

Drug loading (DL) and Encapsulation Efficiency (EE) values of both systems were obtained by UV-Vis quantification dissolving a weighted amount of NPs in DMSO (to promote the NPs disassembly) and detecting the absorbance at λ_{max} 482 nm for DOX and at λ_{max} 274 nm for DTX (***Table 5***).

Table 5 *Drug Loading and Encapsulation Efficiency*

	Drug Loading (%)	**Encapsulation Efficiency (%)**
Star PLA-PEG-RGD/DTX (10:1)	6	57
Star PLA-PEG-RGD/DTX (10:3)	16	69
Star PLA-PEG-RGD/DOX (10:3)	8	35
Star PLA-PEG/DOX (10:3)	5	54

Encapsulation of DTX in NPs was obtained with better results using a 10:3 polymer to drug ratio, achieving 16% of DL and 69% of EE, whereas 6% DL and 57% EE were achieved by the 10:1 formulation. Due to the higher DTX loading and the lower dimension and dispersity of NPs detected by DLS, the 10:3 formulation was selected for the biological investigation.

DOX-loaded NPs owned DL and EE of 8% and 35%, respectively, expectedly lower than the encapsulation achieved for DTX, likely due to the high hydrophobic nature of DTX that favored a more efficient incorporation in the PLA lipophilic core with respect to DOX. However, it was observed that the presence of RGD positively affected DOX loading, since NPs formulated using only undecorated polymer star PLA-PEG achieved lower DL and EE (5% and 54%, respectively)[2].

4.2.2. Stability studies and release profile investigation

The self-assembly of both star PLA-PEG and star PLA-PEG-RGD was investigated by a direct measurement of their CMC in aqueous medium. Solutions of both polymers at increasing concentrations were used to rehydrate identical films of pyrene fluorescent probe. The fluorescence emission intensities of the probe at 338 and 333 nm were monitored as the shift from a lower to a higher wavelength indicated the environment change of the probe, from the aqueous phase to the lipophilic core of the NPs. The intensity ratio of I_{338}/I_{333} plotted against the concentrations of the copolymer allowed to estimate a CMC of 10 μg/mL.

Moreover, stability studies of DTX-loaded nanoformulations re-dispersed after lyophilization were carried out in ultrapure water and in PBS (pH 7.4) at 37°C by monitoring the size distribution and zeta potential, attesting for a good colloidal stability within 7 days.

Release studies in PBS (pH 7.4) were carried out for both drug-loaded nanoformulations by the dialysis bag method at 37°C.

The release study of DTX was very challenging due to the high lipophilicity of the drug and its poor solubility in PBS, requiring the addition of Tween 80 in the release medium to ensure sink condition. Therefore, the release experiment on free DTX was not performed since the high lipophilicity of DTX avoided its solubilization in PBS. For the same reason, to ensure sink conditions and to prevent precipitation of released DTX, Tween 80 was added in the external medium in the release experiment of star PLA-PEG-RGD/DTX. Despite these precautions, an actual release curve for DTX could not be plotted due to the tendency of the released drug to stick to the dialysis membrane, likely due to its high lipophilicity. Therefore, an indirect quantification of the total amount of drug released in 7 days was performed by measuring, by UV-Vis, the amount of unreleased DTX in the internal jacket, resulting about 58%.

Since the release of drug from polymeric NPs is a process mainly associated with the degradation and erosion of the polymer matrix as well as with drug diffusion, the incomplete release of DTX after 7 days may be ascribable to strong interactions between the drug and the polymer itself which is slowly degraded.

Regarding the release of DOX, a stability study of the free drug in PBS was first performed to investigate its tendency to precipitate in physiologically relevant conditions[122,123] (see photograph, ***Figure 38*** *left*) with a proposed mechanism involving a dimerization[124], that would interfere with an accurate estimation of the released drug.

The stability of the free drug was determined monitoring, by UV-Vis analysis, solutions of DOX in PBS at 3 different concentrations at 37 °C within 72 h. The amount of DOX was progressively reducing overtime of the same factor, regardless of the initial concentrations; specifically, 8% of DOX dimer was formed within 5 h and even 50 % after 48 h. A degradation profile of DOX was plotted (***Figure 38,*** *left*) at the same time points used for the release experiment, highlighting how DOX dimerization and precipitation could dramatically affect the release data interpretation. Therefore, our stability study pointed out that a prolonged exposure of DOX in aqueous solution during the release experiments may generate inaccurate results in terms of cumulative percentage release owing to Dox dimer formation and precipitation. Therefore, the

percentage of drug degradation should be considered for a proper interpretation of release data and the ratio between drug release (***Figure 38, right***) and drug degradation (***Figure 38, left***) was responsible for the detected concentration in the receiver compartment.

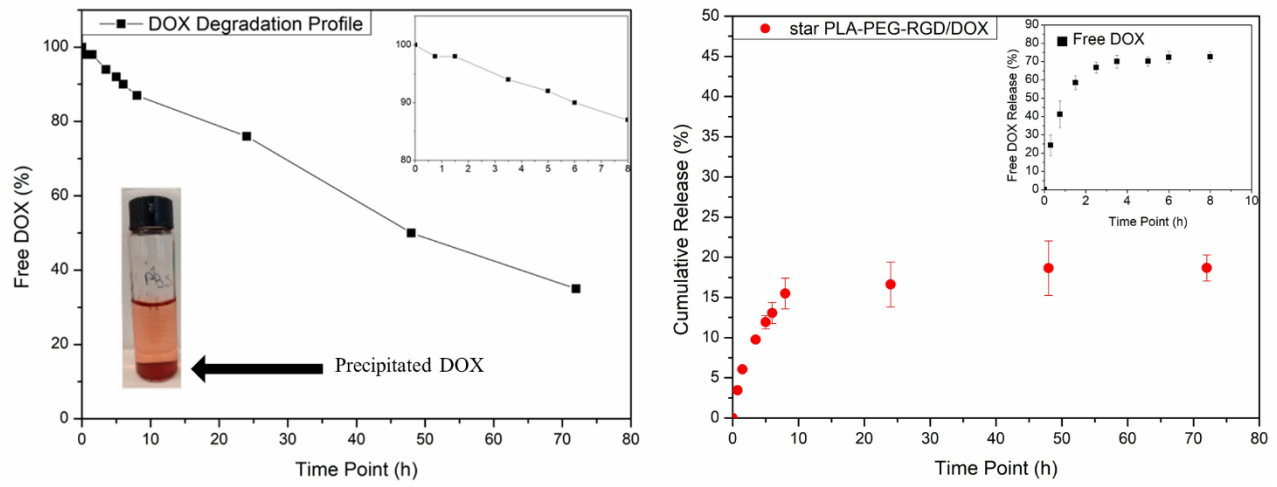

Figure 38 *Degradation profile of DOX in PBS (left); Release profile of DOX in PBS from star PLA-PEG-RGD NPs (right) (●) compared to the release of free DOX (■) (inset) in the same experimental conditions*

The release profile (***Figure 38, right***) showed that free DOX is released much quicker than the drug from star PLA-PEG-RGD NPs, as expected, confirming the ability of polymeric NPs to serve as effective drug carrier for prolonged and sustained release over the time.

Overall, our experiments revealed the pivotal role of RGD-decorated polymeric NPs as protective sleeve for DOX: about 20% of released "monomeric" DOX was detected after 72 hours (***Figure 38, right***); the undetected drug (about 80%), even if partially affected by dimerization over the time, would serve as drug "*reservoir*". Specifically, taking into account a dimer formation ranging from 2 to 65 % within 72 h, about 78-15 % of DOX could be considered still available to be released from the NPs after 72 h confirming the sustained drug release from RGD-decorated star PLA-PEG NPs.

Conversely, star PLA-PEG/DOX NPs without RGD decoration did not release DOX within 72 hours under the same experimental conditions.

4.2.3. Biological assays on star PLA-PEG-RGD/DTX

The first step of the biological investigation of DTX-loaded NPs aimed to exclude any cytotoxic effect of empty RGD-decorated NPs by MTT viability test. Cellular culture of Adipose-derived Mesenchymal Stem Cells (Ad-MSC), used as healthy cells model, were exposed to different concentrations of empty star PLA-PEG-RGD NPs (52, 105, 158 μg/mL) for 24, 48 and 72 hours. The viability test evidenced the absence of toxicity of the polymeric material at any tested concentration and any time points, confirming its biocompatibility (***Figure 39***).

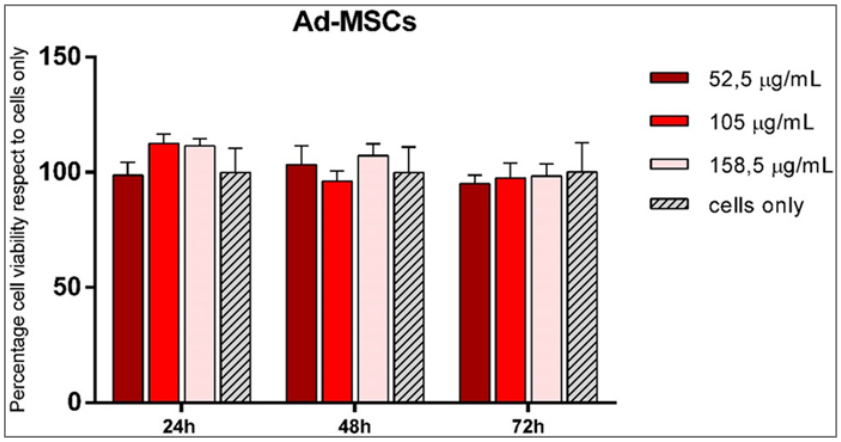

Figure 39 *Absence of cytotoxic effects of empty star PLA-PEG-RGD on healthy cell model (Ad-MSC).*

Further biological experiments were carried out to determine the cytotoxic effect of nanoformulations on cancerous cells. DTX-loaded NPs were tested against human Glioblastoma (U87) (***Figure 40***) and Breast Adenocarcinoma 468 (MDA-MB 468) (***Figure 41***) tumoral cell lines, as models of two most common primary and metastatic tumors. They were exposed for 24, 48 and 72 hours to three different concentrations of DTX-loaded NPs (52, 105, 158 μg/mL of NPs containing 10, 20 and 30 μg/mL of drug, respectively) comparing the effect of free DTX at the same concentrations.

The biological profile was evaluated by MTT (***Figures 40 and 41***), cell morphology analysis (***Figure 42)***, and scratch test (***Figures 43 and 44)***.

The free drug exhibited high cytotoxic effects compared to cells only at all tested concentrations for both cell lines; star PLA-PEG-RGD/DTX NPs were responsible for a significant reduction of viability for both cell lines at all the investigated time points, with a time-dependent cytotoxic effects at all tested concentrations against MDA-MB 468 cells. However, the effects of DTX loaded in NPs appeared to be hidden against both the cell lines as demonstrated by the higher activity of 20 and 30 μg/mL of free DTX compared to the same concentration of loaded drug against U87 cells at 48 and 72 h, likely due to different release kinetics and bioavailability (***Figures 40 and 41***).

Interestingly, an unexpected and relevant anticancer effect was exerted by unloaded RGD-decorated NPs on both cellular lines. Specifically, while at 24 hours the free drug exhibited higher activity compared to both loaded and unloaded NPs against MDA-MB 468 (***Figures 41)***, empty RGD-decorated NPs showed a cytotoxic effect comparable to that of free DTX and star PLA-PEG-RGD/DTX at 48 and 72 hours, (about 40 % and 60 % of dead cells, respectively) at all tested concentrations. Moreover, empty star PLA-PEG-RGD NPs induced a significant reduction of U87 cell viability compared to cells only at 72 hours (about 30 % of dead cells) at the highest concentrations (***Figures 40***).

Overall, our results attested for a high antitumoral effect exerted by DTX, as expected, due to the immediate availability of free drug, while the performance of the nanoformulations dealt with the sustained release of the drug. A significant cytotoxic effect was exerted by DTX-loaded star PLA-PEG-RGD NPs against tumoral cellular lines that is not observed on healthy cells model. Moreover, an unprecedented effect on cell viability was exerted also by empty RGD-decorated NPs, likely due to the enhanced cellular uptake and toxicity promoted by the presence of RGD targeting moiety.

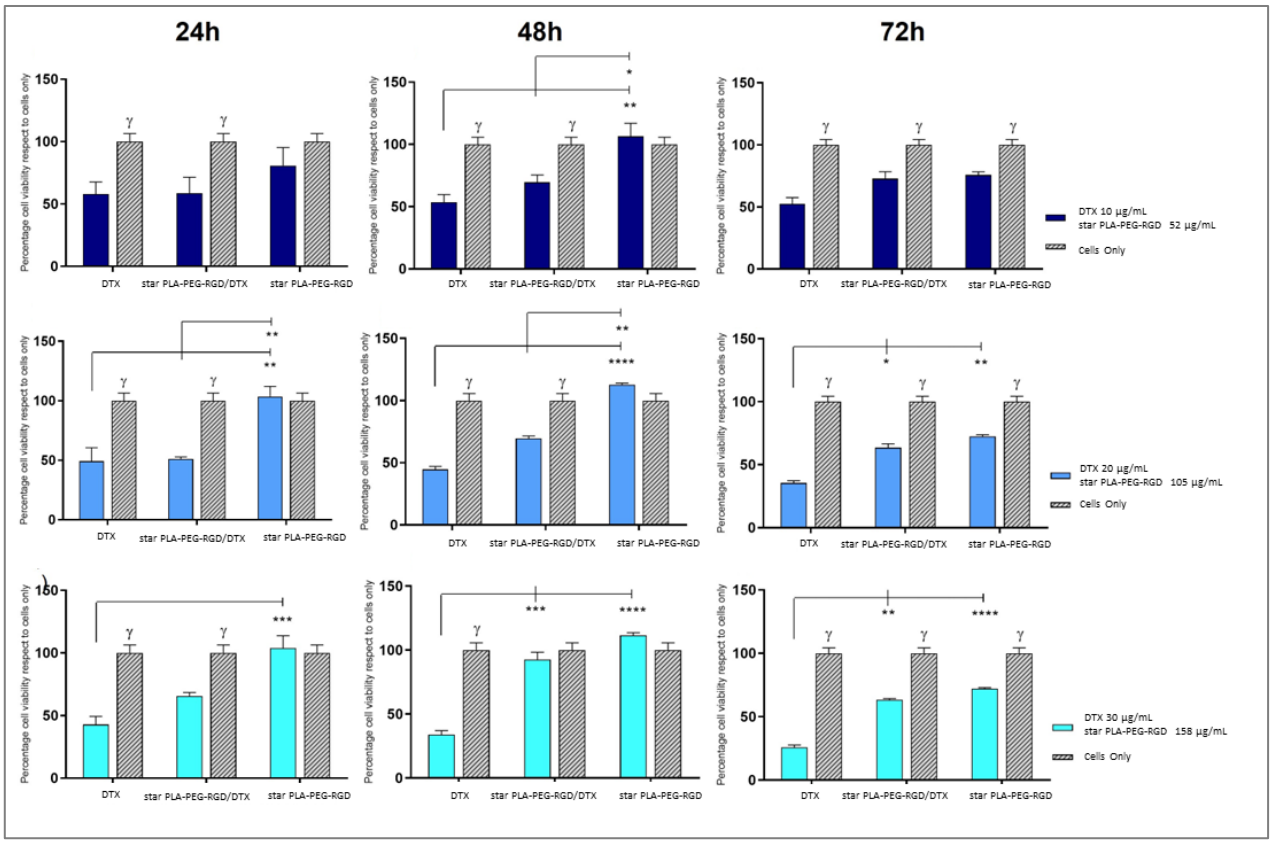

Figure 40 *Cellular vitality assay of U87 glioblastoma treated with free DTX, star PLA-PEG-RGD NPs and empty NPs*

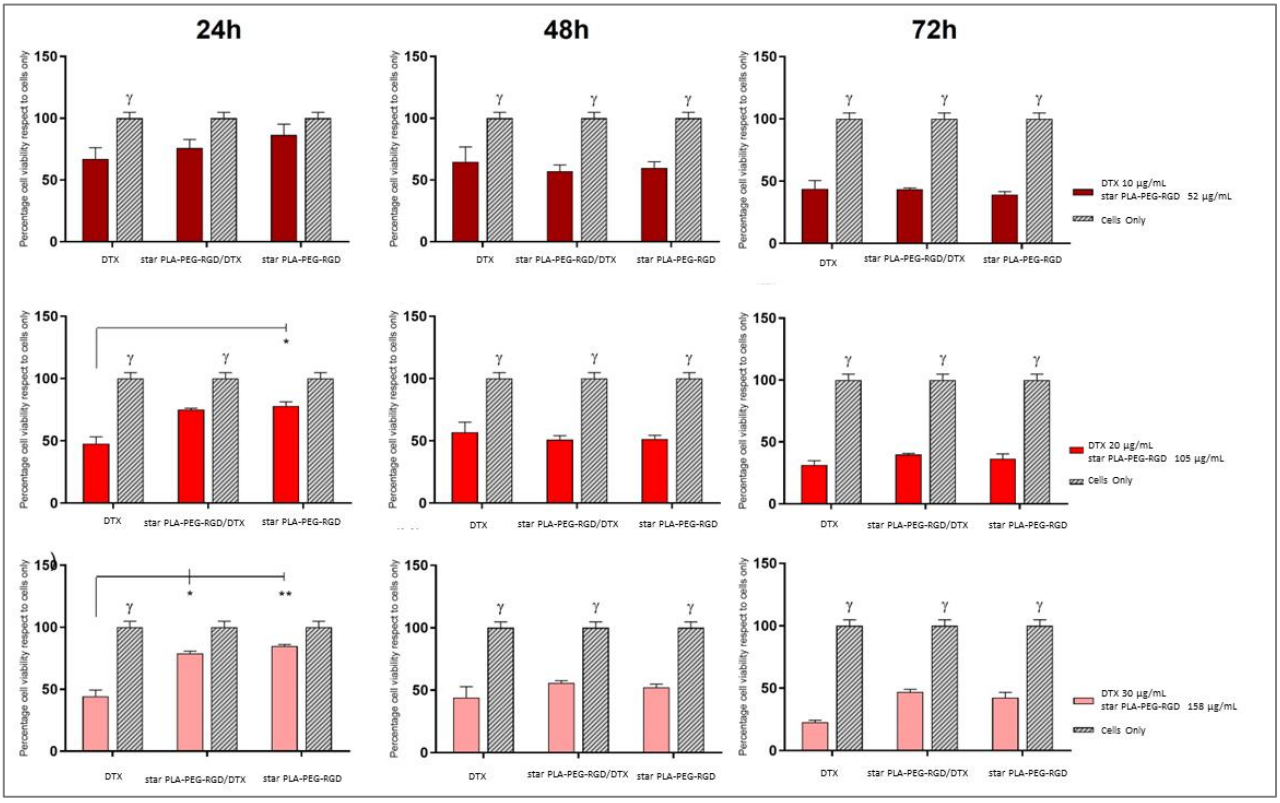

Figure 41 *Cellular vitality assay MDA-MB treated with free DTX, star PLA-PEG-RGD NPs and empty NPs*

Morphological analysis on U87 and MDA-MB treated with free DTX, star PLA-PEG-RGD/DTX NPs and unloaded NPs for 24 hours attested for a compromised morphology especially in U87 cells treated with DTX and star PLA-PEG-RGD/DTX compared to cells only (***Figure 42***). While no morphological alteration was noticed on both cell lines treated with empty NPs at 24 h, a slight reduction of cells number was observed compared to cells only at later time points, confirming the previously reported long-term cytotoxic effects exerted by unloaded NPs.

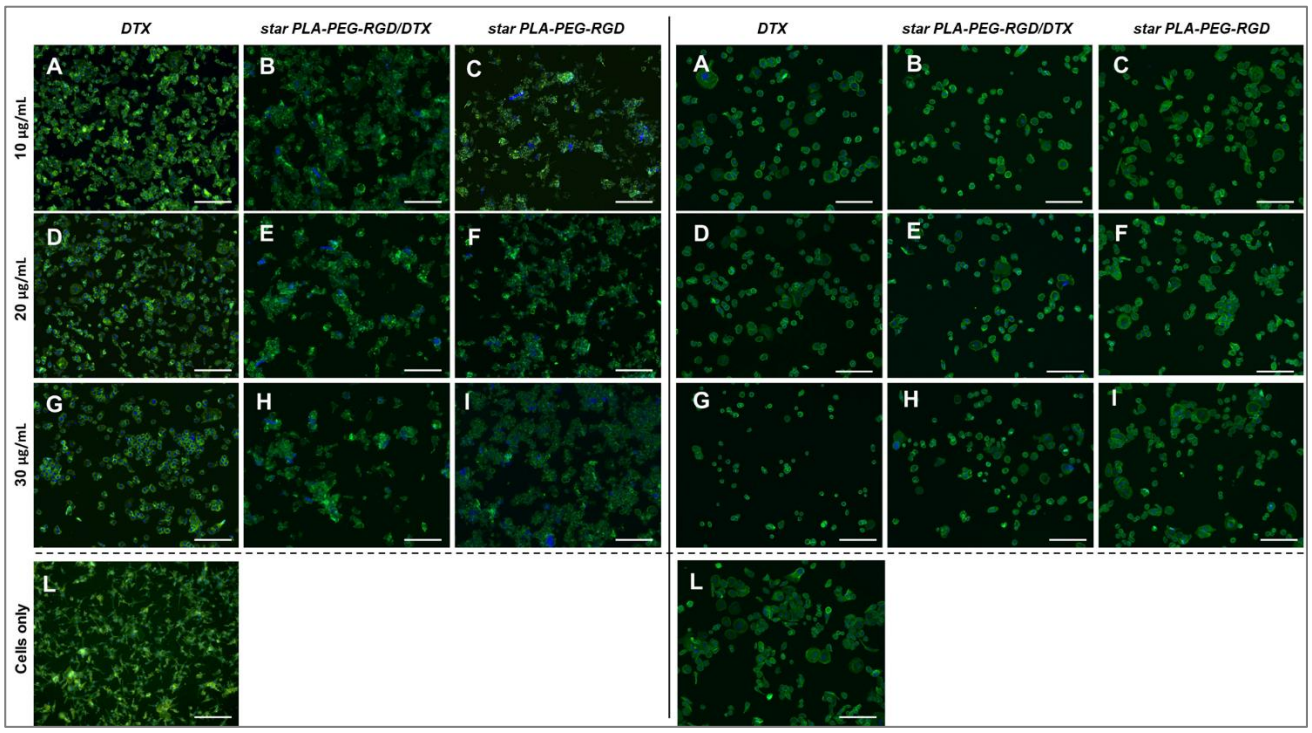

Figure 42 *Morphological analysis of U87 (panel left) and MDA-MB (panel right) cell lines after treatment with free DTX, star PLA-PEG-RGD NPs and empty star PLA-PEG-RGD NPs*

Lastly, a special focus was reserved to the investigation of the role of star PLA-PEG-RGD/DTX NPs in inhibiting cancer cell migration that is associated with the process of metastasis. A scratch test was carried out monitoring the distance (µm) that the tumoral cells were able to cover over time towards the centre of a scratch performed at time 0 in the well (***Figure 43***). Our results highlighted the inhibition of cell migration in the presence of star PLA-PEG-RGD/DTX NPs and free DTX, compared to cells

only, in both U87 (***Figure 43, panel left***) and MDA-MB 468 cells (***Figure 43, panel right***).

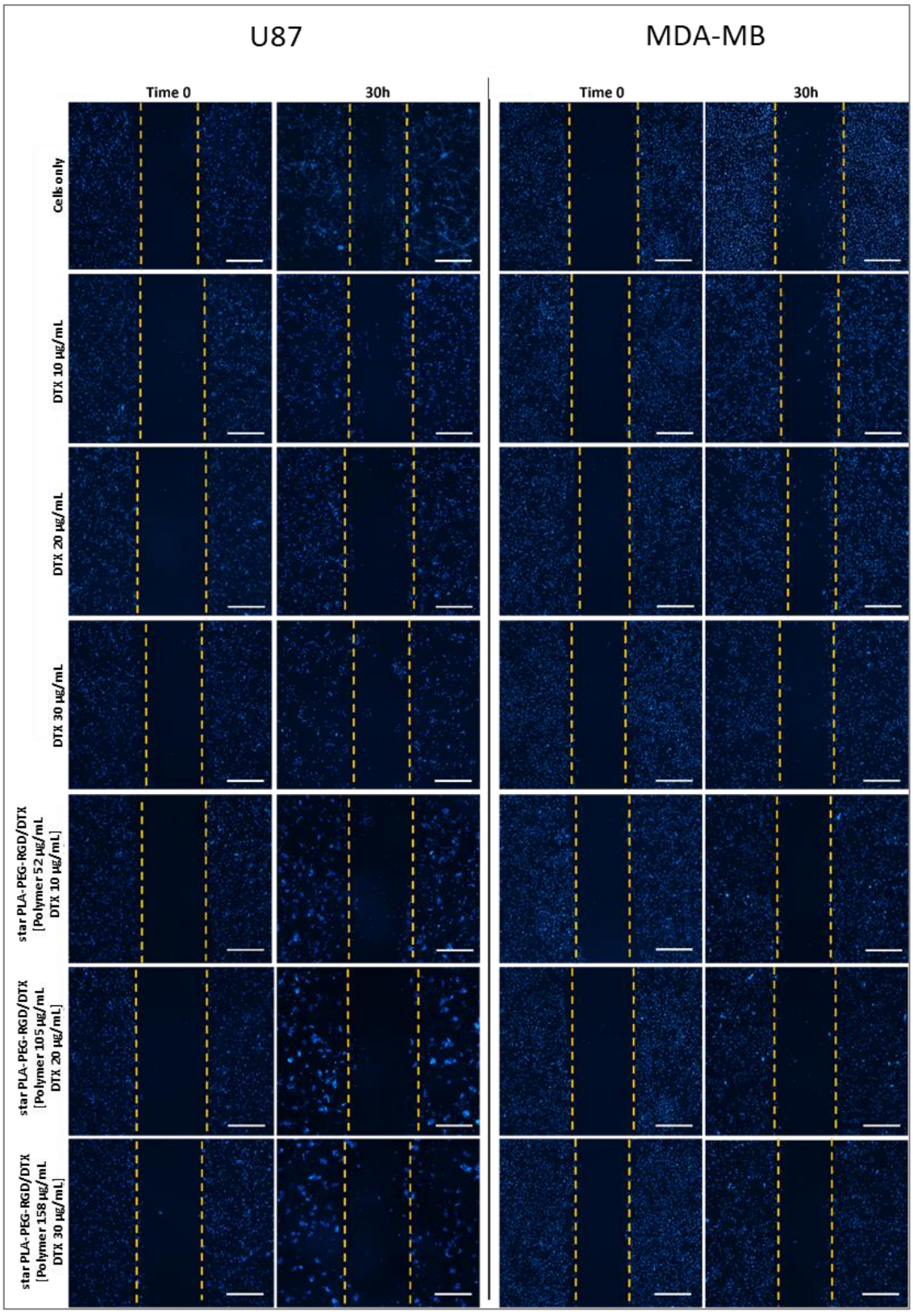

Figure 43 *Scratch test performed on U87 cells (left) and MDA-MB cells (right)*

Overall, cellular migration was significantly inhibited after treatment with free DTX and DTX-loaded NPs for both cancerous cellular lines compared to cells only at all the tested concentration, starting from 24 h (***Figure 44***). Interestingly, the treatment of both cellular lines with NPs incorporating 10 and 30 µg/mL DTX achieved a greater migratory inhibition than the free drug at the same concentrations. More in detail, U87 cells treated with 30 µg/mL of DTX-loaded NPs achieved a migration of 43 µm against the 73 µm covered in the presence of free DTX at the same concentration; MDA-MB 468 showed an even higher susceptibility to the treatment with DTX-loaded NPs, as no migration was observed with 10 µg/mL of DTX-loaded NPs, while a distance of 50 µm was covered in the presence of free drug at the same concentration (***Figure 44***). Overall, the results of the scratch test attested for a good ability of DTX-loaded star PLA-PEG-RGD NPs to reduce tumor propagation and invasiveness, enhancing the typical effect of DTX on metastatization.

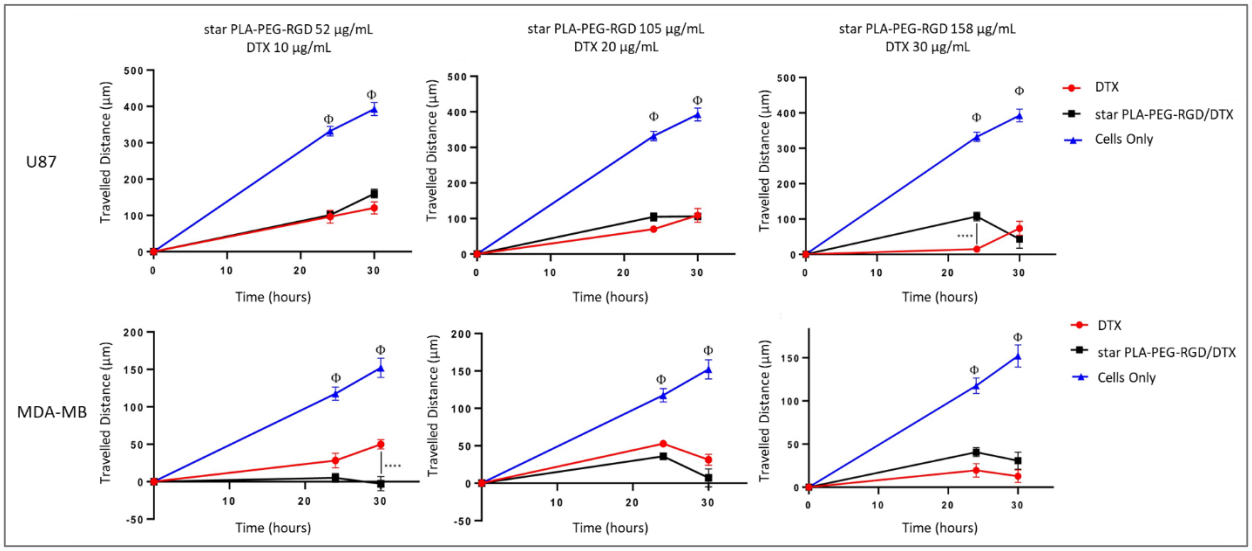

Figure 44 *Migrated distance after scratch test on U87 and MDA-MB cells treated with free DTX and DTX-loaded NPs*

4.2.4. Biological assays on star PLA-PEG-RGD/DOX and star PLA-PEG/DOX NPs

DOX-loaded nanoformulations, both RGD-targeted and untargeted, were tested against MG63, SAOS-2, and U2-OS osteosarcoma cells.

The detection of DOX fluorescence and its colocalization with the blue, DAPI-stained *nuclei*, in cellular uptake experiments, demonstrated that DOX loaded on star PLA-PEG-RGD NPs easily reached the cell nuclei at 72 h, as well as free Dox (***Figure 45***).

On the other hand, DOX loaded in untargeted star PLA-PEG NPs did not achieve nuclear localization as DOX was localized exclusively on the cytoplasm (***Figure 45***). Our investigation on cellular uptake provided preliminary results attesting the crucial role played by RGD moiety, likely promoting an internalization pathway that favored the direct nuclear localization of DOX. In the nucleus, the inhibition of topoisomerase-II was recognized as one of the major cytotoxic effects of DOX[125].

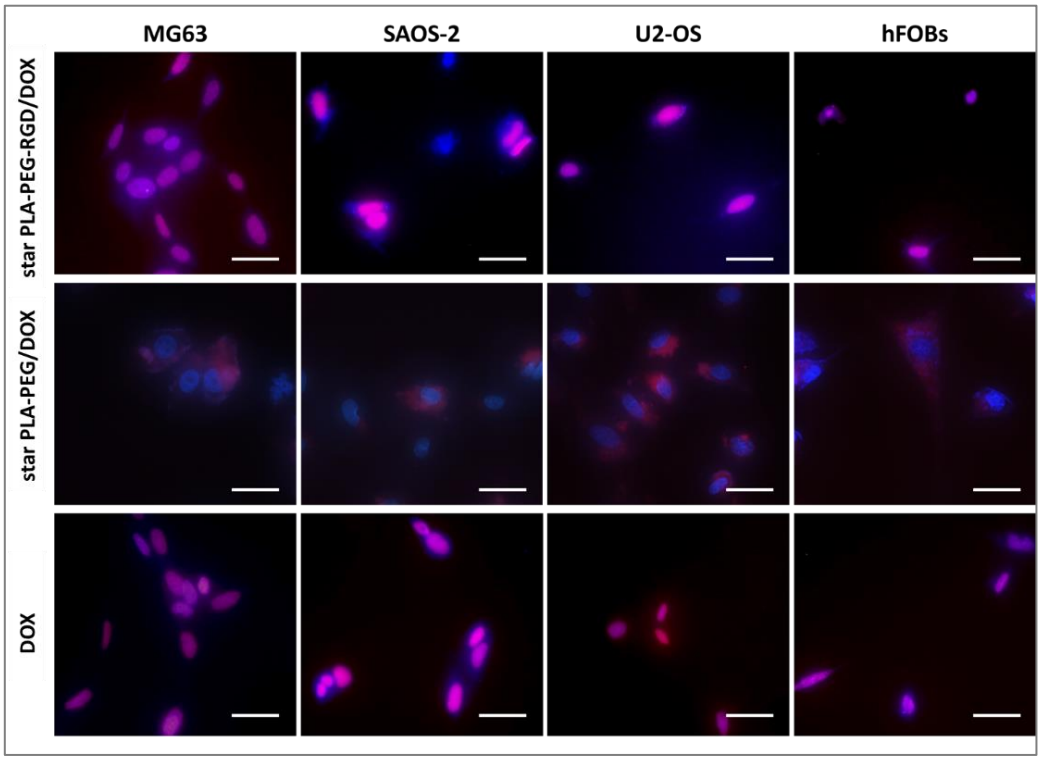

Figure 45 *Investigation of cellular uptake of free DOX and DOX delivered by star PLA-PEG-RGD NPs and untargeted star PLA-PEG NPs*

These results were confirmed by MTT viability assays performed on MG63, SAOS-2, and U2-OS osteosarcoma cells and healthy osteoblasts (hFOBs) (***Figure 46***). RGD-decorated NPs (incorporating 2.7, 5.4 and 10.8 µg/mL of DOX) showed cytotoxic effect comparable to those of free DOX at all tested concentration after 72 hours, according to the observed nuclear localization. Furthermore, accounting for the information obtained by our release and degradation studies (about 20% of active DOX is detected at 72 hours), it's possible to speculate a role of our nanosystem both in protecting the drug from degradation and acting as a *depot* for the payload, able to release the drug overtime in a prolonged and sustained way.

Conversely, star PLA-PEG/DOX NPs did not exert relevant cytotoxic effect compared to the free drug at the same concentration in line with the observed cytoplasmatic localization (data not shown).

Generally, free DOX rapidly diffuses into the cellular nucleus, while DOX released from nanosystems reaches the nucleus within 24-48 h upon their lysosomal processing[126]. However, the exclusive presence of DOX delivered by undecorated star PLA-PEG NPs in the cytoplasm after 72 hours could be likely due to an inefficient acidic and enzymatic lysosomal digestion that did not guarantee the drug release from the NPs and, accordingly, no cytotoxic effect was observed under our experimental conditions.

Lastly, analyzing the effects of empty star PLA-PEG-RGD NPs on osteoblast cells (hFOBs), an expected absence of cytotoxicity was observed (***Figure 46***), confirming the biocompatibility of the material. At the same time, moderate cytotoxic effects were noticed on some cancerous cell lines, likely due to intrinsic biological differences related to expression of $\alpha_v\beta_3$ and $\alpha_v\beta_5$ integrins, that are cell surface receptors of RGD overexpressed in some cancer cells[127,128]. Specifically, a decrease of MG63 viability was detected at every tested concentration, while for SAOS-2 a dose-dependent cytotoxic effect was observed; only U2-OS cells seemed to be not affected by the treatment with empty NPs (***Figure 46***).

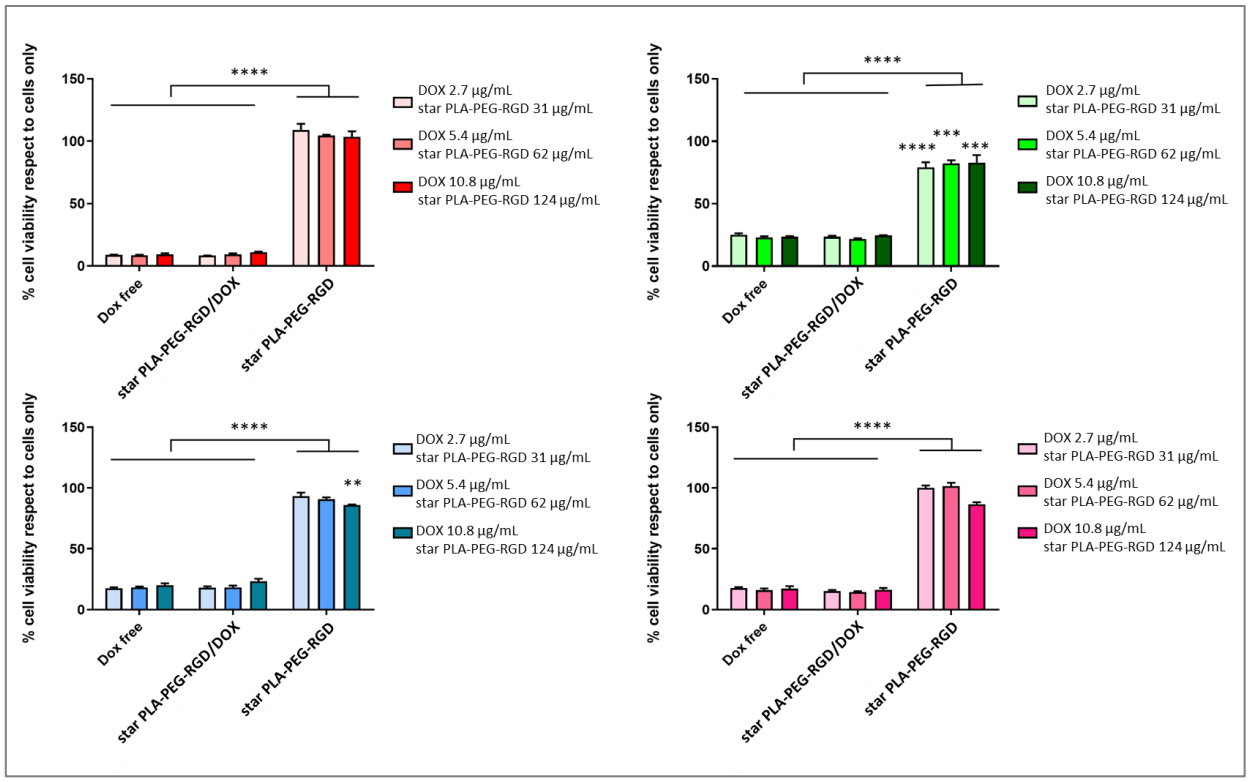

Figure 46 *Viability assays on hFOB (top left), MG63 (top right), SAOS-2 (bottom left) and U2-OS (bottom right) cell lines treated with free DOX, star PLA-PEG-RGD/DOX NPs and empty star PLA-PEG-RGD NPs*

A final morphological analysis of the cells treated with empty star PLA-PEG-RGD NPs produced results in line with the MTT viability assay, showing that, even if present, the cytotoxic effect of our nanosystem was limited since the surviving cells maintained their typical morphology without evident aberrations (***Figure 47***).

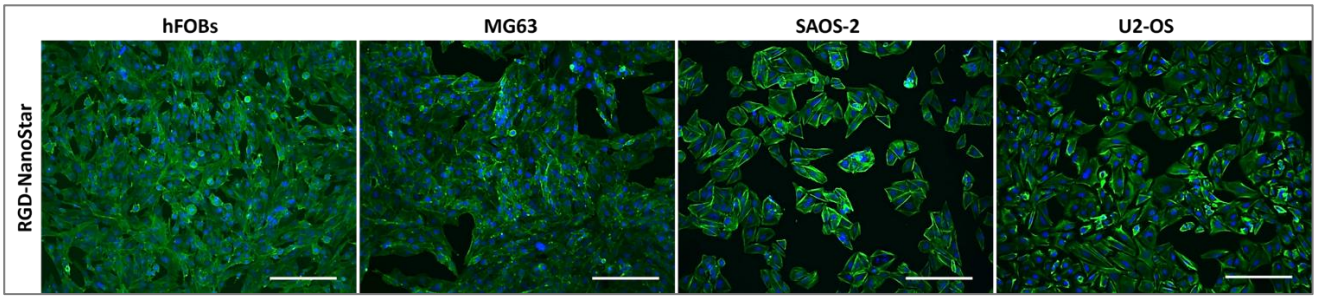

Figure 47 *Morphological analysis of the four cell lines treated with empty star PLA-PEG-RGD NPs*

Overall, our investigations attested that the DDS based on star PLA-PEG turned out to be able to incorporate two different antitumoral drugs (Docetaxel and

Doxorubicin) with satisfying encapsulation efficiency exerting a selective action against tumoral cells. The decoration of our polymeric DDS with RGD targeting moiety promoted the cellular uptake of DTX-loaded NPs enhancing the cytotoxicity. Moreover, RGD receptor-mediated uptake allowed DOX-loaded NPs to selectively drive the payload into the cellular nucleus, allowing for a cytotoxic effect comparable to the free drug but exerted by only a fraction of the total amount of DOX incorporated which is slowly released over the time.

4.3. Formulation of lipodisks for MEDS433 incorporation

During my foreign 6-months abroad at the University of Uppsala (Sweden), under the supervision of Professor Katarina Edwards, my research activity focused on formulation and characterization of lipodisks nanocarriers for the entrapment of the antiviral MEDS433.

MEDS433 is an *in house* dihydroorotate dehydrogenase (hDHODH) inhibitor, acting as Broad Spectrum Antiviral Agent (BSAA) able to reduce the replication of a large virus panel, including SARS-CoV-2. Specifically, MEDS433 developed at the University of Turin (Department of Drug Science and Technology) by Marco L. Lolli's Group[129,130,131] turned out to be one log unit more potent that the best available and FDA-approved therapy, *i.e.* Remdesivir (EC50 0.77 μM). Astonishing preliminary data indicated MEDS433 as capable to potently inhibit the *in vitro* SARS-CoV-2 replication (EC50 0.063 μM, Vero E6 cells) with a great safety and *in vitro*/*vivo* profile (Safety Index (SI) >7900).

Human Dihydroorotate Dehydrogenase (hDHODH) enzyme represents a paradigm for the development of *Host-Targeting Antivirals* (HTAs) that act by interfering with cellular biochemical pathways used by different viruses for the replication; thus they are able to overcome virus specificity and potential viral mutagenesis of virus-directed agents. In fact, hDHODH catalyzes, inside host cells, the

fourth step in the *de novo* biosynthesis of pyrimidines, key building blocks required for DNA and RNA production. While usually human cells can satisfy ongoing demands for such DNA/RNA need through the recycling of pre-existing nucleosides, virally-infected cells require active *de novo* biosynthesis of pyrimidines to fulfil pyrimidines demand resulting from viral replication. Therefore, hDHODH pathway is pivotal for the replication of many viruses[132].

By targeting hDHODH, MEDS433 is able to lead the infected cell in a condition named *"pyrimidine starvation"* (***Figure 48***). In such condition, the virus is unable to replicate and becomes prey of the immune defensive system. Such mechanism could be applied potentially to target any virus and will be effective also when the virus will start to mutate (variants) during pandemic events.

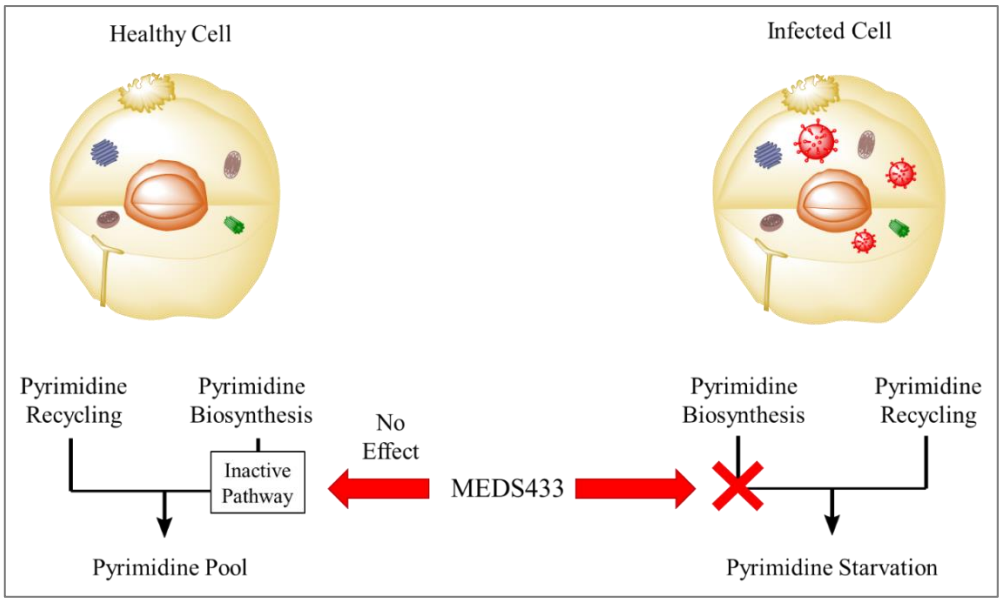

Figure 48 *Mechanism of action of MEDS433, leading to selective pyrimidine starvation of infected cells*

Since March 2020, several independent studies granted by governments, specifically in China[133], have focused on the development of hDHODH inhibitors against COVID-19 with dual action of antiviral activity and immuno-repression, effective against the so-called cytokine/chemokine storm that causes worsening of the disease.

In the framework of VIPER project granted by the NATO *Call* "*Science for Peace and Security"* (*VIPER: "Learning a lesson: fighting SARS-CoV-2 Infection and get ready for other future PandEmic scenarios"*), MEDS433 was incorporated into water soluble DDS based on lipodisks and cyclodextrins suitable for *in vivo* tests with the aim to improve the water solubility (12 μM) and the farmacokinetic profile of MEDS433.

VIPER project aimed to prove the concept of MEDS433 as an effective *in vivo* agent in SARS-CoV-2 and several respiratory viruses, offering a new therapeutic option to reinforce the current arsenal of therapeutic possibilities for COVID-19 as well as future emerging and re-emerging viral diseases. The repositioning of existing safe-in-man BSAAs from a pandemic event to another is certainly faster and cheaper than the development of virus-specific drugs and vaccines.

A series of commercially available phospholipids were employed for the nanoformulation of lipodisks incorporating MEDS433, including 1-palmitoyl-2-oleoyl-sn-glycero-3-phosphocholine (POPC), cholesterol (CHOL), 1,2-distearoyl-sn-glycero-3-phosphoethanolamine-N-[amino(polyethylene glycol)-2000 (DSPE-PEG_{2000}), phosphatidylcholine (HSPC) (***Figure 49***).

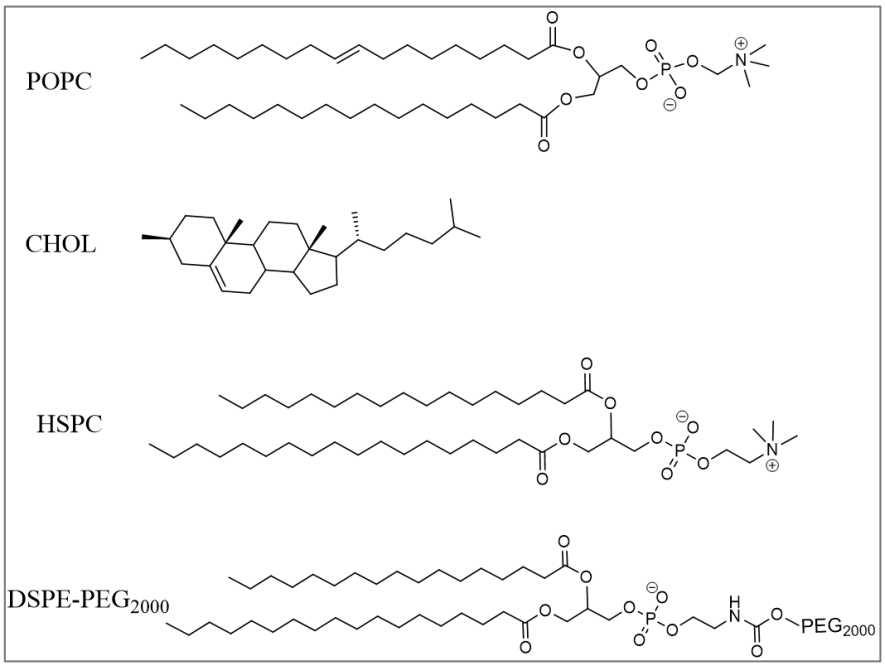

Figure 49 *Structure of phospholipids used for the formulation of lipodisks incorporating MEDS433*

Specifically, two types of lipodisks with different phospholipidic composition were formulated: POPC:CHOL:DSPE-PEG_{2000} (40:40:20) and HSPC:DSPE-PEG_{2000} (80:20). It is well known that the phospholipidic composition affects the stability of the nanosystems as well as the drug loading. Saturated phospholipids (HSPC) assemble into relatively rigid, stable and highly lipophilic bilayer, able to incorporate hydrophobic drug and to prevent its leakage. Conversely, unsaturated components, such as POPC, form loose, unstable structures, unable to withstand drug permeation to the external environment.

Cholesterol is generally included in the formulation to confer to the bilayer a higher rigidity and resistance to permeation[134] and offers the advantage of mimicking biological membranes, facilitating the cellular uptake and the intracellular release of the payload[135,136]. Furthermore, it was observed that cholesterol increased the hydrophobic character of the bilayer, preventing its permeation by water which is more easily adsorbed around the polar heads and facilitates accumulation of more hydrophilic drugs in this external shell[134].

Both our lipodisk formulations (POPC:CHOL:DSPE-PEG_{2000} and HSPC:DSPE-PEG_{2000}) included 20% of PEGylated phospholipid necessary for achieving the exclusive formation of lipodisks without liposome population[79].

Several formulations were investigated using different ratios of phospholipids to MEDS433 (40:1, 30:1 and 20:1), pointing out that the 30:1 ratio of lipids to MEDS433 led to a maximum encapsulation efficiency.

The formulation procedure consisted of preparing a thin “film” of phospholipids and MEDS433 (obtained after dissolving them in methanol and evaporating the solvent) which was rehydrated with HEPES buffer and kept at 65°C for 1 hour while vortexing every 10 minutes to form a heterogeneous suspension of lamellar macroassemblies[137]. Then, in order to homogenize the sample, the macroassemblies are broken apart by means of tip sonication performed for 5 minutes, affording lipodisks.

Extra care is taken into the vortexation and sonication steps ensuring that they're performed at a low intensity. Otherwise, aggressive procedures might lead to formation of cavitation bubbles with consequent PEG degradation, either by direct physical or thermal action or indirectly, by causing the formation of oxygen reactive species[138]. This PEG degradation[139] might reduce its contribution in lipodisks composition below 20% leading to the formation of liposomes alongside lipodisks.

The lipodisks suspension was separated as a supernatant by strong centrifugation (13000 RPM) from the non-incorporated insoluble MEDS433 and any metal residue coming from the tip-sonicator, collected at the bottom of the vial as a precipitate (***Figure 50***).

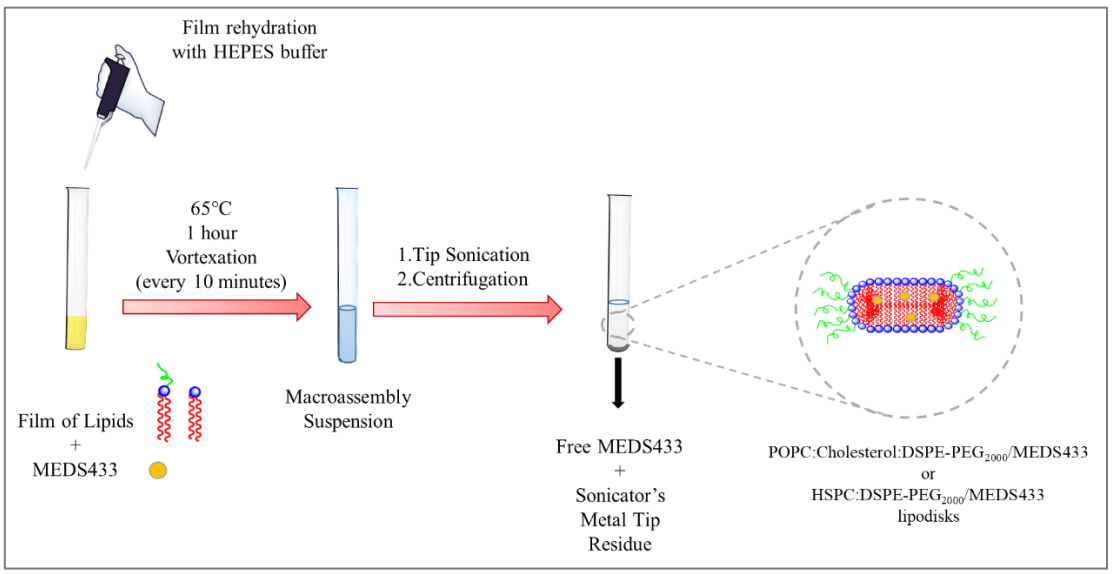

Figure 50 *Nanoformulation method for lipodisks preparation and MEDS433 incorporation*

Physico-chemical characterization was carried out by DLS (***Table 6***) and Cryo-TEM (***Figure 51***). For both type of lipodisks, DLS provided a statistical data regarding the average dimensions of the lipodisks ranging between 24-34 nm with low dispersity (***Table 6***). Cryo-TEM imaging was employed for morphological characterization of the samples: lipodisks are recognizable since they appear as uniformly faint, round objects when *"face on"* to the detector, and as darker sticks if *"edge-on"*[140]. Both formulations are populated only by lipodisks, confirming that no degradation of PEG occurred

during formulation, and the size observed by Cryo-TEM were comparable with the data provided by DLS.

Table 6 *Hydrodynamic diameter of lipodisks incorporating MEDS433*

	Hydrodynamic Diameter (nm)	**PDI**
POPC:CHOL:DSPE-PEG$_{2000}$/MEDS433	33.80	0.12
HSPC:DSPE-PEG$_{2000}$/MEDS433	24.43	0.09

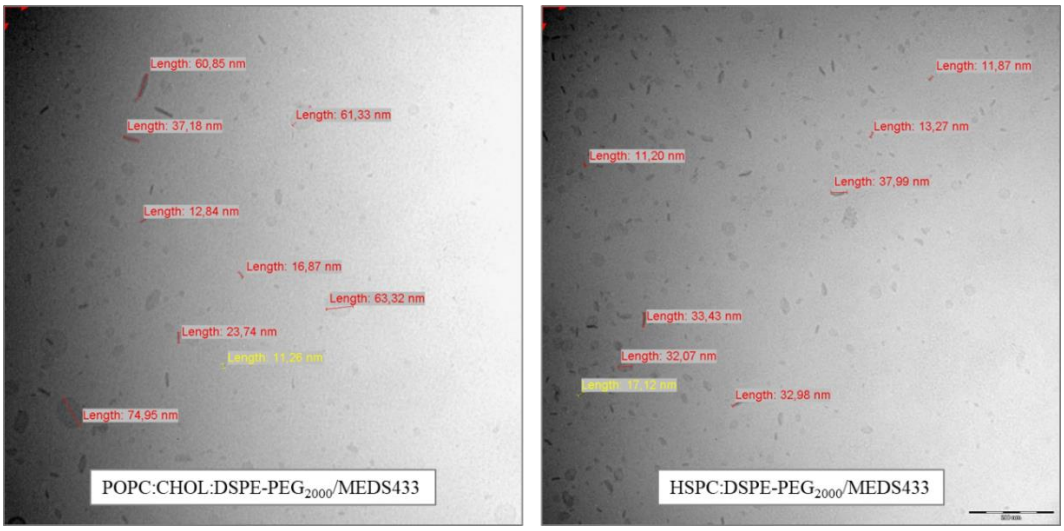

Figure 51 *Cryo-TEM imaging of both formulations of lipodisks*

For Encapsulation Efficiency (EE) determination, 400 µl of suspensions were dissolved in 2 mL of ethanol able to promote the disassembly of the lipodisks and the consequent release of the incorporated MEDS433. The drug was quantified by UV-Vis analysis. Furthermore, the unloaded MEDS433 precipitated after centrifugation was dissolved in the same solvent (400 µl of HEPES buffer and 2 mL of ethanol) and quantified by UV-Vis measurement. Overall, an excellent EE was achieved for both the nanoformulations (84% and 88% for POPC:CHOL:DSPE-PEG$_{2000}$ and HSPC:DSPE-PEG$_{2000}$, respectively).

Moreover, calcination of lipodisks suspension was carried out to determine the amount of phosphorus and, therefore, the exact amount of phospholipids in the formulation.

Having quantified the amount of incorporated drug, the total amount of drug and the exact amount of lipids used in the formulation, the EE and the drug to lipid ratio were calculated (***Table*** 7).

Table 7 *Drug loading and encapsulation efficiency of MEDS433 into lipodisks*

	Drug/Lipid Ratio	**Encapsulation Efficiency (%)**	**Drug Solubility Increase**
POPC:CHOL:DSPE-PEG$_{2000}$/MED433	0.028	84	8.8
HSPC:DSPE-PEG$_{2000}$/MEDS433	0.032	88	9.8

Overall, the two lipodisks formulations with different chemical composition owned comparable dimensions and ability to encapsulate MEDS433. Most importantly, they both achieved a 10-fold increase in drug solubility (***Table 7***).

The stability of the HSPC:DSPE-PEG$_{2000}$/MEDS433 suspension was investigated both at room temperature within 7 days and at refrigerated conditions (4°C) within 2 months monitoring lipodisks' size by DLS measurements, showing no substantial change in the hydrodynamic diameter (***Table 8***), and by Cryo-TEM imaging, confirming that no morphological variation occurred (***Figure 52***).

Table 8 *Stability investigation by hydrodynamic size monitoring of HSPC:DSPE-PEG$_{2000}$/MEDS433 formulation at room temperature and at 4°C*

		Room temperature			**4°C**		
	Fresh	*1 day*	*2 days*	*7 days*	*7 days*	*1 month*	*2 months*
Hydrodynamic Diameter (nm)	25.55	24.36	24.07	26.93	25.12	25.82	24.56

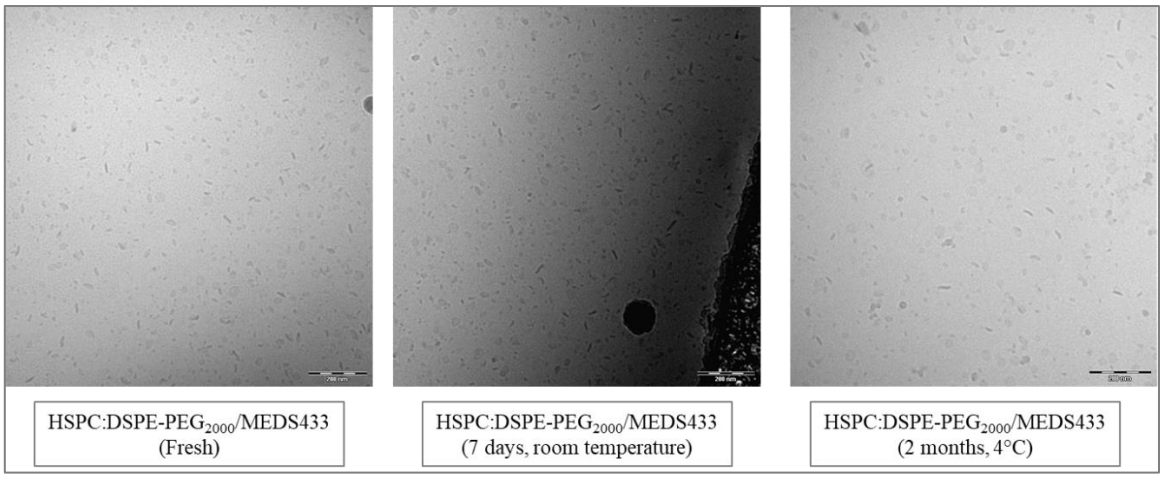

Figure 52 *HSPC:DSPE-PEG$_{2000}$/MEDS433 morphological stability study. Compared to the fresh formulation (left), no shape change is recognizable in the sample after 1 week at room temperature (center) or after 2 months at 4°C (right)*

The release profile of the drug from both the formulations, POPC:CHOL:DSPE-PEG$_{2000}$/MEDS433 and HSPC:DSPE-PEG$_{2000}$/MEDS433, was investigated within 48 hours at 37°C. 500 μL of lipodisks' suspension containing 24 μg of MEDS433 was transferred inside a dialysis bag and dialyzed against 25 mL of HEPES buffer with 0.1% Tween 80 to ensure sink conditions. By fluorimetric analysis the emission of MEDS433 released by the nanosystem was detected. The percentage of drug released at each time point was expressed as the ratio of the emission intensity of MEDS433 in the external medium at every time point and the emission intensity of the total amount of MEDS433 found in the external medium after bursting the dialysis bag at the last time point (48 h, end of the experiment).

The release of free MEDS433 was monitored under the same experimental conditions, but at concentration 12 μM (the solubility limit) and its release profile was compared with the two nanoformulations (***Figure 53***).

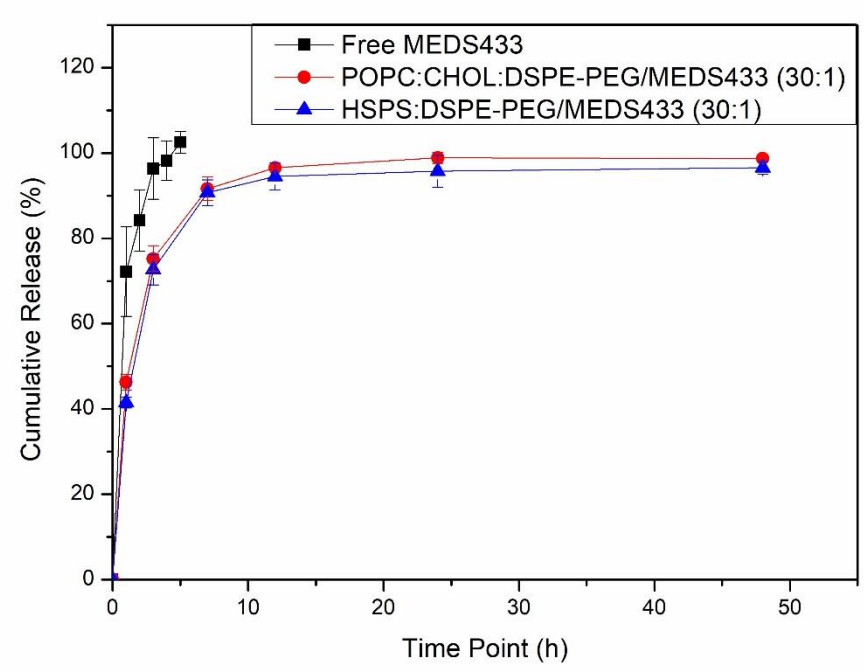

Figure 53 *Cumulative release profile of free MEDS433 (■), POPC:CHOL:DSPE-PEG$_{2000}$/MEDS433 (●), and HSPC:DSPE-PEG$_{2000}$/MEDS433 (▲)*

Both MEDS433-loaded lipodisk formulations showed burst release with about 40% of drug released in the first hour and 75 % within the first 3 hours. Conversely, more than 70% of free MEDS433 was released in the first hour and the total amount within 3 hours. The complete drug release from both lipodisks was obtained within 12 hours.

A preliminary biological assay was carried out *in vitro* to evaluate the ability of both MEDS433-loaded lipodisk formulations to inhibit SARS-CoV-2 replication in Calu-3 cells in comparison with free drug (***Table 9***). The EC50 value of free MEDS433 was 0.075 μM and the value became 0.006 μM for HPSC:DSPE-PEG@MEDS433 and 0.029 μM for POPC:CHOL:DSPE-PEG@MEDS433 pointing out a great increment of the antiviral efficacy of lipodisk formulations. Moreover, a decreased cytotoxicity was registered for both MEDS433-loaded lipodisk formulations (CC50 35.66 and 10.83 μM) respect to the free drug (CC50 > 60 μM).

Table 9 *Evaluation of SARS-CoV-2 replication in Calu-3 treated with MEDS433, HPSC:DSPE-PEG$_{2000}$/MEDS433 and POPC:CHOL:DSPE-PEG$_{2000}$/MEDS433. The values are reported in μM*

Virus	***MEDS433***				***HSPC:DSPE-PEG$_{2000}$/MEDS433***				***POPC:CHOL:DSPE-PEG$_{2000}$/ MEDS433***			
	EC_{50}	**EC_{90}**	**CC_{50}**	**SI**	**EC_{50}**	**EC_{90}**	**CC_{50}**	**SI**	**EC_{50}**	**EC_{90}**	**CC_{50}**	**SI**
SARS-CoV-2	0.075	0.429	>60	>800	0.006	0.101	35.66	59.43	0.0291	0.369	10.83	372

4.4. Cyclodextrin formulations for MEDS433

A series of cyclodextrins-based DDS have been already approved for clinical use[141], most of them based on modified sulfobutylether-β-cyclodextrin (SBE, Captisol®). This clinically approved CD is characterized by charged sulfobutylether moieties replacing hydroxyl groups at position 6 able to enhance solubility and reducing toxicity[142]. Interestingly, Captisol® was recently used for the inclusion of the anti-viral agent Remdesivir against COVID-19[143].

With the aim to improve the water solubility and the farmacokinetic profile of MEDS433, we first attempted the nanoformulation of the drug with two different commercial cyclodextrins, SBE and hydroxypropyl cyclodextrin (CD-HP) exploiting the organic film hydration technique at a 5:1 CD to drug ratio. After filtration with 0.20 μm membrane, to remove the unloaded MEDS433, the filtered solution were analyzed by UV-Vis and compared to free MEDS433 at its solubility limit in water (12 μM) (***Figure 54***) pointing out that both CD managed to improve MEDS433 solubility in water, as the absorbance signals of SBE@MEDS433 and CD-HP@MEDS433 are more intense than that of the free drug, with CD-HP appearing the most efficient CD.

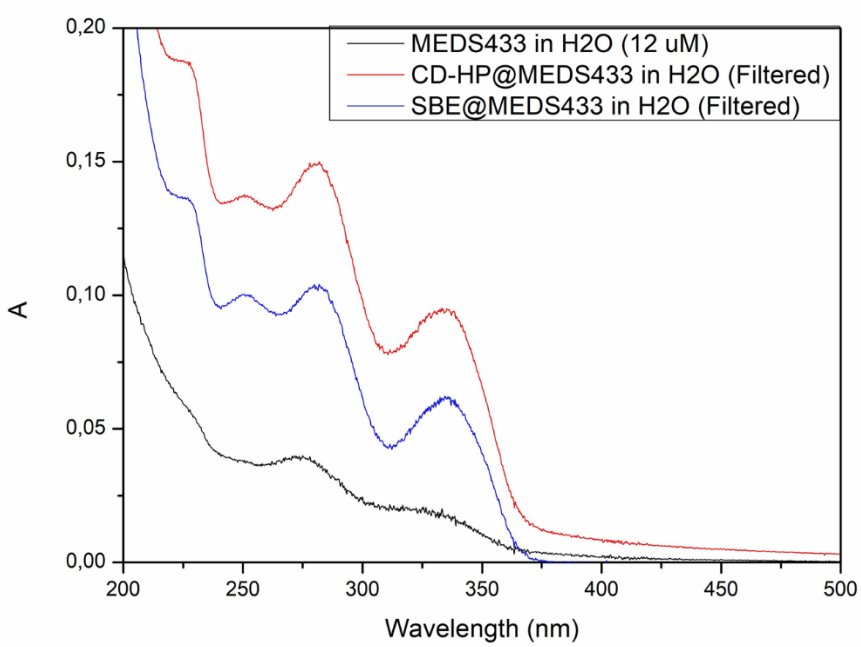

Figure 54 *UV-Vis spectra comparison of SBE@MEDS433, CD-HP@MEDS433 and free MEDS433*

Therefore, the formulations were lyophilized and the concentration of encapsulated drug was determined by UV-Vis analysis by redissolved the samples in methanol (***Figure 55***), using a calibration line in the same solvent. Our results attested for a poor encapsulation efficiency (2.6% and 1.4% for CD-HP and SBE, respectively), revealing that CD-HP and SBE turned out to be unsuitable as carrier for MEDS433 likely due to a dynamic equilibrium between free and complexed drug, resulting in the formation of aggregates of free MEDS433 insoluble in water.

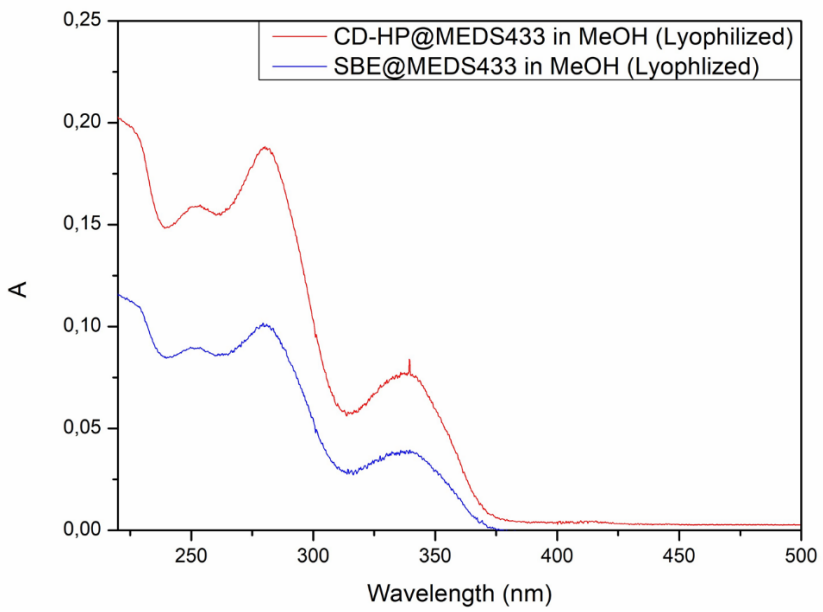

Figure 55 *Spectra of CD-HP@MEDS433 and SBE@MEDS433 redissolved in MeOH after lyophilization*

Based on these findings, we selected for our further studies an amphiphilic CD, heptakis[6-deoxy-6-hexylthio-2-oligo(ethylene glycol)]-β-cyclodextrin[144] (SC6OH) (***Figure 56***) that was widely used as drug carrier[91,92,93].

SC6OH is a semi-synthetic CD substituted with hydrophobic thiohexyl chains at the primary rim (C-6) and hydrophilic oligo(ethyleneglycol) chains at the secondary rim (C-2) accessible in an efficient two-step synthesis[144].

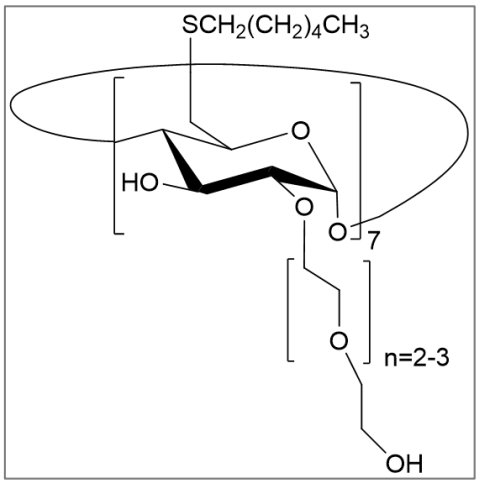

Figure 56 *Structure of SC6OH*

Two different formulations of SC6OH@MEDS433 were prepared using a ratio of CD to drug of 5:1 and 2.5:1. A solution of CD in DCM and a solution of MEDS433 were mixed together respecting the selected ratios and an organic film of the two components was obtained by solvent evaporation. By addition of water and after a brief vortexation, the film was completely rehydrated (***Figure 57***).

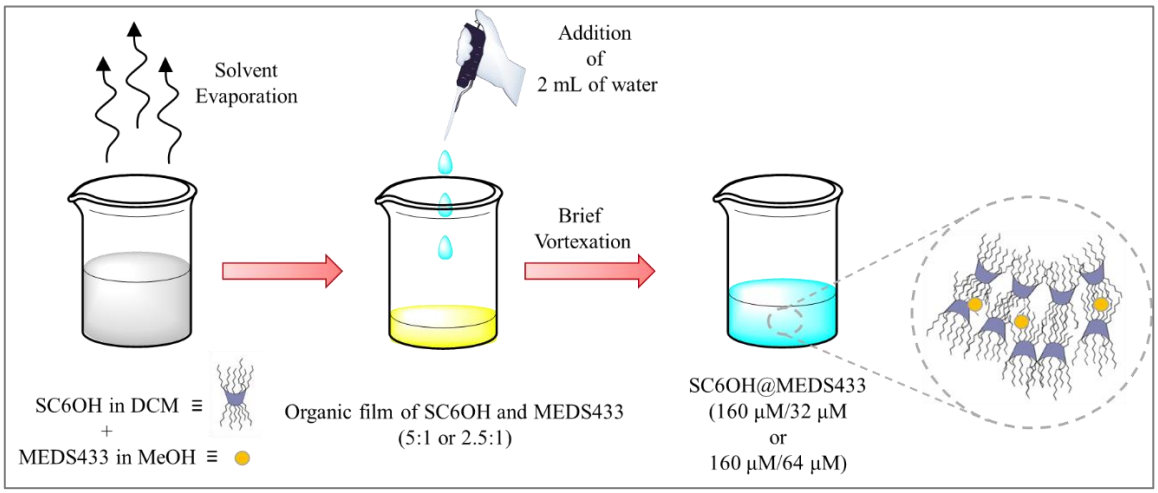

Figure 57 *Formulation procedure of SC6OH@MEDS433 by film rehydration*

The aqueous solutions were directly analyzed by UV-Vis (***Figure 58***) without filtration to measure the concentration of the rehydrated drug and to compare with free MEDS433 at its solubility limit in water (12 µM).

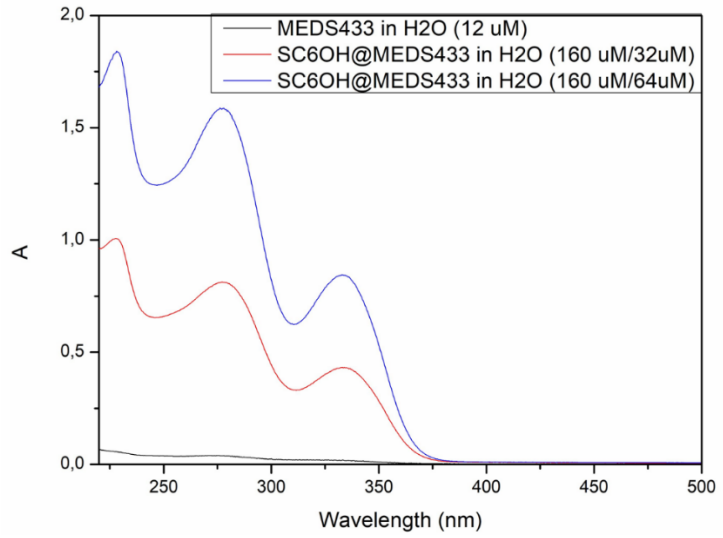

Figure 58 *UV-Vis spectra comparison of SC6OH@MEDS433 (5:1 and 2.5:1) and free MEDS433*

The absorbance of the two SC6OH@MEDS433 complexes in water was higher than the absorbance of free drug at its solubility limit (12 μM) and also higher than the SBE@MEDS433 and CD-HP@MEDS433 complexes previously investigated, attesting for a better performance of SC6OH towards MEDS433 incorporation.

We could speculate that the SC6OH-based assembly can accommodate both free and aggregate MEDS433 in the lipophilic pockets. The release of the drug from SC6OH@MEDS433 was investigated within 72 hours at 37°C (***Figure 59***) on 1 mL of formulation with cyclodextrin and drug concentration of 320 and 128 μM (51 μg of MEDS433), respectively, that was dialyzed against 50 mL of PBS buffer with 0.1% Tween 80 to ensure sink conditions. By fluorimetric analysis the emission of MEDS433 released by the nanosystem was detected, and the percentage of drug released was expressed as the ratio of the emission intensity of the compound in the external medium at every time point and the emission intensity of the total amount of MEDS433 found in the external medium after bursting the dialysis bag at the end of the experiment (72 hours).

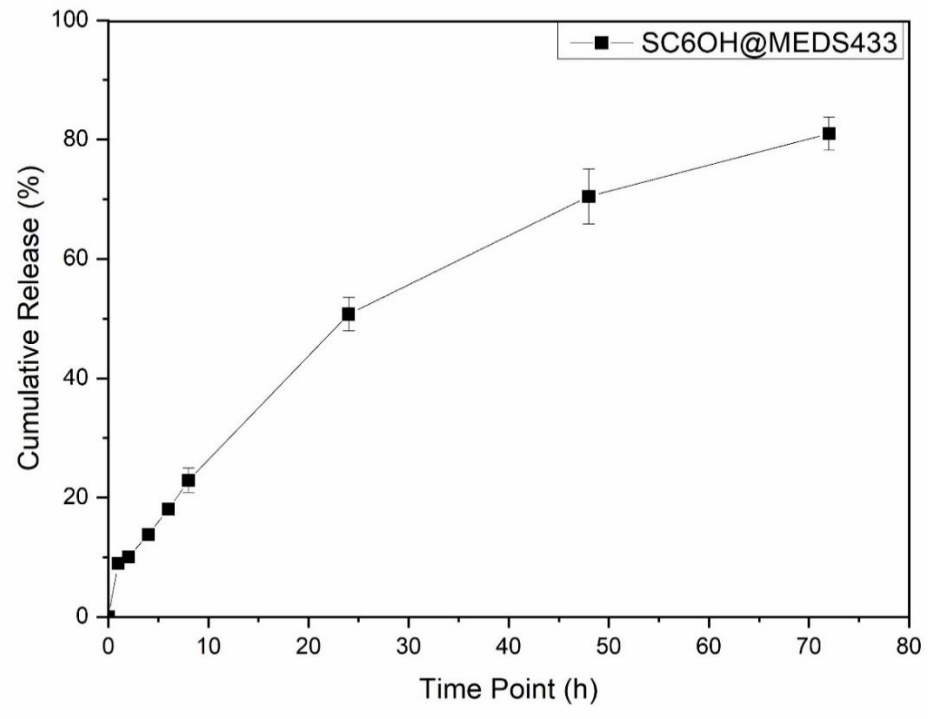

Figure 59*7 Release profile of MEDS433 from SC6OH formulation*

The release study highlighted the ability of the nanosystem to prevent a burst release of MEDS433 as only about 10% and 20% of drug is detected in the external medium at 2 and 6 hours, respectively; 50% of MEDS433 is released after 24 hours and 80% at the end of the experiment (72 hours). The overall performance achieved by the nanosystem is encouraging, considering both the high increase of MEDS433's solubility obtained with the amphiphilic cyclodextrin formulation and the sustained release profile.

A preliminary biological study was carried out *in vitro* to evaluate the ability of SC6OH@MEDS433 to inhibit SARS-CoV-2 replication in Calu-3 cells in comparison with free drug and SC6OH (***Table 10***). The EC50 value of free MEDS433 was 0.065 μM, and the value became almost halved (0.038 μM) for SC6OH@MEDS433 nanoassembly pointing out a significant increment of the antiviral efficacy.

Moreover, a decreased cytotoxicity was registered for SC6OH@MEDS433 (CC50 76.71 μM) respect to the free drug (CC50 54.91 μM). SC6OH did not exert antiviral or cytotoxic effects, as expected. The Selectivity Index (SI) of MEDS433 favorably increased from 844.76 (free drug) to 2018 for SC6OH@MEDS433 attesting for a nanoformulation more active and less toxic respect to the free drug.

Table 10 *Evaluation of SARS-CoV-2 replication in Calu-3 treated with MEDS433, SC6OH@MEDS433 and SC6OH. The values are reported in μM*

Virus	***MEDS433***				***SC6OH@MEDS433***				***SC6OH***			
	EC_{50}	**EC_{90}**	**CC_{50}**	**SI**	**EC_{50}**	**EC_{90}**	**CC_{50}**	**SI**	**EC_{50}**	**EC_{90}**	**CC_{50}**	**SI**
SARS-CoV-2	0.065	0.374	54.91	>845	0.038	0.143	76.71	2018	>1	>1	>120	>120

5. Conclusions and Future Perspectives

Biomaterial design has received a large amount of attention in the last decades, together with the study of their interactions with the surrounding biological milieu. In this context, this PhD thesis reported a deep investigation on chemically-tailored nanoplatforms based on different biomaterials (*i.e.*, amphiphilic copolymers, cyclodextrins and phospholipids) obtained by versatile design strategies for customized antitumoral and antimicrobial applications.

The results reported in this thesis pointed out that a fine control over the chemical composition, molecular weight, hydrophobic: hydrophilic balance, end-functional groups can be obtained by a proper designing and optimization of all the preparation steps of a multifunctional nanoplatform, having a significant effect on its properties (*e.g. self-assembly* and micellization, stability, drug loading and release kinetics, degradation rate and biological profile, targeting abilities and therapeutic efficacy).

Part of my PhD research focused on the development of polymeric NPs obtained by formulation of linear and branched amphiphilic PLA-PEG copolymers.

Linear PLA-PEG copolymers were obtained by combining an EDCI-mediated coupling reaction and a copper-catalyzed azide-alkyne 1,3-dipolar cycloaddition (CuAAC). The material held the typical *self-assembly* ability of amphiphilic species in aqueous environment allowing its formulation in NPs and the encapsulation of the antibiotic Linezolid occurred with satisfactory efficiency.

A sustained and prolonged delivery of Linezolid from NPs was achieved, with 65% of entrapped antibiotic released within 80 h. The biological investigation on PLA-PEG/LNZ NPs highlighted that LNZ retained its bacteriostatic activity against several Gram-positive bacteria responsible for human infections (*i.e. Staphylococcus aureus*, including MRSA, *Staphylococcus epidermidis*, *Staphylococcus lugdunensis* and *vancomycin-resistant Enterococcus faecium).* Moreover, the slow and prolonged release of the drug from the nanosystem granted a sustained and efficient antimicrobial

treatment, unachievable with the administration of free LNZ which is rapidly metabolized. Most importantly, the treatment of MRSA biofilms with PLA-PEG/LNZ NPs afforded a reduction of the biomass, not achieved with free LNZ, attesting the ability of the polymeric NPs to penetrate and deliver more efficiently the drug into such biological matrixes, improving its anti-biofilm efficiency.

The success of the PLA-PEG/LNZ nanoformulation prompted us to investigate an adaptation of the synthetic procedure to obtain a three-armed star PLA-PEG copolymer. In this case, the inclusion of a Ring Opening Polymerization (ROP) of L-lactide using glycerol as trifunctional core allowed to synthetize a three-armed star PLA precursor which was converted into the final star PLA-PEG and star PLA-PEG-RGD by a series of esterification reactions with pentynoic anhydride followed by CuAAC reactions for the conjugation of both the hydrophilic moiety (i.e., PEG) and the targeting ligand (i.e., RGD peptide) to the PLA core.

Both the RGD-decorated and undecorated polymer were nanoformulated and Docetaxel and Doxorubicin were incorporated in polymeric micelles with satisfactory efficiency. The biological profile of the two nanosystems were evaluated against different tumoral cell lines. Specifically, the antitumoral effect of DTX-loaded nanoformulations and the inhibition of tumoral cell migration were evaluated on U87 Human Glioblastoma and MDA-MB 468 Human Breast Adenocarcinoma, as models of two most common primary and metastatic tumors affecting people worldwide; whereas, DOX-loaded nanoformulations were evaluated against MG63, SAOS-2, and U2-OS osteosarcoma cells.

In both cases, it was demonstrated that the antitumoral effect of DOX and DTX delivered by star PLA-PEG-RGD NPs was well preserved. More importantly, our results highlighted the crucial role of RGD targeting moiety.

In fact, one of the main biological findings of our work was that the decoration with RGD peptide strongly influenced the biological profile of our DOX-loaded nanocarrier since only RGD-decorated micelles were able to reach the osteosarcoma cell nuclei, resulting effective; conversely the undecorated micellar nanoassemblies,

without RGD, failed to reach the nucleus, resulting ineffective in our *in vitro* studies, maintaining a cytoplasmic localization.

The stronger ability of DTX-loaded RGD-decorated nanocarrier to reduce tumoral cell migration and invasiveness (associated with metastatization) compared to the free drug in both U87 Human Glioblastoma and MDA-MB 468 Human Breast Adenocarcinoma cell lines at 30 h was one of the most important results of our investigation. Overall, these biological outcomes, together with the absence of toxicity on healthy Ad-MSCs and with the specific interaction and toxicity towards cancer cells, primarily MDA-MB 468 cell line, could be fruitfully exploited for a perspective design of target therapy.

In the framework of VIPER project granted by NATO, I was involved in the development of nanoformulations for the antiviral agent MEDS433 using phospholipids and cyclodextrins. In both cases, the incorporation of the drug into lipodisks and cyclodextrin-based nanoassemblies, respectively, led to a significant improvement of its low solubility in water which was the main hindrance in the clinical development of this powerful Broad Spectrum Antiviral Agent (BSAA).

During my foreign 6-months abroad at the University of Uppsala (Sweden), two optimized lipodisks formulations (POPC:CHOL:DSPE-PEG_{2000} and HSPC:DSPE-PEG_{2000}) were produced and investigated and a 10-fold increase in aqueous solubility of MEDS433 was achieved. The two systems showed very similar performances, with a slower release respect to the free drug and a very good stability up to 2 months in buffered solution in refrigerated conditions, as attested by DLS and SEM analysis.

Furthermore, the ability of commercially available (Sulfobutyether-β-cyclodextrins, SBE and 2-Hydroxypropyl-β-cyclodextrin, HP) and semi-synthetic cyclodextrins (SC6OH) to complex MEDS433 was also investigated, pointing out that hydrophilic SBE and HP were unsuitable carriers for MEDS likely due to a dynamic equilibrium between free and complexed MEDS433, resulting in the formation of aggregates of free drug insoluble in water. Conversely, the amphiphilic SC6OH assembly can accommodate both free and aggregate MEDS433 into the lipophilic

pockets enabling a very high solubility increase from 12 µM to 64 µM in freshly prepared MEDS@SC6OH assembly. Moreover, after reconstitution of lyophilized MEDS@SC6OH sample, the solubility increased even up to 1.6 mM (≈ 2.5 mg/mL).

The results achieved with all the formulated nanosystems are encouraging and pave the way for their further exploration in both antimicrobial and antitumoral field. The polymeric nanocarriers performances may be further investigated after co-encapsulation of different bioactive compounds in order to provide synergistic effects and broaden the range of therapeutic action.

Moreover, the versatility of end-groups functionalization in polymeric structures might allow further tailoring of the performances of the polymeric DDSs by decoration with targeting ligands different from RGD peptide and/or by the inclusion of stimuli-responsive chemical groups (i.e. hydrazone pH sensitive group).

Both cyclodextrin complexes and lipodisk formulations obtained in the framework of the VIPER project are undergoing, at the time of writing, further *in vitro* biological assays to confirm the preliminary results above reported and to compare their performance respect to the free MEDS433.

6. Materials and Methods

6.1 General

Reagents and solvents were purchased from Merck (Italy). RGD-N_3 was purchased from Scintomics. MEDS433 was supplied by University of Turin. All lipids were purchased from Avanti Polar Lipids. SC6OH cyclodextrin was previously obtained following a synthetic procedure described in literature[137] and kindly provided for the research.

DLS and Z-Potential were measured using a Zetasizer Nano ZS, UV-Vis measurements were performed using an Agilent 8453 diode array spectrophotometer, NMR spectra were recorded using a Varian 500 MHz spectrometer. Scanning electron microscopy was performed using a field emission scanning electron microscope Supra35 FE-SEM.

Cryogenic transmission electron microscopy (cryo-TEM) investigations were performed using a Zeiss TEM Libra 120 Transmission Electron Microscope. DLS measurements in Sweden were performed using a setup consisted of a Uniphase He-Ne laser and a Perkin Elmer diode detector connected to an ALV-5000 multiple digital autocorrelator. UV-Vis measurements in Sweden were performed using an Agilent spectrophotometer HP 8453. Fluorescence measurements were performed using a Horiba Fluorolog®-3.

6.2. Synthesis of PLA-Alkyne

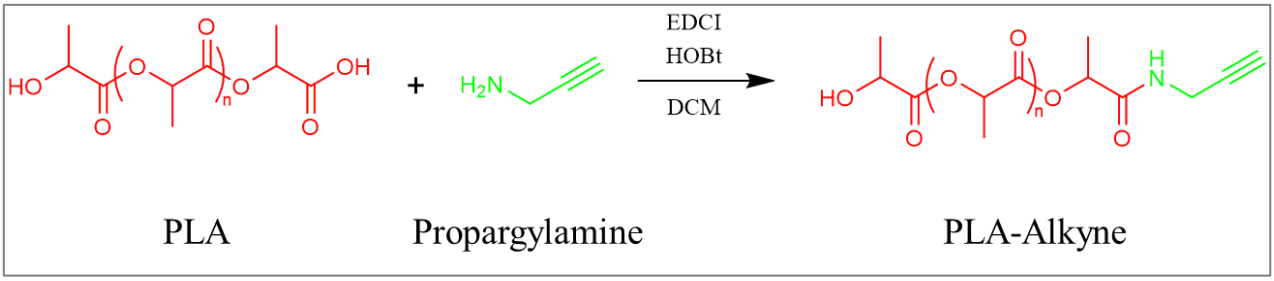

PLA (0.2 g, 1.43×10^{-5} mol) was dissolved in anhydrous dichloromethane (DCM, 10 mL) in nitrogen saturated atmosphere. 1-Ethyl-3-(3-dimethylaminopropyl)carbodiimide (EDCI) (5 equiv) and hydroxybenzotriazole (HOBt) (5 equiv) were added. After 30 minutes under stirring, propargylamine (5 equiv) was added and the reaction mixture was kept stirring in inert atmosphere for 24 hours at room temperature. The organic solution was washed three times with distilled water, the recovered organic phase was dried over anhydrous Na_2SO_4 and evaporated under vacuum to isolate the product PLA-Alkyne as a white solid (0.17 g). ^{1}H NMR (500 MHz, $CDCl_3$, δ): 6.6–6.4 (br s, NH), 5.3–5.1 (m, $[CH]_n$), 4.9–5.0 (m, CH-$COOH_{unreacted}$), 4.3 (q, CH-OH), 4.0–4.1 (m, 2H, $NHCH_2$), 2.2 (m, 1H, C≡CH), 1.6–1.4 (m, $[CH_3]n$). Mn ^{NMR} 11592 Da.

6.3. Synthesis of PLA-PEG

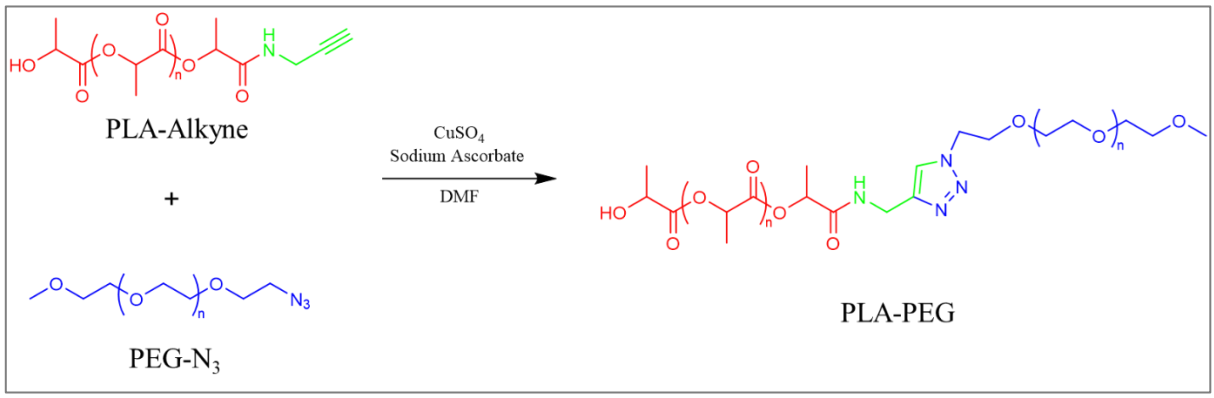

PLA-Alkyne (0.15 g, 1.04×10^{-5} mol) was dissolved in anhydrous dimethylformamide (DMF, 3 mL). mPEG-N_3 (1 equiv), $CuSO_4$ (2 equiv) and sodium ascorbate (4 equiv) were added in nitrogen saturated atmosphere. The reaction mixture was kept stirring in inert atmosphere for 48 hours at room temperature. Water was added until the solution became cloudy. The suspension was centrifuged at 13000 rpm for 20 minutes three times. The residue was lyophilized to obtain the final product PLA-PEG as a white solid (0.11 g). ^{1}H NMR (500 MHz, $CDCl_3$, δ): selected peaks 7.3 (s, H-$5_{triazole}$), 6.6–6.4 (br s, NH), 5.2–5.1 (m, $[CH]_n$), 4.9–5.0 (m, $\underline{CH}$-$COOH_{unreacted}$), 4.35 (q, CH-OH), 3.8–3.6 (s, $[CH_2CH_2O]$), 3.3 (s, CH_3O), 1.6–1.4 (m, $[CH_3]_n$). Mn NMR 13044 Da. From NMR analysis, the content of PEG grafted on PLA was estimated to be ≈ 11 w/w %.

6.4. Formulation of PLA-PEG/LNZ nanoparticles

6.4.1. Nanoprecipitation with acetone

PLA-PEG (30 mg) and LNZ (9 mg) were codissolved in acetone (6 mL) with a polymer:drug ratio mass of 10:3. The organic solution was added dropwise to 12 mL of stirring ultrapure water. After 24 hours, once acetone was evaporated, 300 µl of the suspension were diluted to 1 mL with water and underwent physical characterization to investigate the hydrodynamic diameter and surface charge of the freshly formulated NPs. The remaining suspension was centrifuged at 13000 rpm for 10 minutes and the residue was lyophilized yielding PLA-PEG/LNZ NPs as a white powder. Part of the residue was redispersed in water to investigate physical characterization of the resuspended formulation and part of it was dissolved in DMSO for the UV quatification of the incorporated drug (drug loading determination).

6.4.2. Nanoprecipitation with THF

PLA-PEG (30 mg) LNZ (9 mg) and were codissolved in THF (3 mL) with a polymer:drug ratio mass of 10:3. The solution was added dropwise to 30 mL of stirring ultrapure water. After stirring for 4 h, THF was evaporated under vacuum and 450 μl of the obtained suspension were diluted up to 1.5 mL with water and underwent physical characterization to investigate the hydrodynamic diameter and surface charge of the freshly formulated NPs. The remaining suspension was centrifuged at 13000 rpm for 10 minutes and the residue was lyophilized yielding PLA-PEG/LNZ NPs as a white powder. Part of the residue was redispersed in water to investigate physical characterization of the resuspended formulation and part of it was dissolved in DMSO for the UV quatification of the incorporated drug (drug loading determination).

6.4.3. Dialysis

PLA-PEG (30 mg) and LNZ (9 mg) and were codissolved in 1 mL of DMSO with a polymer:drug ratio mass of 10:3. The organic solution was added dropwise to 20 mL of stirring ultrapure water. After 4 h of stirring, the suspension was transferred into a dialysis membrane (3.5–5 kDa cut-off) previously conditioned in water for 10 minutes. The sealed dialysis tube was immersed in 500 mL of ultrapure water and kept under gentle stirring. The entire volume of water was replaced after 3, 15 and 19 hours. 450 μl of the suspension inside the dialysis bag were diluted up to 1.5 mL with water and underwent physical characterization to investigate the hydrodynamic diameter and surface charge of the freshly formulated NPs. The remaining suspension was lyophilized, yielding PLA-PEG/LNZ NPs as a white powder. Part of the residue was redispersed in water to investigate physical characterization of the resuspended formulation and part of it was dissolved in DMSO for the UV quatification of the incorporated drug (drug loading determination). “Empty” PLA-PEG NPs were prepared following the same method but omitting the drug and used as controls.

6.5. Characterization of PLA-PEG/LNZ nanoparticles

6.5.1. Drug loading and encapsulation efficiency calculation

The amount of LNZ incorporated in the NPs was determined by UV-Vis spectroscopy. A weighted amount of PLA-PEG/LNZ NPs was dissolved in DMSO and the UV-Vis spectrum was recorded. The amount of encapsulated LNZ was calculated at the wavelength of 262 nm using a previously plotted calibration curve of the drug in the same solvent (concentration range 25–150 μg/mL). On the basis of optical absorbance data and molar extinction coefficient ($\varepsilon \cong 17758\ M^{-1}\ cm^{-1}$), DL and EE were calculated using the following equations:

–DL (%) = (Drug weight in the NPs/Weight of the drug-loaded NPs) × 100
–EE (%) = (Drug weight in the NPs/Weight of drug used in the formulation) × 100

6.5.2. Size and ζ-potential investigation

Measurements were performed on the freshly formulated and the lyophilized NPs after reconstitution. The lyophilized white solid was resuspended in ultrapure water to a concentration of 1 mg/mL, sonicated for 15 minutes and diluted to a final concentration of 0.3 mg/mL for DLS and ζ-potential measurements.

6.6. Release study

0.91 mg of PLA-PEG/LNZ NPs containing 32 μg of LNZ were dispersed in 1 mL of PBS (0.01 M, pH 7.4), sonicated for 15 minutes and transferred into a dialysis tube (MWCO 3.5–5 kDa, Spectra/Por®). Dialysis was performed against 5 mL of PBS kept at 37 °C. At fixed times (4, 24, 32, 48, 56 and 80 h), 1 mL of the release medium was withdrawn and replaced with an equal volume of fresh buffer. The withdrawn volume

was analyzed by UV-Vis spectroscopy to quantify the released LNZ using a previously plotted calibration curve calibration curve of LNZ in PBS (concentration range 0.34–25 μg/mL; ε ≅ 18486 M^{-1} cm^{-1}). Free LNZ in PBS was dialyzed at the same concentration as the drug-loaded NPs (32 μg/mL) in similar experimental conditions.

6.7. Biological studies of PLA-PEG/LNZ nanoparticles

6.7.1. Minimal inhibitory concentration and minimal bactericidal concentration

Investigation of minimal inhibitory concentration (MIC) and minimal bactericidal concentration (MBC) of the PLA-PEG/LNZ NPs (containing 32 μg LNZ in 914 μg of NPs), free LNZ and empty PLA-PEG NPs were performed using *S. aureus* ATCC 6538, MRSA ATCC 43300, *S. epidermidis* ATCC 35984, *S. lugdunensis* DSM 4804 and *VREfm* DSM 17050 microorganisms. The samples were diluted twofold in 96-well and overnight bacterial cultures were inoculated to a final concentration of 5×10^5 CFU/mL. After incubation at 37 ˚C for 24 hours, the MBC was determined by seeding 20 μl from all clear wells onto Muller-Hinton agar (MHA) and incubated at 37 ˚C for 24 to 48 hours. The MBC was defined as the lowest concentration which killed 99.9% of the inoculum.

6.7.2. Effect of PLA-PEG/LNZ NPs on planktonic cells

Overnight culture of MRSA ATCC 43300 grown in CAMHB was adjusted to a concentration of 1×10^6 CFU/mL. The standardized inoculum was dispensed in tubes containing PLA-PEG/LNZ NPs at MIC, 2 × MIC, 4 × MIC [incorporating a LNZ content of 8, 16 and 32 μg/mL, respectively, corresponding to a release of drug of about 25% in 24 hours, 46% in 48 hours, and 60% in 72 hours], free LNZ at MIC, 2 × MIC, 4 × MIC (corresponding to 2, 4 and 8 μg/mL, respectively), or empty PLA-PEG NPs (tested at the same polymer concentration used for testing the drug-loaded NPs). The

tubes were incubated at 37 ˚C with shaking (100 rev/min) and after 2, 4, 6, 24, 48, 72 hours the samples were serially diluted in PBS and were plated onto MHA to determine total cell number. The plates were then incubated at 37 ◦C for 24 hours up to 48 hours, CFU were counted and time kill plots were constructed.

6.7.3. Effect of PLA-PEG/LNZ NPs on preformed biofilm

Overnight cultures of MRSA ATCC 43300 in Tryptic Soy Broth (TSB) + 1% glucose (TSBG) were adjusted to 1×10^6 CFU/mL. 100 µL were added individually to each well of a polystyrene flat bottomed 96-microtitre plate. The plates were incubated at 37 ˚C for 24 hours. After incubation, the supernatant was removed and biofilms were carefully washed twice with sterile PBS. Biofilms were treated with 100 µL of PLA-PEG/LNZ NPs at 2 × MIC, 4 × MIC, free LNZ at 2 × MIC, 4 × MIC, empty PLA-PEG NPs or CAMHB (control) for 24 hours at 37◦C. To determine whether the PLA-PEG/LNZ NPs treatment inhibited the growth in biofilm supernatant, the optical density (OD_{492}) was measured at time 0 (T0) and after incubation for 24 hours. The growth inhibition in biofilm supernatant was detected when there was no observable bacterial growth in the wells, confirmed by no increase in optical density compared with the initial reading. To verify the activity on biofilm biomass and cell viability, the supernatant was removed and biofilms were washed twice with PBS before being dried, stained for 1 min with 0.1% safranin and resuspended in 30% (v/v) acetic acid for OD492 evaluation; resuspended in 100 µL of PBS and scraped with sterile pipette tips for evaluation of the bacterial load (CFU) by plating serial dilutions onto MHA.

6.7.4. Effect of PLA-PEG/LNZ NPs on biofilm re-growth

Initially, the influence of a treatment with PLA-PEG/LNZ NPs 4 × MIC (containing a LNZ content of 32 µg/mL and a and corresponding to a release of around

25% in 12 hours) or free LNZ at 4 × MIC (corresponding to 8 µg/mL) for 12 hours on growth of biofilm supernatant and viable cells of MRSA ATCC 43300 was evaluated. Subsequently, to determine whether PLA-PEG/LNZ NPs and free LNZ treatment prevented the re-growth of bacteria embedded in the biofilm, the medium was removed, the biofilm was washed with PBS and fresh CAMHB was added. Plates were re-incubated at 37◦C overnight and the biofilm supernatant and viable cells were evaluated in similar fashion to the one describe in the previous paragraph.

6.8. Synthesis of star PLA-PEG-RGD

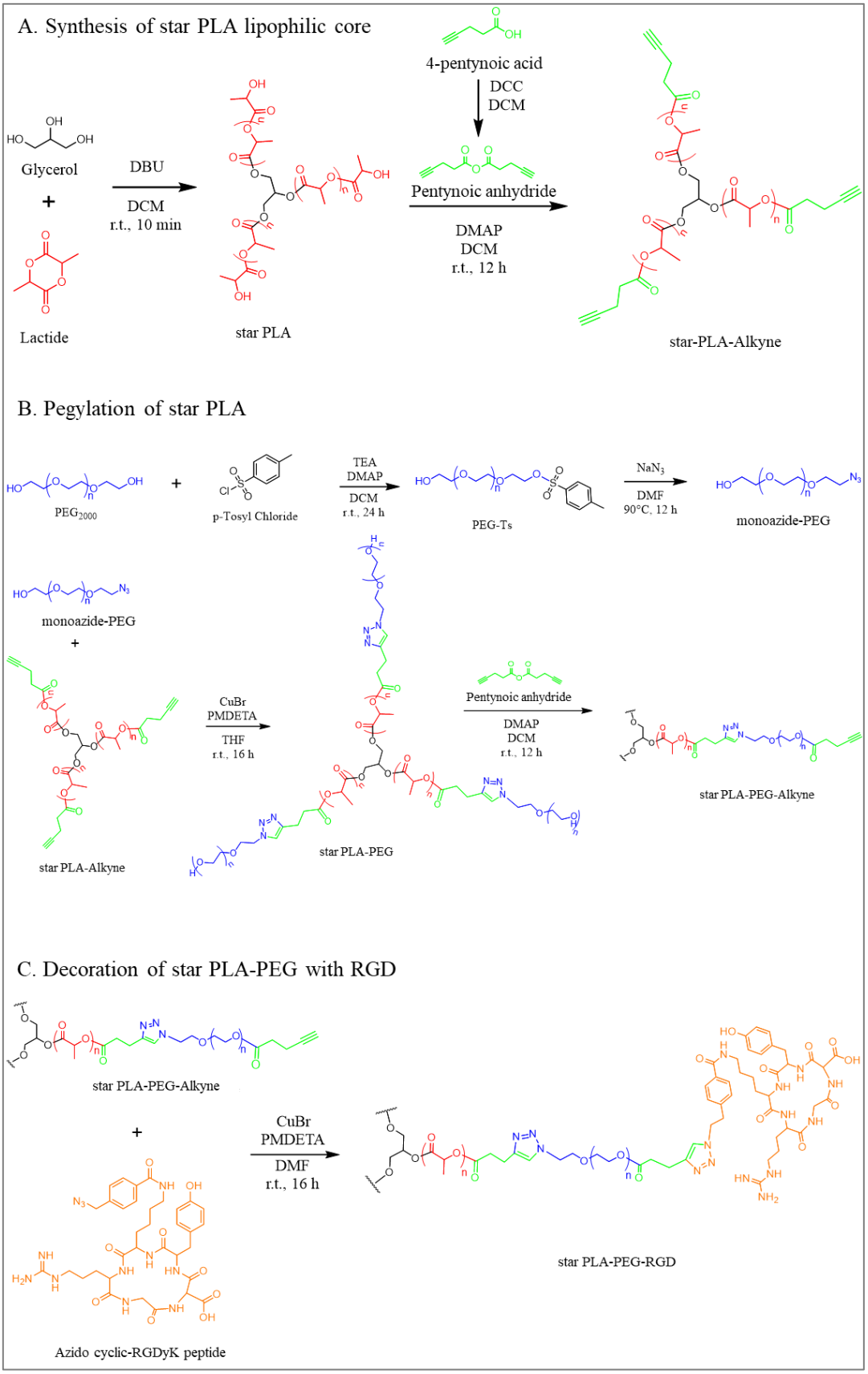

A. Synthesis of star PLA lipophilic core

In a glove box, under inert atmosphere, glycerol (6.6 mg, $7 \cdot 10^{-5}$ mol, 1 equiv) and DBU (2 equiv) were solubilized in 2 mL of anhydrous DCM. Separately, L-Lactide (97 equiv) was solubilized in 5 mL of anhydrous DCM and added to the first solution. The reaction was left to stir 12 min, a solution of benzoic acid (2.4 equiv) in 0.2 mL of anhydrous DCM was added to stop the reaction. Outside the glove box, the volume of the solution was reduced under vacuum. The solution was precipitated into cold methanol, centrifuged and the residue was dried for 5 hours into a vacuum oven at 60 °C. The final product star PLA was obtained as a white powder (980 mg). ^{1}H NMR (500 MHz, $CDCl_3$, δ): 1.57 (m, 3H, $[CH_3]_n$), 4.22 (m, 5H, $-CH_2CHCH_2$), 4.36 (m, 1H, CHOH), 5.15 (m, 1H, $[CH]_n$). Polymerization Degree $^{1H\ NMR}$ = 97, $Mn^{1H\ NMR}$ = 14.000 g/mol, SEC: $Mn^{SEC,app}$ = 21.019 g/mol, $Đ_M$ = 1.12.

The retrieved amount of star PLA (980 mg, $7 \cdot 10^{-5}$ mol, 1 equiv), DMAP (4 equiv) and pentynoic anhydride (4 equiv) were dissolved in 30 mL of DCM and the solution was kept stirring for 12 hours at room temperature. The solution was washed three times with a saturated solution of $NaHCO_3$ and three times with a saturated solution of NaHSO4. The recovered organic phase was dried over Na_2SO_4 and concentrated under vacuum. The solution was precipitated into cold methanol, centrifuged and the residue was dried for 5 hours into a vacuum oven at 60◦C. The product star PLA-Alkyne was obtained as a white powder (900 mg). ^{1}H NMR (500 MHz, $CDCl_3$, δ): 1.57 (m, 3H, -$[CH_3]_n$-), 2.65 (m, 2H, $CH_2CH_2C{\equiv}CH$), 2.52 (m, 2H, $CH_2CH_2C{\equiv}CH$), 1.98 (t, 1H, J = 2.5 Hz, C≡CH), 4.22 (m, 5H, -CH_2CHCH_2-), 5.15 (m, 1H, -$[CH]_n$-). Polymerization Degree$^{1H\ NMR}$ = 97, $Mn^{1H\ NMR}$ = 14.294 g/mol, SEC: $Mn^{SEC,app}$ = 21.207 g/mol, $Đ_M$ = 1.13.

B. Pegylation of star PLA

In a glove box, under inert atmosphere, PEG (500 mg, $2.5 \cdot 10^{-4}$ mol, 1 equiv) was dissolved in 10 mL of DCM and stirred until complete dissolution. TEA (3 eq) and DMAP (3 eq) were added. Tosyl chloride (0.75 eq) is dissolved in 5 mL of DCM and added to the solution that is left to stirr overnight. The reaction mixture is washed twice with a saturated solution of NH_4Cl and dried over Na_2SO_4, solvent is evaporated by rotary evaporation and the product obtained as white powder. ^{1}H NMR and MALDI-ToF analysis demonstrated that it is a mixture of mono-tosyl PEG and unreacted PEG diol (ratio 1:1), that was directly used in the next synthetic step, without further purification. ^{1}H NMR (500 MHz, $CDCl_3$, δ): 2.44 (s, 3H, CH_3), 3.64 (m, 4H, -$[CH_2CH_2O]_n$-), 4.15 (t, 2H, J = 5 Hz, CH_2OTs), 7.33 (d, 2H, J = 8.5 Hz, Ar H), 7.79 (d, 2H, J = 8.5 Hz, Ar H).

The mixture of PEG and PEG-Ts obtained in the previous synthetic step (574 mg, containing $6.65 \cdot 10^{-5}$ mol of mono-tosyl PEG, 1 equiv) and NaN_3 (5 equiv) were dissolved into 5 mL of anhydrous DMF. The mixture was kept under stirring for 12 hours at 90◦C. DMF was then evaporated under vacuum and the crude product was dissolved in DCM to be washed two times with brine and two times with water. The recovered organic phase was, dried over Na_2SO_4 and evaporated under vacuum to obtain a white solid (120 mg). ^{1}H NMR and MALDI-ToF analyses demonstrated that it is a mixture of mono-azide PEG and unreacted PEG diol (ratio 1:1). ^{1}H NMR (500 MHz, $CDCl_3$, δ): 3.39 (t, 2H, J = 5 Hz, -CH_2N_3), 3.64 (m, 4H, -$[CH_2CH_2O]_n$).

In a glove box, under inert atmosphere, star PLA-Alkyne (650 mg, $4.56 \cdot 10^{-5}$ mol, 1 equiv) and the mixture of PEG diol and monoazide-PEG (555 mg, containing 3 equiv of mono-azide PEG) were dissolved in 2 mL of anhydrous THF. CuBr (0.1 equiv) and PMDETA (0.1 equiv) were added to the reaction mixture. The solution was kept stirring at room temperature for 16 h. Outside the glove box the solvent was evaporated under vacuum, the residue was washed three times with 5 mL of water to remove the unreacted PEG-diol and the centrifuged at 2800 rpm for 50 min at 10◦C. The solid was

dried at 40◦C in a vacuum oven for 4 hours to obtain the product star PLA-PEG (891 mg). ^{1}H NMR (500 MHz, $CDCl_3$, δ): 1.57 (d, 3H, -$[CH_3]_n$-), 2.82 (t, 2H, J = 5 Hz, $CH_2CH_2C_{triazole}$), 3.06 (t, 2H, J = 7.5 Hz, $CH_2N_{triazole}$), 3.64 (m, 4H, -$[CH_2CH_2O]_n$-), 4.22 (m, 5H, -CH_2CHCH_2-), 4.49 (t, 2H, J = 5 Hz, $CH_2CH_2C_{triazole}$), 5.15 (m, 1H, -$[CH]_n$-), 7.53 (s, 1H, $CH_{triazole}$). $Mn^{SEC,\ app}$ = 32.212 g/mol, $Đ_M$ = 1.14.

Star PLA-PEG (891 mg, $4.38•10^{-5}$ mol, 1 equiv), DMAP (4 equiv) and pentynoic anhydride (4 equiv) were dissolved in 30 mL of DCM. The reaction mixture was kept stirring for 12 hours at room temperature. The solution was washed three times with water and the recovered organic phase was dried over Na_2SO_4 and dried under vacuum to obtain star PLA-PEG-Alkyne as a white powder (788 mg). ^{1}H NMR (500 MHz, $CDCl_3$, δ): 1.57 (d, 3H, -$[CH_3]_n$-), 1.98 (t, 1H, J = 2.7 Hz, C≡CH), 2.52 (dt, 2H, J = 2.7, J = 6.5 Hz, CH_2CH_2C≡CH), 2.67 (t, 2H, J = 6.5 Hz, CH_2CH_2C≡CH), 2.82 (t, 2H, J = 5 Hz, $CH_2CH_2C_{triazole}$), 3.06 (t, 2H, J = 7.5 Hz, $CH_2N_{triazole}$), 3.64 (m, 4H, -$[CH_2CH_2O]_n$-), 4.22 (m, 5H, -CH_2CHCH_2-), 4.27 (t, 2H, J = 5 Hz, OCH_2CH_2OCO), 4.49 (t, 2H, J = 5 Hz, $CH_2CH_2C_{triazole}$), 5.15 (m, 1H, -$[CH]_n$-), 7.53 (s, 1H, $CH_{triazole}$). $Mn^{SEC,app}$ = 34.203 g/mol, $Đ_M$ = 1.16

C. Synthesis of star PLA-PEG-RGD

In a glove box, under inert atmosphere star PLA-PEG-Alkyne (137 mg, $6.18•10^{-6}$ mol, 1 equiv) and azide-RGD (2 equiv) were dissolved into 2 mL of anhydrous DMF. CuBr (0.1 equiv) and PMDETA (0.1 equiv) were added and the reaction mixture was kept stirring at room temperature for 16 hours. The solvent was evaporated under vacuum and the residue was washed two times with water. The suspension was centrifuged at 2800 rpm for 50 min at 10◦C and the residue dried in a vacuum oven at 40◦C for 2 hours to obtain star PLA-PEG-RGD (80 mg) as a brown solid. ^{1}H NMR (500 MHz, d7-DMF, δ): selected peaks 1.53 (d, 3H, -$[CH_3]_n$-), 1.98 (t, 1H, J = 2.7 Hz C≡CH), 2.52 (m, 2H, CH_2CH_2C≡CH), 2.65 (m, 2H, CH_2CH_2C≡CH), 2.82 (t, 2H, J = 5

Hz, $CH_2CH_2C_{triazole}$), 2.99 (m, 2H, $CH_2N_{triazole}$), 3.58 (m, 4H, -$[CH_2CH_2O]_n$-), 4.19 (m, 2H, CH_2), 4.22 (t, 2H, J = 5 Hz, OCH_2CH_2OCO), 4.38 (m, 5H, -CH_2CHCH_2-), 4.56 (t, 2H, J = 5 Hz, $CH_2CH_2C_{triazole}$), 5.28 (m, 1H, -$[CH]_n$-), 6.65 (br s, 1H, NH), 6.72 (d, 2H, Ar H, J = 8 Hz), 7.02 (d, 2H, Ar H, J = 8 Hz), 7.39 (s, 1H, $CH_{triazole}$), 7.43 (d, 2H, Ar H, J = 8 Hz), 7.60 (br s, 1H, NH), 7.78 (br s, 1H, NH), 7.97 (d, 2H, ArH, J = 8 Hz), 8.39 (br s, 1H, NH), 8.55 (br s, 1H, NH), 8.74 (br s, 1H, NH)

6.9. Formulation of star PLA-PEG-RGD/DTX nanoparticles

Star PLA-PEG-RGD (3 mg), star PLA-PEG (27 mg) and DTX (3 mg or 9 mg) were dissolved in 3 mL of THF. The organic solution was added dropwise to 30 mL of stirring water and the mixture was kept stirring at room temperature for 4 h. THF was then evaporated under vacuum and the suspension was gently centrifuged (1500 rpm), the supernatant suspension was lyophilized to obtain star PLA-PEG-RGD/DTX NPs. Similarly, empty NPs were prepared with the same method omitting the drug and used as control.

6.10. Characterization of star PLA-PEG-RGD/DTX nanoparticles

6.10.1. Drug loading and encapsulation efficiency calculations

The amount of DTX incorporated in the NPs was determined by UV-Vis spectroscopy. A weighted amount of star PLA-PEG-RGD/DTX NPs was dissolved in DMSO and the UV-Vis spectrum was recorded. The amount of encapsulated DTX was calculated at the wavelength of 274 nm using a previously plotted calibration curve of the drug in the same solvent. On the basis of optical absorbance data and molar extinction coefficient previously calculated in the same solvent ($\varepsilon \cong 1021\ M^{-1}\ cm^{-1}$), DL and EE were calculated using the following equations:

–DL (%) = (Drug weight in the NPs/Weight of the drug-loaded NPs) × 100

–EE (%) = (Drug weight in the NPs/Weight of drug used in the formulation) × 100

6.10.2. Size and ζ-potential investigation

Measurements were performed on the freshly formulated and the lyophilized NPs after reconstitution. The lyophilized solid was resuspended in ultrapure water, sonicated for 15 minutes and diluted to a final concentration of 0.3 mg/mL for DLS and ζ-potential measurements. The samples obtained from resuspension of lyophilized material were also monitored over a week for the stability check.

6.10.3. Evaluation of CMC

The CMC of star PLA-PEG and star PLA-PEG-RGD was determined by fluorescence spectra. Films of pyrene were obtained by evaporation of solvent from identical volumes of a solution of pyrene in acetone (6×10^{-6} M). The films were rehydrated using polymers solutions of different concentrations (1×10^{-3} - 0.1 mg/mL) and left to equilibrate at room temperature overnight. The fluorescence emission wavelength was fixed at 390 nm and the emission fluorescence intensities at 338 and 333 nm were monitored. The intensity ratios of I^{338}/I^{333} were plotted as a function of logarithm of two copolymer concentrations. The excitation spectrum red-shift from 333 to 338 nm indicated the transfer of pyrene molecules from an aqueous environment to the hydrophobic micelle core.

6.11. Release study

2.07 mg of star PLA-PEG-RGD/DTX NPs (containing 331.2 μg of DTX) were resuspended in 1 mL of PBS, sonicated for 15 minutes and transferred in dialysis kit (MWCO = 3.5-5 kDa, Spectra/Por®). The sample was dialyzed against 5 mL under

gentle stirring of PBS 10% v/v of Tween 80 to fulfil the sink condition. At fixed times (1, 2, 4, 6, 8, 24, 32, 48, 56, 72, 80, 96, 104 hours and 7 days) the release medium was withdrawn, replaced with an equal volume of fresh buffer, lyophilized, re-disperded in DMSO and analysed by UV-Vis. After 7 days, the inner bag solution was withdrawn and directly analyzed by UV-Vis; then the inner bag was filled with ethanol and, after 1 hour, the ethanolic solution was also analyzed by UV-Vis to directly quantify the amount of DTX not released and/or sticked to the bag.

6.12. Biological study of star PLA-PEG-RGD/DTX nanoparticles

6.12.1. MTT assay

The effect of empty star PLA-PEG-RGD NPs was tested on Ad-MSCs as model of healthy cells. Empty and DTX-loaded star PLA-PEG-RGD NPs were tested on U87 and MDA-MB 468 tumoral cell lines using free DTX as positive control and cells only as negative control. Briefly, star PLA-PEG-RGD/DTX NPs (1 mg contains 160 μg of DTX) were tested at 10 μg/mL, 20 μg/mL and 30 μg/mL (drug concentration in culture media). Unloaded NPs were tested at the same concentration used for testing the drug-loaded nanoparticles: 52 μg/mL, 105 μg/mL and 158 μg/mL concentrations of polymeric micelles for 10 μg/mL, 20 μg/mL and 30 μg/mL DTX, respectively. Loaded and unloaded NPs were reconstituted after lyophilization in MilliQ water at 1 mg/mL and sonicated for 5 minutes, while DTX free was reconstituted in DMSO at 1 mg/mL on before dilution in culture media.

The effect of empty NPs on Ad-MSCs were evaluated after 24, 48 and 72 hours. Cell viability assay of cancer cell lines incubated with loaded and unloaded NPs was performed at 24, 48 and 72 hours. At each time point, MTT assay was performed following the manufacturer's instructions. Briefly, the MTT reagent [3- (4,5-dimethylthiazol-2-yl)-2,5-diphenyltetrazolium bromide] (5 mg/mL) was dissolved in PBS and the cells were incubated with MTT solution for 2 hours at 37◦C, 5 % CO_2 and

controlled humidity conditions. The media was replaced by 15 minutes incubation in DMSO under slight stirring conditions and the absorbance was read at 570 nm by using a Multiskan FC Microplate Photometer. The values of absorbance are directly proportional to the number of metabolically active cells able to convert MTT reagent in a formazan-based by-product. All cell lines were seeded at a density of 15.000 cells/cm^2 in 96 well-plates. One experiment was carried out and a biological triplicate for each condition was performed.

6.12.2. Cell morphology evaluation

The morphology of cancer cell lines after 24 h of treatment with NPs was investigated. Cells were fixed in 4% PFA and permeabilized in PBS with 0.1% (v/v) Triton X-100 for 5 minutes at room temperature. F-actin filaments were highlighted by green-fluorescent Alexa Fluor 488® phalloidin probe incubated for 20 minutes at room temperature. DAPI counterstaining was performed for cell nuclei identification. The images were acquired at the Inverted Ti-E Fluorescent Microscope. One experiment was carried out and a biological replicate for each condition was performed.

6.12.3. Migration analysis

DTX-loaded NPs ability in inhibiting the migration of cancer cells was evaluated by performing the scratch test. Cells were seeded with a density of 50.000 cells/cm^2 in 24 well-plates. 24 hours after cell seeding, a scratch was made in each well using a p200 tip and culture media was substituted with the drug and micelles diluted in scratch media consisting of basal media with 2% FBS and 1% pen/strep. Cells cultured with scratch media only were used as negative control. The scratch was monitored over time and images were acquired at time 0, 24 and 30 hours by using the Inverted Ti-E Fluorescent Microscope. One experiment was carried out and a biological triplicate for each condition was performed. A representative panel of the scratch trend was proved

by 4% buffered Paraformaldehyde (PFA) fixation of cells at time 0 and 30 hours followed by DAPI staining of cell nuclei.

6.13. Formulation of star PLA-PEG/DOX and star PLA-PEG-RGD/DOX nanoparticles

Dox HCl (9 mg) was dissolved in THF (1.5 mL), TEA (2.2 μl) was added and the solution was kept stirring for 15 min to achieve DOX deprotonation. A mixture of star PLA-PEG (27 mg) and star PLA-PEG-RGD (3 mg) dissolved in THF (1.5 mL) was added. After stirring for 5 minutes, the organic solution was added dropwise to 30 mL of stirring water. After 4 hours, THF was evaporated under reduced pressure and the suspension was centrifuged twice at 13000 rpm for 15 minutes. The residue was lyophilized to obtain star PLA-PEG-RGD/DOX NPs. Similarly, empty NPs were prepared using the same method omitting the drug and used as a blank; star PLA-PEG/DOX NPs were formulated using the same method starting from 30 mg of star PLA-PEG.

6.14. Characterization of star PLA-PEG/DOX and star PLA-PEG-RGD/DOX nanoparticles

6.14.1. Drug loading and encapsulation efficiency calculations

The amount of DOX incorporated in the NPs was determined by UV-Vis spectroscopy. A weighted amount of star PLA-PEG/DOX NPs or and star PLA-PEG-RGD/DOX was dissolved in DMSO and the UV-Vis spectrum was recorded. The amount of encapsulated DOX was calculated at the wavelength of 482 nm using a previously plotted calibration curve of the drug in the same solvent. On the basis of

optical absorbance data and molar extinction coefficient ($\varepsilon \cong 11450\ M^{-1}\ cm^{-1}$), DL and EE were calculated using the following equations:

–DL (%) = (Drug weight in the NPs/Weight of the drug-loaded NPs) × 100
–EE (%) = (Drug weight in the NPs/Weight of drug used in the formulation) × 100

6.14.2. Size and surface potential investigation

Measurements were performed on lyophilized NPs after reconstitution. The lyophilized solid was resuspended in ultrapure water, sonicated for 15 minutes and diluted to a final concentration of 0.3 mg/mL for DLS and ζ-potential measurements.

6.14.3. Morphological analysis

Morphological and structural investigation of NPs was performed by scanning electron microscopy (SEM). Empty and DOX-loaded NPs were dispersed in water at the concentration of 0.03 mg/mL, were deposited by drop-casting on a silicon substrate, dried, and analyzed using low energy (3 keV) electron beam, to prevent any damaging of the nanoassemblies.

6.15. Release study

2 mg of star PLA-PEG-RGD/DOX NPs (containing 160 μg of DOX) were dispersed in 1 mL of PBS, sonicated for 15 minutes and transferred into a dialysis tube (Spectra Por® Pre-wetted RC Tubing MWCO 3.5–5 kDa). The sample was dialyzed against 5 mL under gentle stirring at 37 ◦C. At fixed time points (45 minutes, 1 hour and 30 minutes, 3 hours and 30 minutes, 5, 6, 8, 24, 48 and 72 hours), 1 mL of the release medium was withdrawn and replaced with an equal volume of fresh buffer. Every volume withdrawn was analyzed by UV–Vis spectroscopy to quantify the

released DOX (λ = 480 nm) using a calibration curve of the drug in PBS previously plotted in the concentration range 3.3–149 μg/mL (ε ≅ 9752 M^{-1} cm^{-1}). Free DOX and star PLA-PEG/DOX NPs were dialyzed in similar conditions at the same concentration (160 μg/mL). The amount of released DOX was corrected taking into account the dimerization and precipitation of the drug under our experimental conditions. To test DOX stability, three DOX solutions in PBS (300, 60 and 6 μM) were kept at 37°C and monitored by UV-Vis analysis at fixed times (45 minutes, 1 hour 30 minutes, 3 hours 30 minutes, 5, 6, 8, 24, 48 and 72 hours) to quantify DOX concentration in solution and to indirectly measure DOX degradation.

6.16. Biological Studies of star PLA-PEG/DOX and star PLA-PEG-RGD/DOX nanoparticles

6.16.1. In vitro study

The biological activity of empty and DOX-loaded NPs was tested in vitro on three osteosarcoma cell lines (MG63, SAOS-2, U2-OS) and on Human Fetal Osteoblasts (hFOBs) as a model of healthy cells, using DOX HCl as a positive control and cells only as a negative control. Star PLA-PEG/DOX and empty star PLA-PEG NPs were tested in vitro at 5.4 μg/mL drug concentration and 105 μg/mL polymer concentration. Star PLA-PEG-RGD/DOX was tested at 2.7 μg/mL, 5.4 μg/mL and 10.8 μg/mL drug concentration. Unloaded star PLA-PEG-RGD NPs were tested at the same concentration used to test DOX-loaded RGD-decorated NPs (31, 62 and 124 μg/mL of polymeric NPs for 2.7 μg/mL, 5.4 μg/mL and 10.8 μg/mL of DOX, respectively). The samples were reconstituted in MilliQ water at a concentration of 1 mg/mL and they were resuspended in tip sonicator for 5 minutes before final dilution in culture media. All cell lines were seeded at a density of 5000 cells/well in 96 well-plates.

The viability of all cell lines grown in the presence of the samples was evaluated after 72 hours of culture by MTT assay. The MTT reagent [3-(4,5-dimethylthiazol-2-

yl)-2,5-diphenyltetrazolium bromide] (5 mg/mL) was dissolved in PBS and the cells were incubated with MTT solution for 2 hours at 37◦C, 5 % CO_2 and controlled humidity conditions. The medium was replaced by incubation for 15 minutes in DMSO with slight stirring and the absorbance was read at 570 nm using a Multiskan FC Microplate Photometer. Absorbance values were directly proportional to the number of metabolically active cells. One experiment was performed and a biological triplicate was performed for each condition.

6.16.2. Cellular uptake

The cellular uptake of both undecorated and RGD-decorated NPs loaded with DOX (5.4 µg/mL) was investigated in all the osteosarcoma cell lines after 72 hours of culture with respect to free DOX. The cells were fixed in 4 % buffered paraformaldehyde (PFA), permeabilized in PBS with 0.1 % (v/v) Triton X-100, and DAPI (600 nM)) counterstaining was performed to highlight cell nuclei. Images of the TRITC and DAPI filters were acquired using an inverted Ti-E fluorescence microscope and merged to observe the nuclear internalization of Dox in the cells. One experiment was performed and a biological duplicate was performed for each condition.

6.16.3. Cell morphology evaluation

The morphology of all the cell lines was analyzed after 72 hours of culture with unloaded RGD-decorated NPs (124 µg/mL). Briefly, cells were fixed in 4% PFA and permeabilized in PBS with 0.1% (v/v) Triton X-100. F-actin filaments were highlighted using a green-fluorescent Alexa Fluor 488® phalloidin probe for 20 minutes incubation and DAPI counterstaining was performed for cell nuclei identification. Images were acquired using an Inverted Ti-E fluorescence microscope. One experiment was performed and a biological duplicate was performed for each condition.

6.17. Lipodisks formulation

For lipodisks preparation, in one case HSPC (5.02 mg) and DSPE-PEG_{2000} (4.46 mg) were used in molar ratio 80:20; in the other case POPC (2.40 mg), CHOL (1.24 mg) and DSPE-PEG_{2000} (4.46 mg) in molar ratio 40:40:20 were used. MEDS433 (0.107 mg, withdrawn from a stock solution in MeOH) was co-dissolved with the lipids in chloroform keeping a 1:30 drug to lipids molar ratio. A uniform film of lipids and MEDS433 was obtained by evaporation of the solvent and it was kept overnight under vacuum. The film was rehydrated with 2 mL of HEPES buffer and it was kept at 65°C for 1 hour, gentle vortexing the forming suspension every 5-10 minutes. The obtained suspension was tip-sonicated for 5 minutes and then centrifuged at 13000 RPM for 6 minutes. The lipodisks suspension was collect as the surnatant, while the residue consisted of the unloaded MEDS433 and metal debris from the tip of the sonicator.

6.18. Characterization of lipodisks formulations

6.18.1. Drug loading and encapsulation efficiency calculation

400 µl of suspension were diluted with 2 mL of ethanol to disassemble the lipodisks and release the MEDS433. The drug was directly quantify by UV-Vis using a previously plotted calibration curve of the drug in the same solvent (concentration range 5-30 µg/mL). The amount of encapsulated MEDS433 was calculated on the basis of optical absorbance data at the wavelength of 282 nm and molar extinction coefficient ($\varepsilon \cong 27550\ M^{-1}\ cm^{-1}$). The volume of supernatant left with the residue is measured and a volume of ethanol is added respecting the same buffer to solvent ratio. The amount of MEDS433 in this solution is measured via UV-Vis and, knowing the concentration of MEDS433 in the suspension from the previous quantification, it is possible to calculate the actual quantity of MEDS433 not encapsulated.

Volumes of 5, 8 and 10 µl of supernatant were mineralized at 400°C, then treated to develop a coloration directly proportional to the concentration of phosphorous in the solution which was quantified via UV-Vis using a previously plotted calibration line of the analyte in the same solvent mixture. Knowing that the amount of phosphorous in the solution comes from the amount of phospholipids used in the formulation, their exact amount can be calculated.

Knowing the total amount of lipids in the formulation, the total amount of MEDS433 used and the amount of drug encapsulated, DL and EE were calculated using the following equations:

–DL (%) = (Drug moles in formulation/Lipids moles in formulation) × 100

–EE (%) = (Drug weight in the NPs/drug weight used in the formulation) × 100

6.18.2. Morphological investigation, size and stability studies

1 µl of suspension was frozen and used for morphological evaluation via Cryo-TEM imaging. 100 µl of suspension were diluted with 900 µl of HEPES buffer and used as such for DLS measurements. The stability of the suspension was monitored by repeating the same measurements on a formulation kept for a week at room temperature and on a formulation kept for two months in refrigerated conditions (4°C).

6.19. Release study

The release study was carried out transferring 500 µl of suspension inside a dialysis membrane. This was then put inside 25 mL of HEPES buffer containing 1% v/v Tween 80 to ensure sink conditions. The whole apparatus was kept at 37°C and at predetermined time points (1, 3, 7 12, 24 and 48 hours) 1 mL of the external medium was withdrawn and replaced with fresh HEPES buffer. At the end of the release experiment, the dialysis membrane was torn and the inner solution was thoroughly

mixed with the external medium. Therefore, a sample of the unreleased drug was obtained at the same dilution of the samples of the previous time point. 400 μL of each withdrawn volume was diluted with 2 mL of ethanol and analyzed by fluorimetry (excitation wavelength = 282 nm and emission wavelength = 401 nm). The release profile of free MEDS433 was investigated under the same experimental conditions at its solubility limit (12 μM).

6.20. Cyclodextrin formulations

The formulation of SC6OH cyclodextrin incorporating MEDS433 was performed via film rehydration of the drug with an aqueous solution of CD (940 μg in 2 mL of ultrapure water). A film of MEDS433 (26 or 51 μg for 5:1 and 2.5:1 ratio, respectively) was prepared by solvent evaporation and rehydrated with the SC6OH aqueous solution. The solution was vortexed until total rehydration and dissolution of the film to obtain two SC6OH@MEDS433 formulations at concentrations 160 μM:64 μM and 160 μM:32 μM.

6.21. Characterization of cyclodextrin formulations

The two SC6OH@MEDS433 formulations were characterized by UV-Vis analysis and the profile and intensity were compared to that of free MEDS433 solution.

6.22. Release study

The release study was carried out transferring inside a dialysis membrane 1 mL of binary formulation with cyclodextrin and MEDS433 at concentrations 320 μM and 128 μM, respectively (MEDS433 content of 51 μg). This was then put inside 50 mL of PBS buffer containing 1% v/v Tween 80 to ensure sink conditions. The whole apparatus was kept at 37°C and at predetermined time points (1, 2, 4, 6, 8, 24, 48 and

72 hours) 1 mL of the external medium was withdrawn and replaced with fresh buffer. At the end of the release experiment, the solution inside the internal jacket was diluted 50 times to achieve the same dilution factor of MEDS433 in the external medium. Fluorimetric analysis (excitation wavelength = 315 nm and emission wavelength = 406 nm) was carried out for MEDS433 quantification and a release profile was plotted.

Legend of Abbreviations

BSAA = Broad Spectrum Antiviral Agent

CuAAC = Copper-catalyzed Azide-Alkyne Cycloaddition

DDS = Drug Delivery System

DOX = Doxorubicin

DTX = Docetaxel

hDHODH = human DiHydroOrotate DeHydrogenase

LNZ = Linezolid

MRSA = Methicillin Resistant Staphilococcus Aureus

Mtb = Multidrug Resistant-Mycobacterium Tubercolosis

NPs = Nanoparticles

PCL = Polycaprolactone

PEG = PolyEthylene Glycol

PLA = PolyLactic Acid

PLGA = PolyLactic-co-Glycolic Acid

ROP = Ring Opening Polymerization

Publications

- Serena Maria Torcasio, **Roberto Oliva**, Monica Montesi, Silvia Panseri, Giada Bassi, Antonino Mazzaglia, Anna Piperno, Olivier Coulembier, Angela Scala, *Three-armed RGD-decorated starPLA-PEG nanoshuttle for docetaxel delivery*, Biomaterials Advances 140, 2020, 213043.
- **Roberto Oliva**, Giovanna Ginestra, Anna Piperno, Antonino Mazzaglia, Antonia Nostro, Angela Scala. *Harnessing the power of PLA-PEG nanoparticles for Linezolid delivery against methicillin-resistant Staphylococcus aureus*. International Journal of Pharmaceutics 642, 2023, 123067.
- **Roberto Oliva**, Serena M. Torcasio, Olivier Coulembier, Anna Piperno, Antonino Mazzaglia, Arianna Rossi, Giada Bassi, Silvia Panseri, Monica Montesi, Angela Scala. *RGD-tagging of star-shaped PLA-PEG Micelles enhances Doxorubicin Efficacy against Osteosarcoma.* International Journal of Pharmaceutics 657, 2024, 124183.

Conference Proceedings

- 2 December 2021: Convegno SCI della Sezione Sicilia. Oral Communication (OC5): "*Sintesi e potenzialità biologiche di copolimeri anfifilici a stella a base di PLA-PEG*".
- 13-17 June 2022: 20th International Ciclodextrin Symposium. Poster Presentation (P40): *"Supramolecular assembly of adamantane-functionalized bodipy and polylactide-cyclodextrin conjugate".*
- 11-15 September 2022: XL Convegno Nazionale della Divisione di Chimica Organica della Società Chimica Italiana. Poster presentation (PC-71): *"Synthesis of BODIPY-labeled β-Cyclodextrin-grafted Star-PLA-PEG Copolymers"*
- 11-15 September 2022: XL Convegno Nazionale della Divisione di Chimica Organica della Società Chimica Italiana. Poster presentation (PC72): *"Three-armed RGD-decorated Star-PLA-PEG Nanoshuttle for Antitumoral Drugs Delivery".*
- 5-7 June 2024: 8th Milan Polymer Days International Congress (MIPOL2024). Oral Communication MYOC (Mipol Young Oral Communication) *"Synthesis of linear and branched amphiphilic PLA-PEG copolymers for drug delivery".*

Periods as Visiting PhD student

- 01/10/2022-31/03/2023 (6 months): Uppsala University, Sweden. Supervisor: Prof. Katarina Edwards.
- 04/10/2023-22/12/2023 (3 months): Université de Mons, Belgium. Supervisor: Prof. Olivier Coulembier.

References

[1] S. M. Torcasio, R. Oliva, M. Montesi, S. Panseri, G. Bassi, A. Mazzaglia, A. Piperno, O. Coulembier, A. Scala, "Three-armed RGD-decorated starPLA-PEG nanoshuttle for docetaxel delivery", *Biomaterials Advances 140*, **2022**, 213043

[2] R. Oliva, S. M. Torcasio, O. Coulembier, A. Piperno, A. Mazzaglia, S. Scalese, A. Rossi, G. Bassi, S. Panseri, M. Montesi, A. Scala, "RGD-tagging of star-shaped PLA-PEG micellar nanoassemblies enhances doxorubicin efficacy against osteosarcoma", *International Journal of Pharmaceutics 657*, **2024**, 124183

[3] C. Foti, A. Piperno, A. Scala, O. Giuffrè, "Oxazolidinone Antibiotics: Chemical, Biological and Analytical Aspects", *Molecules 26*, **2021**, 4280

[4] R. Oliva, G. Ginestra, A. Piperno, A. Mazzaglia, A. Nostro, A. Scala, "Harnessing the power of PLA-PEG nanoparticles for Linezolid delivery against methicillin-resistant *Staphylococcus aureus*", *International Journal of Pharmaceutics 642*, **2023**, 123067

[5] M. Oleksy, K. Dynarowicz, D. Aebisher, "Advances in Biodegradable Polymers and Biomaterials for Medical Applications—A Review", *Molecules 28*, **2023**, 6213

[6] R. Álvarez-Chimal, J. A. Arenas-Alatorre, M. A. Álvarez-Pérez, "Nanoparticle-polymer composite scaffolds for bone tissue engineering. A review", *European Polymer Journal 213*, **2024**, 113093

[7] R. R. Naik, A. A. Roy, S. Mutalik, N. Dhas, "Unleashing the power of polymeric nanoparticles — Creative triumph against antibiotic resistance: A review", *International Journal of Biological Macromolecules 278*, **2024**, 134977

[8] V. Rahimkhoei, A. H. Alzaidy, M. J. Abed, S. Rashki, M. Salavati-Niasari, "Advances in inorganic nanoparticles-based drug delivery in targeted breast cancer theranostics", *Advances in Colloid and Interface Science 329*, **2024**, 103204

[9] R. Saker, G. Regdon jr., Tamás Sovány, "Pharmacokinetics and toxicity of inorganic nanoparticles and the physicochemical properties/factors affecting them", *Journal of Drug Delivery Science and Technology 99*, **2024**, 105979

[10] V. K. Panthi, K. E. Fairfull-Smith, N. Islam, "Antibiotic loaded inhalable liposomal nanoparticles against lower respiratory tract infections: Challenges, recent advances, and future perspectives", *Journal of Drug Delivery Science and Technology 94*, **2024**, 105517

[11] K. Panthi, K. E. Fairfull-Smith, N. Islam, "Liposomal drug delivery strategies to eradicate bacterial biofilms: Challenges, recent advances, and future perspectives", *International Journal of Pharmaceutics 655*, **2024**, 124046

[12] Y. Mei, J. Hu, Y. Cao, X. Gao, L. Tang, W. Wang, "Versatile hydrogel-based drug delivery platform for multimodal cancer therapy from bench to bedside", *Applied Materials Today 39*, **2024**, 102341

[13] J. Gong, L. Hou, Y. C. Ching, K. Y. Ching, N. D. Hai, C. H. Chuah, "A review of recent advances of cellulose-based intelligent-responsive hydrogels as vehicles for controllable drug delivery system", *International Journal of Biological Macromolecules 264*, **2024**, 130525

[14] R. J. Sarode, H. S. Mahajan, "Dendrimers for drug delivery: An overview of its classes, synthesis, and applications", *Journal of Drug Delivery Science and Technology 98*, **2024**, 105896

[15] L. T. Thuya, N. Kanga, M. Choia, M. Leeb, J. S. Choi, "Dendrimeric micelles composed of polyamidoamine dendrimer-peptide cholesterol conjugates as drug carriers for the treatment of melanoma and bacterial infection", *Journal of Industrial and Engineering Chemistry 114*, **2022**, 361-376

[16] Y. Jia, Y. Jiang, Y. He, W. Zhang, J. Zou, K. T. Magar, H. Boucetta, C. Teng, W. He, "Approved Nanomedicine against Diseases", *Pharmaceutics 15*, **2023**, 774

[17] A. Albanese, P. S. Tang, W. C. W. Chan, "The Effect of Nanoparticle Size, Shape, and Surface Chemistry on Biological Systems", *Annual Review of Biomedical Engineering 14*, **2012**, 1-16

[18] J. G. Henn, T. A. S. Aguirre, M. Nugent, D. J. Moura, "Cancer nanomedicine: Recent developments in drug delivery systems and strategies to overcome eventual barriers to achieve a better outcome", *Journal of Drug Delivery Science and Technology 91*, **2024**, 105254

[19] Q. Fang, X. Pan, "A systematic review of antibiotic resistance driven by metal-based nanoparticles: Mechanisms and a call for risk mitigation", *Science of The Total Environment 916*, **2024**, 170080

[20] A. Sharma, M. Singh, V. Sharma, A. Vashishth, M. Raj, S. K. Upadhyay, S. Singh, S. Ramniwas, K. Dhama, A. K. Sharma, S. K. Bhatia, "Current paradigms in employing self-assembled structures: Drug delivery implications with improved therapeutic potential", *Colloids and Surfaces B: Biointerfaces 234*, **2024**, 113745

[21] Q. Liu, J. Zou, Z. Chen, W. He, W. Wu, "Current research trends of nanomedicines", *Acta Pharmaceutica Sinica B 13 (11)*, **2023**, 4391-4416

[22] P. Tang, T. Shen, H. Wang, R. Zhang, X. Zhang, X. Li, W. X, "Challenges and opportunities for improving the druggability of natural product: Why need drug delivery system?", *Biomedicine & Pharmacotherapy 164*, **2023**, 114955

[23] A. Kumar, R. K. Mishra, S. M. Aldosari, C. K. Maity, S. Verma, R. Patel, V. K. Thakur, "A comprehensive review of various biopolymer composites and their applications: From biocompatibility to self-healing", *Materials Today Sustainability 23*, **2023**, 100431

[24] M. H. Syed, M. A. K. M. Zahari, M. M. R. Khan, M. D. H. Beg, N. Abdullah, "An overview on recent biomedical applications of biopolymers: Their role in drug delivery systems and comparison of major systems", *Journal of Drug Delivery Science and Technology 80*, **2023**, 104121

[25] W. A. Akbar, H. U. Rahim, F. A. Rutigliano, "Microbial- and seaweed-based biopolymers: Sources, extractions and implications for soil quality improvement and environmental sustainability - A review", *Journal of Environmental Management 359*, **2024**, 120964

[26] B. B. Yerramathi, B. A. Muniraj, M. Kola, K. K. Konidala, P. K. Arthala, T. S. K. Sharma, "Alginate biopolymeric structures: Versatile carriers for bioactive compounds in functional foods and nutraceutical formulations: A review", *International Journal of Biological Macromolecules 253*, **2023**, 127067

[27] P. Rakshit, T. K. Giri, K. Mukherjee, "Research progresses on carboxymethyl xanthan gum: Review of synthesis, physicochemical properties, rheological characterization and applications in drug delivery", *International Journal of Biological Macromolecules 226*, **2024**, 131122

[28] A. N. Amitaye, E. E. Elemike, H. B. Akpeji, E. Amitaye, I. Hossain, J. I. Mbonu, A. E. Aziza, "Chitosan: A sustainable biobased material for diverse applications", *Journal of Environmental Chemical Engineering 12*, **2024**, 113208

[29] S. Xu, H. Xu, W. Wang, S. Li, H. Li, T. Li, W. Zhang, X. Yu, L. Liu, "The role of collagen in cancer: from bench to bedside", *Journal of Translational Medicine 17*, **2019**, 309

[30] B. An, Y. Lin, B. Brodsky, "Collagen interactions: Drug design and delivery", *Advanced Drug Delivery Reviews 97*, **2016**, 69-84

[31] M. W. Ndinguri, A. Zheleznyak, J. L. Lauer, C. J. Anderson, G. B. Fields, "Application of Collagen-Model Triple-Helical Peptide-Amphiphiles for CD44-Targeted Drug Delivery Systems", *Journal of Drug Delivery 2012*, **2012**, 592602

[32] Z. Dong, X. Meng, W. Yang, J. Zhang, P. Sun, H. Zhang, X. Fang, D. Wang, C. Fan, "Progress of gelatin-based microspheres (GMSs) as delivery vehicles of drug and cell", *Materials Science & Engineering C 122*, **2021**, 111949

[33] M. Diba, B. Pape, A. Klymov, Y. Zhang, J. Song, D. W. P. M. Löwik, H. Seyednejad, S. C. G. Leeuwenburgh, "Nanostructured raspberry-like gelatin microspheres for local delivery of multiple biomolecules", *Acta Biomaterialia 58*, **2017**, 67-79

[34] K. De Clercq, F. Xie, O. De Wever, B. Descamps, A. Hoorens, A. Vermeulen, W. Ceelen, C. Vervaet, "Preclinical evaluation of local prolonged release of paclitaxel from gelatin microspheres for the prevention of recurrence of peritoneal carcinomatosis in advanced ovarian cancer", *Scientific Reports 9:1*, **2019**, 14881

[35] A. Passi, D. Vigetti, "Hyaluronan as tunable drug delivery system", *Advanced Drug Delivery Reviews 146*, **2019**, 83-96

[36] M. Hussaina, S. M. Khana, M. Shafiqa, N. Abbas, "A review on PLA-based biodegradable materials for biomedical applications", *Giant 18*, **2024**, 100261

[37] A. K. Shakya, M. Al-Sulaibi, R. R. Naik, H. Nsairat, S. Suboh, A. Abulaila, "Review on PLGA Polymer Based Nanoparticles with Antimicrobial Properties and Their Application in Various Medical Conditions or Infections", *Polymers 15*, **2023**, 3597

[38] S. Ladhari, N. Vu, C. Boisvert, A. Saidi, P. Nguyen-Tri, "Recent Development of Polyhydroxyalkanoates (PHA)-Based Materials for Antibacterial Applications: A Review", *ACS Applied Bio Materials 6:4*, **2023**, 1398-1430

[39] A. Bhadran, T. Shah, G. K. Babanyinah, H. Polara, S. Taslimy, M. C. Biewer, M. C. Stefan, "Recent Advances in Polycaprolactones for Anticancer Drug Delivery", *Pharmaceutics 15*, **2023**, 1977

[40] T. A. Swetha, A. Bora, K. Mohanrasu, P. Balaji, R. Raja, K. Ponnuchamy, G. Muthusamy, A. Arun, "A comprehensive review on polylactic acid (PLA) – Synthesis, processing and application in food packaging", *International Journal of Biological Macromolecules 234*, **2023**, 123715

[41] B. Tyler, D. Gullotti, A. Mangraviti, T. Utsuki, H. Brem, "Polylactic acid (PLA) controlled delivery carriers for biomedical applications", *Advanced Drug Delivery Reviews 107*, **2016**, 163-175

[42] A. Kolate, D. Baradia, S. Patil, I. Vhora, G. Kore, A. Misra, "PEG — A versatile conjugating ligand for drugs and drug delivery systems", *Journal of Controlled Release 192*, **2014**, 67-81

[43] J. S. Suka, Q. Xua, N. Kima, J. Hanesa, L. M. Ensigna, "PEGylation as a strategy for improving nanoparticle-based drug and gene delivery", *Advanced Drug Delivery Reviews*, **2016**, 28-51

[44] M. Ghezzi, S. Pescina, C. Padula, P. Santi, E. Del Favero, L. Cantù, S. Nicoli, "Polymeric micelles in drug delivery: An insight of the techniques for their characterization and assessment in biorelevant conditions", *Journal of Controlled Release 332*, **2021**, 312-336

[45] K. Knop, R. Hoogenboom, D. Fischer, U. S. Schubert, "Poly(ethylene glycol) in Drug Delivery: Pros and Cons as Well as Potential Alternatives", *Angewandte Chemie International Edition 49*, **2010**, 6288-6308

[46] G. Pasut, F. M. Veronese, "State of the art in PEGylation: The great versatility achieved after forty years of research", *Journal of controlled release 161*, **2012**, 161, 461-472

[47] L. Shi, J. Zhang, M. Zhao, S. Tang, X. Cheng, W. Zhang, W. Li, X. Liu, H. Peng, Q. Wang, "Effects of polyethylene glycol on the surface of nanoparticles for targeted drug delivery", *Nanoscale 13*, **2021**, 10748-10764

[48] S. Vasvani, P. Kulkarni, D. Rawtani, "Hyaluronic acid: A review on its biology, aspects of drug delivery, route of administrations and a special emphasis on its approved marketed products and recent clinical studies", *International Journal of Biological Macromolecules 151*, **2020**, 1012-1029

[49] A. P. Pandey, K. K. Sawant, "Polyethylenimine: A versatile, multifunctional non-viral vector for nucleic acid delivery", *Materials Science and Engineering C 68*, **2016**, 904-918

[50] J. Casper, S. H. Schenk, E. Parhizkar, P. Detampel, A. Dehshahri, J. Huwyler, "Polyethylenimine (PEI) in gene therapy: Current status and clinical applications", *Journal of Controlled Release 362*, **2023**, 667-691

[51] T. Pulingam, P. Foroozandeh, J. Chuah, K. Sudesh, "Exploring Various Techniques for the Chemical and Biological Synthesis of Polymeric Nanoparticles", *Nanomaterials 12*, **2022**, 576

[52] M. Turchi, A. P. Karcz, M. P. Andersson, "First-principles prediction of critical micellar concentrations for ionic and nonionic surfactants", *Journal of colloid Science 606*, **2022**, 618-627

[53] X. Jin, P. Sun, G. Tong, X. Zhu, "Star polymer-based unimolecular micelles and their application in bio-imaging and diagnosis", *Biomaterials 178*, **2018**, 738-750

[54] J. M. Ren, T. G. McKenzie, Q. Fu, E. H. H. Wong, J. Xu, Z. An, S. Shanmugam, T. P. Davis, C. Boyer, G. G. Qiao, "Star Polymers", *Chemical Reviews 116*, **2016**, 6743-6836

[55] B. Mendrek, N. Oleszko-Torbus, P. Teper, A. Kowalczuk, "Towards next generation polymer surfaces: Nano- and microlayers of star macromolecules and their design for applications in biology and medicine", *Progress in Polymer Science 139*, **2023**, 101657

[56] R. Joy, J. George, Franklin John, "Brief Outlook on Polymeric Nanoparticles, Micelles, Niosomes, Hydrogels and Liposomes: Preparative Methods and Action", *ChemistrySelect 7*, **2022**, e202104045

[57] M. Qi, Y. Zhou, "Multimicelle aggregate mechanism for spherical multimolecular micelles: from theories, characteristics and properties to applications", *Material Chemistry Frontiers 3*, **2019**, 1994-2009

[58] Y. Barenholz, "Doxil® — The first FDA-approved nano-drug: Lessons learned", *Journal of Controlled Release 160*, **2012**, 117-134

[59] N. Wanga, M. Chenb, T. Wang, "Liposomes used as a vaccine adjuvant-delivery system: From basics to clinical immunization", *Journal of Controlled Release 303*, **2019**, 130-150

[60] J. Szebeni, B. Kiss, T. Bozó, K. Turjeman, Y. Levi-Kalisman, Y. Barenholz, M. Kellermayer, "Insights into the Structure of Comirnaty Covid-19 Vaccine: A Theory on Soft, Partially Bilayer-Covered Nanoparticles with Hydrogen Bond-Stabilized mRNA−Lipid Complexes", *ACS Nano 17*, **2023**, 13147-13157

[61] R. P. Singh, H. V. Gangadharappa, K. Mruthunjaya, "Phospholipids: Unique carriers for drug delivery systems", *Journal of Drug Delivery Science and Technology 39*, **2017**, 166-179

[62] D. E. Large, R. G. Abdelmessih, E. A. Fink, D. T. Auguste, "Liposome composition in drug delivery design, synthesis, characterization, and clinical application", *Advanced Drug Delivery Reviews 176*, **2021**, 113851

[63] H. Nsairat, D. Khater, U. Sayed, F. Odeh, A. Al Bawab, W. Alshaer, "Liposomes: structure, composition, types, and clinical applications", *Heliyon 8*, **2022**, e09394

[64] A. Gabizon, H. Shmeeda, E. Tahover, G. Kornev, Y. Patil, Y. Amitay, P. Ohana, E. Sapir, S. Zalipsky, "Development of Promitil®, a lipidic prodrug of mitomycin c in PEGylated liposomes: From bench to bedside", *Advanced Drug Delivery Reviews 154-155*, **2020**, 13-26

[65] K. Ren, X. Cao, L. Zheng, S. Liu, L. Li, L. Cheng, T. Tian, X. Tong, H. Wang, L. Jiang, "Liposomes decorated with β-conglycinin and glycinin: Construction, structure and in vitro digestive stability", *International Journal of Biological Macromolecules 269*, **2024**, 131900

[66] E. Gazzano, I. Buondonno, A. Marengo, B. Rolando, K. Chegaev, J. Kopecka, S. Saponara, M. Sorge, C. M. Hattinger, A. Gasco, R. Fruttero, M. Brancaccio, M. Serra, B. Stella, E. Fattal, S. Arpicco, C. Riganti, "Hyaluronated liposomes containing H2S-releasing doxorubicin are effective against P-glycoprotein-positive/doxorubicin-resistant osteosarcoma cells and xenografts", *Cancer Letters 456*, **2019**, 2-39

[67] D. Wei, Y. Huang, M. Liang, P. Ren, Y. Tao, L. Xu, T. Zhang, Z. Ji, Q. Zhang, "Polypropylene composite hernia mesh with anti-adhesion layer composed of PVA hydrogel and liposomes drug delivery system", *Colloids and Surfaces B: Biointerfaces 223*, **2023**, 113159

[68] S. Park, H. K. Kim, "Development of skin-permeable flexible liposome using ergosterol esters containing unsaturated fatty acids", *Chemistry and Physics of Lipids 250*, **2023**, 105270

[69] G. Wang, C. Peng, M. Tang, Y. Wang, J. Li, H. Chen, X. Chang, Z. Shu, N. He, J. Guo, S. Gui, "Simultaneously boosting inflammation resolution and osteogenic differentiation in periodontitis using folic acid-modified liposome-thermosensitive hydrogel composites", *Materials & Design 234*, **2023**, 112314

[70] Y. Tao, Y. Chen, S. Wang, W. Chen, D. Zhou, D. Chen, C. Zhang, Z. Wu, J. Yan, H. Zhang, Y. Wei, J. Su, "Optimizing the modification density of acid oligopeptides to enhance the bone-targeting activity of liposomes", *Composites Part B 247*, **2022**, 110288

[71] H. Nsairat, I. S. Mahmoud, F. Odeh, D. Abuarqoub, H. Al-Azzawi, R. Zaza, M. I. Qadri, S. Ismail, A. Al Bawab, A. Awidiefi, W. Alshaer, "Grafting of anti-nucleolin aptamer into preformed and remotely loaded liposomes through aptamercholesterol post-insertion", *RSC Advances 10*, **2020**, 36219–36229

[72] A. I. Antoniou, S. Giofrè, P. Seneci, D. Passarella, S. Pellegrino, "Stimulus-responsive liposomes for biomedical applications", *Drug Discovery Today 26*, **2021**, 8

[73] Y. Wei, J. Lv, S. Zhu, S. Wang, J. Su, C. Xu, "Enzyme-responsive liposomes for controlled drug release", *Drug Discovery Today 29*, **2024**, 7

[74] J. Lou, M. D. Best, "A General Approach to Enzyme-Responsive Liposomes", *Chemistry 26*, **2020**, 8597-8607

[75] B. dos Santos Rodriguesa, H. Oueb, A. Banerjeea, T. Kanekiyob, J. Singh, "Dual functionalized liposome-mediated gene delivery across triple co-culture blood brain barrier model and specific in vivo neuronal transfection", *Journal of Controlled Release 286*, **2018**, 264-278

[76] D. Guiamarãraes, A. Cavaco-Paulo, E. Nogueira, "Design of liposomes as drug delivery system for therapeutic applications", *International Journal of Pharmaceutics 601*, **2021**, 120571

[77] K. Edwards, M. Johnsson, G. Karlsson, M. Silvander, "Effect of Polyethyleneglycol-Phospholipids on Aggregate Structure in Preparations of Small Unilamellar Liposomes", *Biophysical Journal 73*, **1997**, 258-266

[78] E. S. Levy, J. Yu, A. Estevez, J. Mao,·L. Liu, E. Torres, D. Leung, C. Yen, "A Systematic Approach for Liposome and Lipodisk Preclinical Formulation Development by Microfuidic Technology", *The AAPS Journal 23*, **2021**, 111

[79] M. M. Zetterberg, S. Ahlgren, V. A. Hernández, N. Parveen, K Edwards, "Optimization of lipodisk properties by modification of the extent and density of the PEG corona", *Journal of Colloid and Interface Science 484*, **2016**, 86-96

[80] S. Lundsten, V. A. Hernández, L. Gedda, T. Sarén, C. J. Brown, D. P. Lane, K. Edwards, M. Nestor, "Tumor-Targeted Delivery of the p53-Activating Peptide VIP116 with PEG-Stabilized Lipodisks", *Nanomaterials 10*, **2020**, 783

[81] S. Ahlgren, K. Reijmar, K. Edwards, "Targeting lipodisks enable selective delivery of anticancer peptides to tumor cells", *Nanomedicine: Nanotechnology, biology, and Medicine 13*, **2017**, 2325-2328

[82] K. M. Sahu, S. Patra, S. K. Swain, "Host-guest drug delivery by β-cyclodextrin assisted polysaccharide vehicles: A review", *International Journal of Biological Macromolecules 240*, **2023**, 124338

[83] A. Cid-Samamed, J. Rakmai, J. C. Mejuto, J. Simal-Gandara, G. Astray, "Cyclodextrins inclusion complex: Preparation methods, analytical techniques and food industry applications", *Food Chemistry 384*, **2022**, 132467

[84] L. Ferreira, F. Mascarenhas-Melo, S. Rabaça, A. Mathur, A. Sharma, P. S. Giram, K. D. Pawar, A. Rahdar, F. Raza, F. Veiga, P. G. Mazzola, A. C. Paiva-Santos, "Cyclodextrin-based dermatological formulations: Dermopharmaceutical and cosmetic applications", *Colloids and Surfaces B: Biointerfaces 221*, **2023**, 113012

[85] Y. Li, F. Liu, T. Abdiryim, X. Liu, "Cyclodextrin-derived materials: From design to promising applications in water treatment", *Coordination Chemistry Reviews 502*, **2024**, 215613

[86] A. C. Peralta, F. J. R. Mejías, J. Ayuso, C. Rial, J. M. G. Molinillo, J. A. Álvarez, S. Schwaiger, F. A. Macías, "Host–guest complexation of phthalimide-derived strigolactone mimics with cyclodextrins. Application in agriculture against parasitic weeds", *Organic & Biomolecular Chemistry 21*, **2023**, 3214-3225

[87] P. Singh, R. Mahar, "Cyclodextrin in drug delivery: Exploring scaffolds, properties, and cutting-edge applications", *International Journal of Pharmaceutics 662*, **2024**, 124485

[88] H. Liu, S. Guo, S. Wei, J. Liu, B. Tian, "Pharmacokinetics and pharmacodynamics of cyclodextrin-based oral drug delivery formulations for disease therapy", *Carbohydrate Polymers 329*, **2024**, 121763

[89] B. Sharmah, J. Das, P. Manna, "Insight into the drug delivery efficacy and anti-diabetic potential of cyclodextrin against hyperglycemia", *Inorganic Chemistry Communications 161*, **2024**, 112034

[90] M. H. Asim, M. Ijaz, A. C. Röscha, A. Bernkop-Schnürch, "Thiolated cyclodextrins: New perspectives for old excipients", *Coordination Chemistry Reviews 420*, **2020**, 213433

[91] R. Zagami, V. Rapozzi, A. Piperno, A. Scala, C. Triolo, M. Trapani, L. E. Xodo, L. Monsù Scolaro, A. Mazzaglia, "Folate-Decorated Amphiphilic Cyclodextrins as Cell-Targeted Nanophototherapeutics", *Biomacromolecules 20*, **2019**, 2530-2544

[92] M. L. Bondì, A. Scala, G. Sortino, E. Amore, C. Botto, A. Azzolina, D. Balasus, M. Cervello, A. Mazzaglia, "Nanoassemblies Based on Supramolecular Complexes of Nonionic Amphiphilic Cyclodextrin and Sorafenib as Effective Weapons to Kill Human HCC Cells", *Biomacromolecules 16*, **2015**, 3784-3791

[93] C. Conte, A. Scala, G. Siracusano, G. Sortino, R. Pennisi, A. Piperno, A. Miro, F. Ungaro, M. T. Sciortino, F. Quaglia, A. Mazzaglia, "Nanoassemblies based on non-ionic amphiphilic cyclodextrin hosting Zn(II)-phthalocyanine and docetaxel: Design, physicochemical properties and intracellular effects", *Colloids and Surfaces B: Biointerfaces 146*, **2016**, 590-597

[94] A. Mazzaglia, G. Natale, R. Tosto, A. Scala, G. Sortino, A. Piperno, M. P. Casaletto, A. Riminucci, M. L. Giuffrida, P. G. Mineo, V. Villari, N. Micali, G. Pappalardo, "KLVFF oligopeptide-decorated amphiphilic cyclodextrin nanomagnets for selective amyloid beta recognition and fishing", *Journal of Colloid and Interface Science 613*, **2020**, 814

[95] M. Trapani, A. Scala, P. G. Mineo, A. Pistone, A. Díaz-Moscoso, A. Fragoso, L. M. Scolaro, A. Mazzaglia, "Thiolated amphiphilic β-cyclodextrin-decorated gold colloids: Synthesis, supramolecular nanoassemblies and controlled release of dopamine", *Journal of Molecular Liquids 336*, **2021**, 116880

[96] H. M. S. H. Soe, T. Loftsson, P. Jansook, "The application of cyclodextrins in drug solubilization and stabilization of nanoparticles for drug delivery and biomedical applications", *International Journal of Pharmaceutics 666*, **2024**, 124787

[97] J. S. Negi, P. Chattopadhyay, A. K. Sharma, V. Ram, "Preparation of gamma cyclodextrin stabilized solid lipid nanoparticles (SLNS) using stearic acid–c-cyclodextrin inclusion complex", *Journal of Inclusion Phenomena and Macrocyclic Chemistry 80*, **2014**, 359-368

[98] S. Somsri, A. Prasertsab, P. Pornsetmetakul, "Synthesis of cyclodextrin-stabilized gold nanoparticles supported hierarchical zeolites for the facile production of furandicarboxylic acid (FDCA) from 5-hydroxymethylfurfural (HMF)", *Microporous and Mesoporous Materials 354 (51)*, **2023**, 112559

[99] F. Topuz, T. Uyar, "Cyclodextrin-assisted synthesis of tailored mesoporous silica nanoparticles", *Beilstein Journal of Nanotechnology 9*, **2018**, 693-703

[100] A. Scala, A. Piperno, S. M. Torcasio, A. Nicosia, P. G. Mineo, G. Grassi, ""Clickable" polylactic acids obtained by solvent free intra-chain amidation", European Polymer Journal 109, 2018, 341-346

[101] R. Liénard, M. Montesi, S. Panseri, S. M. Dozio, F. Vento, P. G. Mineo, A. Piperno, J. De Winter, O. Coulembier, A. Scala, "Design of naturally inspired jellyfish-shaped cyclopolylactides to manage osteosarcoma cancer stem cells fate", *Materials Science & Engineering C 117*, **2020**, 111291

[102] A. M. Ribeiro, B. N. Estevinho, F. Rocha, "The progress and application of vitamin E encapsulation – A review", *Food Hydrocolloids 121*, **2021**, 106998

[103] E. Fazio, A. Scala, S. Grimato, A. Ridolfo, G. Grassi, F. Neri, "Laser light triggered smart release of silibinin from a PEGylated–PLGA gold nanocomposite", *Journal of Material Chemistry B 3*, **2015**, 9023-9032

[104] J. Huang, Z. Chen, Y. Li, L. Li, G. Zhang, "Rifapentine-linezolid-loaded PLGA microspheres for interventional therapy of cavitary pulmonary tuberculosis: preparation and in vitro characterization", *Drug Design, Development and Therapy 11*, **2017**, 585-592

[105] M. Glinka, K. Filatova, J. Kucinska-Lipka, E. Domincova Bergerova, A. Wasik, V. Sedlarík, "Encapsulation of Amikacin into Microparticles Based on Low-Molecular-Weight Poly(lactic acid) and Poly(lactic acid-co-polyethylene glycol)", *Molecular Pharmaceutics 28*, **2021**, 2986-2996

[106] L. Abad, V. Tafani, J. Tasse, J. Josse, C. Chidiac, S. Lustig, T. Ferry, A. Diot, F. Laurent, F. Valour, "Evaluation of the ability of linezolid and tedizolid to eradicate intraosteoblastic and biofilm-embedded Staphylococcus aureus in the bone and joint infection setting", *Journal of Antimicrobial. Chemotherapy 74*, **2018**, 625–632

[107] V. Cafiso, T. Bertuccio, D. Spina, S. Purrello, S. Stefani, "Tigecycline inhibition of a mature bio¢lm in clinical isolates of Staphylococcus aureus: comparison with other drugs", *Immunology and Medical Micorbiology 59*, **2010**, 466-469

[108] F. Sivori, I. Cavallo, D. Kovacs, M. Guembe, I. Sperduti, M. Truglio, M. Pasqua, G. Prignano, A. Mastrofrancesco, L. Toma, F. Pimpinelli, A. Morrone, F. Ensoli, E. G. Di Domenico, "Role of Extracellular DNA in Dalbavancin Activity against Methicillin-Resistant Staphylococcus aureus (MRSA) Biofilms in Patients with Skin and Soft Tissue Infections", *Microbiology Spectrum 10*, **2022**, 2

[109] K. Kalishwaralal, S. BarathManiKanth, S. R. K. Pandian, V. Deepak, S. Gurunathan, "Silver nanoparticles impede the biofilm formation by *Pseudomonas aeruginosa* and *Staphylococcus epidermidis*", *Colloids and Surfaces B: Biointerfaces 79*, **2010**, 340-344

[110] D. Da Costa, C. Exbrayat-Héritier, B. Rambaud, S. Megy, R. Terreux, B. Verrier, C. Primard, "Surface charge modulation of rifampicin-loaded PLA nanoparticles to improve antibiotic delivery in Staphylococcus aureus bioflms", *Journal of Nanobiotechnology 19*, **2021**, 12

[111] N. Hadjichristidis, M. Pitsikalis, H. Iatrou, P. Driva, G. Sakellariou, M. Chatzichristidi, "Polymers with Star-Related Structures: Synthesis, Properties, and Applications", *Polymer Science: A Comprehensive Reference 6*, **2012**, 29-111

[112] C. Garofalo, G. Capuano, R. Sottile, R. Tallerico, R. Adami, E. Reverchon, E. Carbone, L. Izzo, D. Pappalardo, "Different Insight into Amphiphilic PEG-PLA Copolymers: Influence of Macromolecular Architecture on the Micelle Formation and Cellular Uptake", *Biomacromolecules 15*, **2014**, 403-415

[113] R. Mahou, C. Wandrey, "Versatile Route to Synthesize Heterobifunctional Poly(ethylene glycol) of Variable Functionality for Subsequent Pegylation", *Polymers 4*, **2012**, 561-589

[114] U. K. Marelli, F. Rechenmacher, T. R. A. Sobahi, C. Mas-Moruno, H. Kessler, "Tumor targeting via integrin ligands", *Frontiers in Oncology 3*, **2013**, 222

[115] C. Li, W. Wang, Y.i Xi, J. Wang, J. Chen, J. Yun, Y. Le, "Design, preparation and characterization of cyclic RGDfK peptide modified poly(ethylene glycol)-block-poly(lactic acid) micelle for targeted delivery", *Materials Science and Engineering C 64*, **2016**, 303-309

[116] O. Diou, E. Fattal, V. Delplace, N. Mackiewicz, J. Nicolas, S. Mériaux, J. Valette, C. Robic, N. Tsapis, "RGD decoration of PEGylated polyester nanocapsules of perfluorooctyl bromide for tumor imaging: Influence of pre or post-functionalization on capsule morphology", *European Journal of Pharmaceutics and Biopharmaceutics 87*, **2014**, 170-177

[117] H. J. Kreuzer, R. L. C. Wang, M. Grunze, "Hydroxide Ion Adsorption on Self-Assembled Monolayers", *Journal of American Chemical Society 125*, **2003**, 27

[118] C. Zhang, W. Wang, T. Liu, Y. Wu, H. Guo, P. Wang, Q. Tian, Y. Wang, Z. Yuan, "Doxorubicin-loaded glycyrrhetinic acid-modified alginate nanoparticles for liver tumor chemotherapy", *Biomaterials 33*, **2012**, 2187-2196

[119] M. Johnsson, A. Wagenaar, J. B. F. N. Engberts, "Sugar-Based Gemini Surfactant with a Vesicle-to-Micelle Transition at Acidic pH and a Reversible Vesicle Flocculation near Neutral pH", *Journal of American Chemical Society 125*, **2003**, 757-760

[120] A. Rahmani, F. Rahimi, M. Iranshahi, H. Kahroba, A. Zarebkohan, M. Talebi, R. Salehi, H. Z. Mousavi, "Co-delivery of doxorubicin and conferone by novel pH-responsive β-cyclodextrin grafted micelles triggers apoptosis of metastatic human breast cancer cells", *Scientific Reports 11*, **2021**, 21425

[121] V. Karmegam, S. S. Kuruppu, C. M. Udamulle Gedara, M. C. Biewer, M. C. Stefan, "Enhanced DOX loading in star-like benzyl functionalized polycaprolactone micelles", *hournal of Polymer Science 59*, **2021**, 3040-3052

[122] L. Dornjak, M. Kovačić, K. Ostojić, A. Angaits, J. Szpunar, I. Urlić, A. Rogina, "Chitosan-Boric Acid Scaffolds for Doxorubicin Delivery in the Osteosarcoma Treatment", *Polymers 14*, **2022**, 4753

[123] T. Kovshova, N. Osipova, A. Alekseeva, J. Malinovskaya, A. Belov, A. Budko, G. Pavlova, O. Maksimenko, S. Nagpal, S. Braner, H. Modh, V. Balabanyan, M. G. Wacker, S. Gelperina, "Exploring the Interplay between Drug Release and Targeting of Lipid-Like Polymer Nanoparticles Loaded with Doxorubicin", *Molecules 26*, **2021**, 831

[124] Y. Yamada, "Dimerization of Doxorubicin Causes Its Precipitation", *ACS Omega 5*, **2020**, 33235 -33241

[125] M. A. Mitry, J. G. Edwards, "Doxorubicin induced heart failure: Phenotype and molecular mechanisms", *IJC Heart & Vasculature 10*, **2016**, 17-24

[126] S. Nandi, N. Kale, A. Patil, S. Banerjee, Y. Patil, J. Khandare, "A graphene-sandwiched DNA nano-system: regulation of intercalated doxorubicin for cellular localization", *Nanoscale Advances 2*, **2020**, 5746-5759

[127] J. E. Visvader, "Cells of origin in cancer", *Nature 469*, **2011**, 314-322

[128] Z. Fang, Y. Sun, H. Xiao, Peng Li, M. Liu, Fan Ding, W. Kan, R. Miao, "Targeted osteosarcoma chemotherapy using RGD peptide-installed doxorubicin-loaded biodegradable polymeric micelle", *Biomedicine & Pharmacotherapy 85*, **2017**, 160–168

[129] S. Sainas, A. C. Pippione, E. Lupino, M. Giorgis, P. Circosta, V. Gaidano, P. Goyal, D. Bonanni, B. Rolando, A. Cignetti, A. Ducime, M. Andersson, M. Järvå, R. Friemann, M. Piccinini, C. Ramondetti, B. Buccinnà, S. Al-Karadaghi, D. Boschi, G. Saglio, M. L. Lolli "Targeting Myeloid Differentiation Using Potent 2-Hydroxypyrazolo[1,5-a]pyridine Scaffold-Based Human Dihydroorotate Dehydrogenase Inhibitors", *Journal of Medicinal Chemistry 61*, **2018**, 6034-6055

[130] S. Sainas, A. C. Pippione, M. Giorgis, E. Lupino, P. Goyal, C. Ramondetti, B. Buccinnà, M. Piccinini, R. C. Braga, C. H. Andrade, M. Andersson, A. Moritzer, R. Friemann, S. Mensa, S. Al-Karadaghi, D. Boschi, M. L. Lolli, "Design, synthesis, biological evaluation and X-ray structural studies of potent human dihydroorotate dehydrogenase inhibitors based on hydroxylated azole scaffolds", *European Journal of Medicinal Chemistry 129*, **2017**, 287-302

[131] M. L. Lolli, M. Giorgis, P. Tosco, A. Foti, R. Fruttero, A. Gasco, "New inhibitors of dihydroorotate dehydrogenase (DHODH) based on the 4-hydroxy-1,2,5-oxadiazol-3-yl (hydroxyfurazanyl) scaffold", *European Journal of Medicinal Chemistry 49*, **2012**, 102-109

[132] L. Zhang, J. Zhang, J. Wang, C. Ren, P. Tang, L. Ouyang, Y. Wang, "Recent advances of human dihydroorotate dehydrogenase inhibitors for cancer therapy: Current development and future perspectives", *European Journal of Medicinal Chemistry 232*, **2022**, 114176

[133] R. Xiong, L. Zhang, S. Li, Y. Sun, M. Ding, Y. Wang, Y. Zhao, Y. Wu, W. Shang, X. Jiang, J. Shan, Z. Shen, Y. Tong, L. Xu, Y. Chen, Y. Liu, G. Zou, D. Lavillete, Z. Zhao, R. Wang, L. Zhu, G. Xiao, K. Lan, H. Li, K. Xu, "Novel and potent inhibitors targeting DHODH are broad-spectrum antivirals against RNA viruses including newly-emerged coronavirus SARS-CoV-2", *Protein & Cell 11(10)*, **2020**, 723-739

[134] M. Chountoulesi, N. Naziris, N. Pippa, C. Demetzos, "The significance of drug-to-lipid ratio to the development of optimized liposomal formulation", *Journal of Liposome Research 28(3)*, **2017**, 249-258

[135] E. Johansson, A. Lundquist, S. Zuo, K. Edwards, "Nanosized bilayer disks: Attractive model membranes for drug partition studies", *Biochimica et Biophysica Acta 1768*, **2007**, 1518–1525

[136] E. Johansson, C. Engvall, M. Arfvidsson, P. Lundahl, K. Edwards, "Development and initial evaluation of PEG-stabilized bilayer disks as novel model membranes", *Biophysical Chemistry 113*, **2005**, 183 – 192

[137] R. D. Worsham, V. Thomas, S. S. Farid, "Potential of Continuous Manufacturing for Liposomal Drug Products", *Biothecnology Journal 1700740*, **2018**, 1-8

[138] M. Ashokkumar, "The characterization of acoustic cavitation bubbles – An overview", *Ultrasonics Sonochemistry 18*, **2011**, 864-872

[139] V. S. Murali, R. Wang, C. A. Mikoryak, P. Pantano, R. Draper, "Rapid detection of polyethylene glycol sonolysis upon functionalization of carbon nanomaterials", *Experimental Biology and Medicine 240*, **2015**, 1147–1151

[140] S. Ahlgren, A. Fondell, L. Gedda, K. Edwards, "EGF-targeting lipodisks for specific delivery of poorly water-soluble anticancer agents to tumour cells", *RSC Advances 7*, **2017**, 22178-22186

[141] J. Ghitman, S. I. Voicu, "Controlled drug delivery mediated by cyclodextrin-based supramolecular self-assembled carriers: From design to clinical performances", *Carbohydrate Polymer Technologies and Applications 5*, **2023**, 100266

[142] C. V. Pardeshi, R. V. Kothawade, A. R. Markad, S. R. Pardeshi, A. D. Kulkarni, P. J. Chaudhari, M. R. Longhi, N. Dhas, J. B. Naik, S. J. Surana, M. C. García. "Sulfobutylether-β-cyclodextrin: A functional biopolymer for drug delivery applications", *Carbohydrate Polymers 301*, **2023**, 120347

[143] Y. N. Lamb, "Remdesivir: First Approval", *Drugs 80 (13)*, **2020**, 1355-1363

[144] A. Mazzaglia, R. Donohue, B. J. Ravoo, R. Darcy, "Novel Amphiphilic Cyclodextrins: Graft-Synthesis of Heptakis(6-alkylthio-6- deoxy)-β-cyclodextrin 2-Oligo(ethylene glycol) Conjugates and Their ω-Halo Derivatives", *European Journal of Organic Chemistry*, **2001**, 1715-1721